EFFECT OF ELECTRIC CONDUCTIVITY IN FERROELECTRIC STRUCTURES

ZHOU YAN

M. PHIL.

THE HONG KONG
POLYTECHNIC UNIVERSITY

2006

CERTIFICATE OF ORIGINALITY

I hereby declare that this thesis is my own work and that, to the best of my knowledge and belief, it reproduces no material previously published or written nor material which has been accepted for the award of any other degree or diploma, except where due acknowledgement has been made in the text.

_____ (Signed)

Zhou Yan (Name of student)

Acknowledgements

I would like to deeply thank my chief supervisor Prof. F. G. Shin for his excellent supervision and invaluable advice throughout the whole study period. I would also like to thank Dr. C. H. Lam, Dr. V. C. Lo and Mr. H. K. Chan, for their helpful comments and advice during my MPhil study.

I am deeply indebted to my parents and my brother for their support and encouragement in all the time of study and writing of this thesis.

It is my pleasure to thank Dr. Y. W. Wong, Dr. Y. M. Poon, Dr. K. H. Chew, Dr. C. K. Wong, Mr. C. H. Tsang, Mr. W. F. Wong and Mr. C. H. Ho for their assistance on my research and coursework studies.

Finally, I am grateful to The Hong Kong Polytechnic University for affording me the opportunity of pursuing the master's degree at the Department of Applied Physics.

Table of Contents

Abstract

Although ferroelectric materials are usually regarded as insulators, their small but finite conductivities have recently been taken into account to satisfactorily explain a number of new phenomena, which otherwise may be difficult to understand. Chan *et al.* [Chan *et al.*, 2004] have demonstrated that the time-dependent space-charge-limited (TDSCL) conduction could be a possible origin of the polarization offset in graded ferroelectrics. Wong *et al.* [Wong *et al.*, 2002; Wong and Shin, 2005] have systematically investigated the effects of electrical conductivity of the constituents on the dielectric, pyroelectric and piezoelectric properties of ferroelectric particulate composites. In this thesis, we focus on the study of the effect of electric conductivity in two kinds of ferroelectric structures: ferroelectric thin films and ferroelectric 0-3 composites.

We have investigated theoretically the dependence of the "polarization offset" of hysteresis loops (also known as vertical or charge offset) on various parameters in compositionally graded ferroelectric thin films. Our model adopts the Landau-Khalatnikov equation to describe hysteresis behavior and takes the time-dependent space-charge-limited conductivity into account to study the effects of polarization and permittivity gradients, thickness and charge mobilities in graded ferroelectric thin films. We have found that both polarization and permittivity gradients are requisite for the occurrence of the offset phenomena. It is also found that larger gradients of remanent polarization and permittivity, a smaller thickness and larger charge mobilities can generally enhance the vertical offsets. The qualitative

agreement between simulation and experiment further supports our notion that the asymmetric conduction current arising as a result of the composition gradient is an important factor leading to the “polarization offset” phenomenon.

Theoretical models have been developed to explain the horizontal shifting of the measured D-E hysteresis loops (imprint effect) of ferroelectric thin films. The time-dependent space-charge-limited conduction is adopted to describe the spatial and temporal variation of electrical conductivity in the films. It is found that the imprint phenomenon can be explained by considering three mechanisms or their multiple effects: (1) stress induced by film/electrode lattice mismatch or clamping, (2) domain pinning induced by e.g. oxygen vacancies, or (3) degradation of ferroelectric properties in film/electrode surface layers.

For film type ferroelectrics, we also studied theoretically the enhancement of remanent polarization and dielectric permittivity of interfacial-coupled ferroelectric superlattices based on the Landau-Ginzburg theory. Our model adopts the Landau-Khalatnikov equation to describe hysteresis behavior and takes the time-dependent space-charge-limited conductivity into account to investigate the ferroelectric and dielectric properties of ferroelectric superlattices. The results are in good agreement with recent experimental observations on the enhancement of remanent polarization and permittivity of $BaTiO_3/SrTiO_3$ superlattices and heterolayered $Pb(Zr, Ti)O_3$ thin films [Shimuta *et al.*, 2002; Pontes *et al.*, 2004].

The effect of electrical conductivity is also essential to understanding the behavior of ferroelectric composites. We use a simple dynamic model to include the

effect of the electrical conductivity of both constituent phases on the electrostriction behavior of a 0-3 composite comprising ferroelectric ceramic particles (lead-zirconate-titanate) embedded in a polymer matrix (polyurethane). Ohmic conductivity has been demonstrated to be sufficient to account for the electrostriction strain characteristics of this ferroelectric 0-3 composite system. Good agreement up to 30% volume fraction of lead-zirconate-titanate (PZT) is obtained for the butterfly shaped strain-electric-field loops with those observed in experiment [Lam *et al.* 2005]. The critical switching fields decrease while the electrostriction strain magnitudes increase with increasing PZT volume fraction, in good agreement with the experimental results. On the other hand, a relatively simple model for studying the magnetostrictively induced deformation behavior of magnetostrictive composites is also investigated. We use a conceptually simple and convenient approach to investigate magnetostriction for particulate composites of magnetostrictive inclusions in elastically isotropic, nonmagnetostrictive matrices. We calculate the magnetostriction responses of composites containing Terfenol-D and nickel. The macroscopic longitudinal strains parallel to the applied magnetic field for Terfenol-D/glass composites and both longitudinal and transverse strains for nickel/epoxy composites are obtained. Comparison with published experimental data [Nersessian *et al.* 2004; Chen *et al.* 1999a] indicates that good agreement up to very high volume fraction of inclusion particles has been achieved.

The magnetostriction model is then extended to study magnetoelectric (ME) effect of mildly conducting magnetostrictive/piezoelectric particulate composites by

taking the constituents' Ohmic conductivity into account. For illustrative purpose, we calculate the magnetoelectric voltage coefficients of particulate composites of nickel ferrite and lead zirconate titanate (NFO/PZT). The effects of electrical conductivity of both phases of the composite material are also studied. Our calculation demonstrates that the ME effect is larger for composites with low conductivity constituents and that the range over which notable ME effect is observed becomes smaller when conductivity increases. These trends are observed in recent experiments with particulate composites of nickel zinc ferrite/lead zirconate titanate (NZFO/PZT) and nickel ferrite/barium lead zirconate titanate (NFO/BLZT) [Laletin *et al.* 2002; Srinivasan *et al.* 2004]. The calculated longitudinal magnetoelectric voltage coefficient gradually increases with increasing frequency *f*, which is also experimentally observed in particulate composites of NFO/PZT [Zeng *et al.* 2004].

Chapter 1 Introduction

1.1 Background

In recent years, ferroelectric thin films and multi-phase ferroelectric materials have attracted much interest. This is because ferroelectric thin films usually exhibit a wide variety of interesting properties such as high dielectric permittivity, polarizability, piezoelectricity and pyroelectricity not found in bulk materials. On the other hand, single-phase ferroelectric materials may have some inherent limitations for technological applications. In addition, modern applications desire diverse properties of materials which often cannot be obtained in single phase materials. For example, although several magnetoelectric single phase materials have been discovered since the first experimental observation of linear ME effect in the antiferromagnetic Cr_2O_3 crystal in 1960 [2], these monophase ME materials only exhibit a very weak ME effect, and most of them have Neel or Curie temperature far below room temperature, which makes them difficult to find any practical applications in technology. Alternatively, some multiferroic composites made by combining ferroelectric and ferromagnetic substances together have attracted much interest because they can exhibit a much stronger ME effect in a wide temperature range.

Recently, various anomalous phenomena have been observed experimentally in ferroelectric thin films or composites. Some of these anomalous phenomena have

been satisfactorily explained by taking small but finite electrical conductivity into account, which otherwise may be difficult to understand. Notedly, Chan *et al.* have demonstrated that the time-dependent space-charge-limited conduction could be a possible origin of the polarization offset of the hysteresis loops of graded ferroelectrics as would be measured from a Sawyer-Tower circuit (see Figs. 1.1 and 1.2) [Chan *et al.*, 2004]; Wong *et al.* [Wong *et al.*, 2002; Wong and Shin, 2005] have systematically investigated the effects of electrical conductivity of the constituents on the dielectric, pyroelectric and piezoelectric properties of ferroelectric particulate composites.

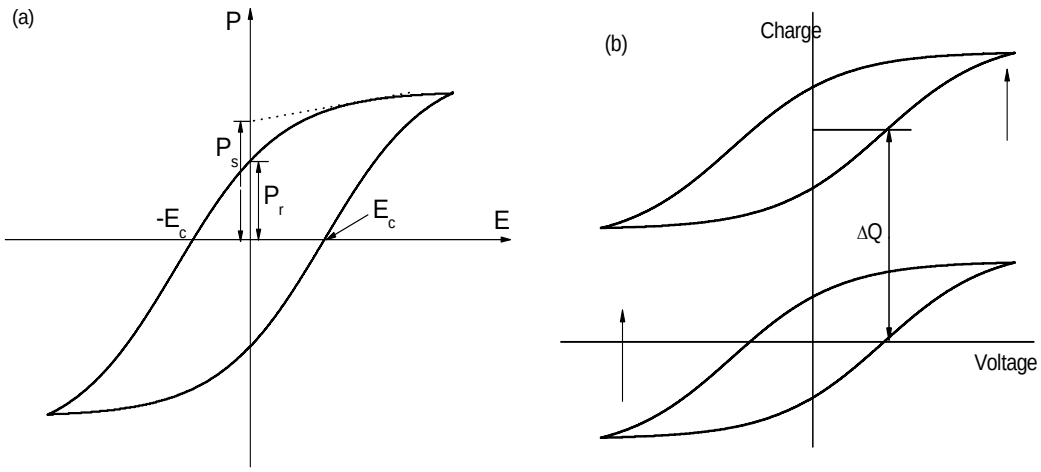

FIG. 1.1 (a) A typical ferroelectric hysteresis loop. (b) The hysteresis loop with a charge offset ΔQ.

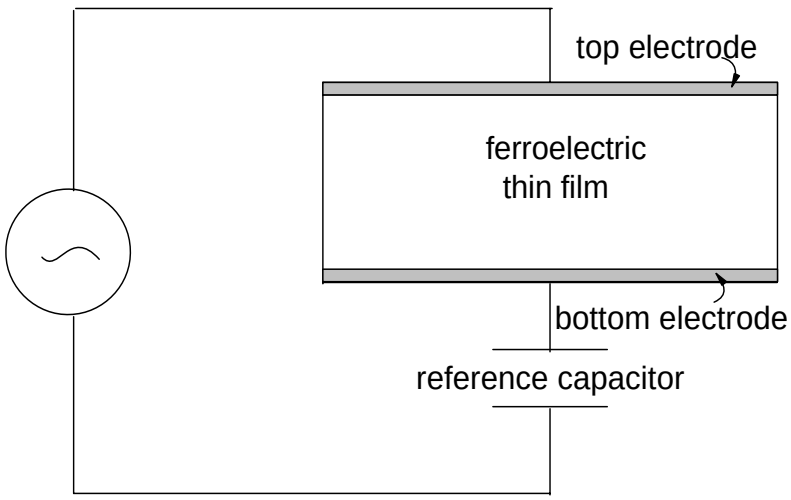

FIG. 1.2 Schematic diagram of the Sawyer–Tower circuit.

All ferroelectrics must possess some finite conductivity. It should be noted that the electrical conductivity may vary with electric field, temperature and the frequency of applied field. Moreover, asymmetric conduction behaviors have been observed in ferroelectric films [Zheng *et al.* 1996; Furuya and Cuchiaro, 1998; Yang *et al.*, 2002]. Although a number of distinct groups have reported on the asymmetric conduction behavior of ferroelectric thin films, its origin is still under debate. Zheng *et al.* suggested that the bottom electrode usually received high temperature cycles during film deposition and postannealing, while the top electrode received less or no heat cycles [Zheng *et al.*, 1996]. Hence different barrier heights may be formed at the bottom and top interfaces, which leads to the asymmetric leakage current characteristic for different polarities. Another possible explanation is that ferroelectric films are normally deposited on a substrate, with the polarization perpendicular to its surface. One side of the film is next to the substrate, while the other exposed to air or vacuum. This difference in contact may lead to the

asymmetry.

In summary, although ferroelectric materials are usually regarded as insulators, the small but finite conductivities have recently been demonstrated in many situations to be a key factor in determining ferroelectric properties and other characteristics. This thesis will focus on the interpretation of some phenomena or characteristics which in our opinion are induced by or enhanced by electrical conductivity.

1.2 Scope and outline of this thesis

This project focuses on some phenomena which are induced by the participation of electrical conductivity in ferroelectric films and composites. Phenomena studied in this project include: horizontal and vertical shifts of hysteresis loop in ferroelectric films, enhancement of dielectric and ferroelectric properties in ferroelectric superlattices, electrostriction behavior of a 0-3 composite comprising ferroelectric ceramic particles (lead-zirconate-titanate) embedded in a polymer matrix (polyurethane), the magnetostriction behavior of particulate composites of magnetostrictive inclusions in elastically isotropic, nonmagnetostrictive matrices, and magnetoelectric effect (ME) of mildly conducting magnetostrictive/piezoelectric particulate composites. This project demonstrates that considerations of electrical conductivity of the ferroelectric/ferromagnetic materials can quite naturally account for these phenomena which may be difficult to understand from the assumption of perfectly insulating materials. The TDSCL and Ohmic conduction are respectively employed for the explanation of most phenomena presently investigated. In this project, both film type ferroelectrics and 0-3 composites are investigated. Calculated results are as far as possible compared with experimental data. By understanding these phenomena, new device applications may be developed and ferroelectric systems can be more effectively designed for specific applications.

This thesis is divided into six chapters. Chapter 1 introduces the background information. In Chapter 2, a thermodynamic model was proposed that shows that

systematic variations in the polarization and permittivity would result in asymmetric conduction currents which could be the origin of vertical offset in the polarization hysteresis loop measurement. It is demonstrated that the gradients of remanent polarization and permittivity, film thickness, and charge mobilities are all key factors determining the charge offset of graded ferroelectric thin film. In chapter 3, we proposed a thermodynamic model to study the effects of stress, domain pinning and degradation of ferroelectric properties at film/electrode surface on the horizontal shifting of measured D-E hysteresis loops (imprint) of ferroelectric thin films. In chapter 4, we studied theoretically the enhancement of remanent polarization and dielectric permittivity of interfacial-coupled ferroelectric superlattices based on the Landau-Ginzburg theory. We use a simple dynamic model to include the effect of the electrical conductivity of both constituent phases on the electrostriction behavior of a 0-3 composite comprising ferroelectric ceramic particles (lead-zirconate-titanate) embedded in a polymer matrix (polyurethane) in chapter 5. A simple model for studying the magnetostrictively induced deformation behavior of magnetostrictive composites is also proposed in this chapter. In the last chapter, the magnetostriction model is extended to study magnetoelectric (ME) effect of mildly conducting magnetostrictive/piezoelectric particulate composites by taking the constituents' Ohmic conductivity into account.

In all, the results of this project will present a further step toward a more detailed understanding of the effect of electrical conductivity in ferroelectric thin films and composites, which is essential for the application of ferroelectrics in various devices.

1.3 Literature review

This section reviews some past research works on the vertically and horizontally shifted hysteresis behavior in thin films, electrostriction and magnetostriction models of particulate composites, and some known models of ME effect of magnetostrictive/piezoelectric dilute particulate composites.

1.3.1 Miller *et al.*'s model for lossy ferroelectric films

Miller *et al.* [Miller *et al.*, 1990] proposed that the behavior of electrical circuits containing a non-ideal ferroelectric can be modeled by a stacked structure, with switching ferroelectric and non-switching dielectric layers. The electric displacement D is defined by

$$D = \varepsilon_0 E_f + P_t(E)\,, \tag{1.1}$$

where E_f is the electric field in the ferroelectric and P_t is the total ferroelectric polarization which can be written as the sum of the linear contribution to the displacement and the contribution due to switching dipoles in the ferroelectric film:

$$D = \varepsilon_0 E_f + \varepsilon_0 \chi_f E_f + P_d = \varepsilon_f E_f + P_d\,, \tag{1.2}$$

where χ_f is the electric susceptibility and $\varepsilon_f = \varepsilon_0 + \varepsilon_0 \chi_f$ is the linear dielectric permittivity of the ferroelectric layer. P_d is the polarization due to the switching dipoles only.

The stacked structure is placed in a Sawyer-Tower circuit (see Fig. 1.3) and the output voltage V_o may be numerically integrated from the following expression:

$$\frac{dV_o}{dt} = \frac{\gamma_3 C_f [dV_i / dt] + V_i / R_f + V_o (1/R_n + 1/R_f)}{C_n + \gamma_3 C_f}, \tag{1.3}$$

where

$$\gamma_3 = \frac{1}{\gamma_2}\left(1 + \frac{1}{\varepsilon_f}\frac{\partial P_d(E)}{\partial E}\right), \tag{1.4}$$

$$\gamma_2 = 1 - \frac{d_p}{d_f}\left[1 - \frac{\varepsilon_f}{\varepsilon_p}\left(1 + \frac{1}{\varepsilon_f}\frac{\partial P_d(E)}{\partial E}\right)\right], \tag{1.5}$$

$$C_f = (\varepsilon_f / d_f) A_f, \tag{1.6}$$

and V_i is the input voltage, E is the electric field across the stacked structure. d_p and d_f are the thickness of the dielectric layer and the total thickness of the film. A_f is area, ε_p is the permittivity of the non-switching dielectric layer, C_f is the capacitance of the ferroelectric capacitor and C_n is the capacitance of the reference capacitor. R_f and R_n represent resistance of the ferroelectric capacitor and the input impedence of the instrument utilized to measure the output voltage, respectively.

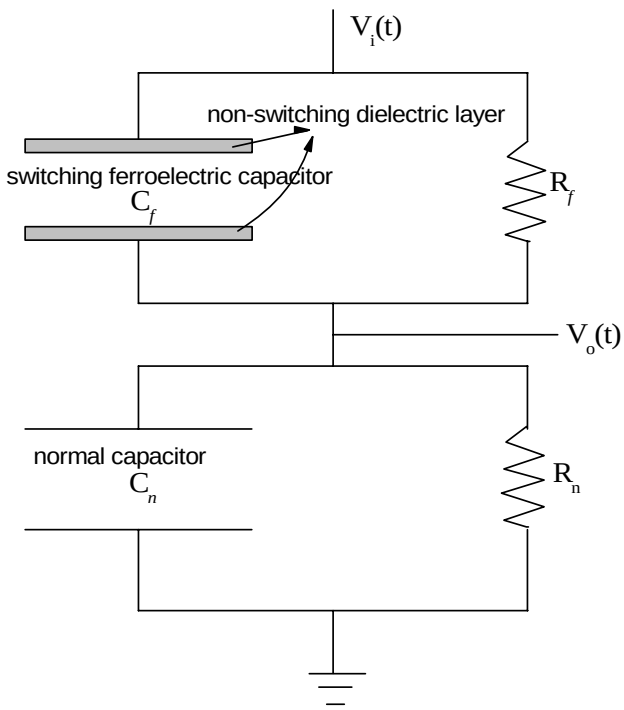

FIG. 1.3 Modified Sawyer-Tower characterization circuit in which the ferroelectric capacitor circuit

element containing a switching ferroelectric layer and nonswitching dielectric layers adjacent to the electrodes in Miller's model.

The *P-E* relation of the ferroelectric layer is described by a mathematical model as:

$$\frac{\partial P_d(x,t)}{\partial E_f(x,t)} = \left[1 - \tanh\sqrt{\frac{P_d(x,t) - P_{sat}(x,t)}{\xi(x,t)P_s(x,t) - P_d(x,t)}}\right]\frac{\partial P_{sat}(x,t)}{\partial E_f(x,t)}, \tag{1.7}$$

where

$$P_{sat}(x,t) = \xi(x,t)P_s(x,t)\tanh\left[\frac{\xi(x,t)E_f(x,t) - E_c(x,t)}{2E_c(x,t)}\ln\left(\frac{P_s(x,t) + P_r(x,t)}{P_s(x,t) - P_r(x,t)}\right)\right]. \tag{1.8}$$

In this model, $\xi(x,t) = +1$ for increasing fields and $\xi(x,t) = -1$ for decreasing fields. $P_r(x,t)$, $P_s(x,t)$ and $E_c(x,t)$ denote remanent polarization, spontaneous polarization and coercive field of the ferroelectric layer respectively.

1.3.2 Mantese *et al.*'s Slater model for GFD

Mantese *et al.* [Mantese *et al.*, 1997] proposed that Slater's empirical model [Slater, 1950] for ferroelectric materials could be extended to describe thin films with polarization gradients normal to the growth surface, i.e., graded ferroelectric devices (GFD).

In their opinion, there should be a spontaneous potential difference which should appear across a graded ferroelectric upon the application of an oscillatory electric field. This "built-in" potential difference is proportional to the gradient in composition, temperature or stress [Mantese and Schubring, 2001].

For a linearly graded composition normal to the growth surface, the dielectric

permittivity ε and spontaneous polarization P_s are approximately linearly related to the composition *c*. The "built-in" potential difference V_s across the material is calculated as:

$$V_s = \frac{[P_s(c_0)]^2 (t/c_0)\nabla c}{12eN\varepsilon_0}. \tag{1.9}$$

c_0 is the composition at some reference plane along the composition gradient, *t* is thickness of the material, *e* is the electronic charge and *N* is the number of dipoles per unit volume. ∇c gives the compositional gradient.

Polycrystalline ferroelectric materials have often been characterized by a field dependence of the form: $P_s \propto P_s^{'}(c_0)E_{\max}^{\gamma}$, where $E_{\max}^{\gamma}$ is the maximum applied field and $P_s^{'}(c_0)$ is a constant. γ is typically, but not exclusively, in the range, $1 \le \gamma \le 2$. Thus Eq. (1.9) is rewritten as $V_s = \frac{[P_s^{'}(c_0)E_{\max}^{\gamma}]^2 (t/c_0)\nabla c}{12eN\varepsilon_0}$.

Thus a traditional Sawyer-Tower measurement of the hysteresis behavior of a graded ferroelectric should result in a nonsymmetric charge offset ΔQ given by:

$$\Delta Q = \frac{\varepsilon A[P_s^{'}(c_0)E_{\max}^{\gamma}]^2 \nabla c/c_0}{12eN\varepsilon_0}, \tag{1.10}$$

where A is the area of the film.

1.3.3 Ban *et al.*'s generalized Landau-Ginzburg model for GFD

Ban *et al.* [Ban *et al.*, 2003] proposed a generalized Landau-Ginzburg model for graded ferroic structures and devices in which the inhomogeneities are assumed to arise from compositional, temperature, or stress gradients.

The graded ferroelectric is considered as being composed of "layers" with a non-uniform polarization along the *z* direction which is perpendicular to the *xy* plane.

Starting from the well-known Landau-Ginzburg-Devonshire (LGD) theory, the free energy (per unit area) of the graded ferroelectric is written as:

$$F = \int_0^L \left[\frac{\alpha P^2}{2} + \frac{\beta P^4}{4} + \frac{\gamma P^6}{6} + \frac{A}{2}(\frac{dP}{dz})^2 - \frac{1}{2}E^D P - EP + F_{el}^i \right] dz \,, \tag{1.11}$$

where α, β, γ, and A are the free-energy expansion coefficients. E^D and L are the depolarization field and film thickness, respectively. F_{el}^i represents the contribution due to the internal stresses resulting from variation of the lattice parameter within the compositionally graded or temperature graded unconstrained ferroelectric bar.

Using the mechanical boundary conditions, the total internal elastic energy for each ‘‘layer’’ can then be expressed as:

$$F_{el}^i(z) = \bar{C}\left\{ Q_{12}\left[P^2(z) - \langle p \rangle^2 \right] + \frac{24(z - L/2)}{L^3}\int_0^L (z - L/2) Q_{12}\left[P^2(z) - \langle P \rangle^2 \right] dz \right\}^2 \,, \tag{1.12}$$

where Q_{12} is the electrostrictive coefficient and $\langle P \rangle$ is the average polarization. $\bar{C}$ is an effective elastic constant given by

$$\bar{C} = C_{11} + C_{12} - \frac{2C_{12}^2}{C_{11}} \,, \tag{1.13}$$

and C_{ij} are the elastic moduli at constant polarization.

The minimization of the free energy with respect to the polarization in the absence of an external electric field yields the Euler-Lagrange equation:

$$A\frac{d^2P}{dz^2} = \bar{\alpha}P + \bar{\beta}P^3 + \gamma P^5 \,, \tag{1.14}$$

where A, $\bar{\alpha}$ and $\bar{\beta}$ are the position-dependent expansion coefficients through which the inhomogeneous nature of the three graded systems is reflected with respect to composition, spatial temperature, and strain variations.

The “built-in” potential that finds its origin in the attendant polarization gradient

that arises as the result of the compositional gradient, temperature gradient or external stress gradient is given by:

$$V_{\text{int}} = -\frac{1}{C_F L}\int_0^L z\left(\frac{dP(z)}{dz}\right)dz\,, \tag{1.15}$$

where C_F is the ferroelectric capacitance. Then, the charge offset due to this built-in potential is:

$$\Delta Q = C_Q V_{\text{int}} = \frac{k}{L}\int_0^L z\left(\frac{dP(z)}{dz}\right)dz\,, \tag{1.16}$$

where k is the ratio of the capacitance of a load capacitor C_Q in the Sawyer-Tower circuit to the capacitance of the graded ferroelectric C_F.

Although a succession of theoretical models developed by the groups of Alpay and Mantese [Mantese *et al.*, 1997; Mantese and Schubring, 2001; Ban *et al.*, 2003] can partially account for some experimental features related to the charge offset phenomena, their models can not satisfactorily explain the experimental observations where very large vertical offset were reported, e.g. values as large as $420\mu C/cm^2$ obtained in lead-zirconate-titanate (PZT) graded structures [Brazier *et al.*, 1998]. In addition, their models have not explained the dynamic nature of the charge offsets in compositionally graded structures.

1.3.4 Chen et al.'s model for compositionally graded ferroelectics

Chen *et al.* [Chen *et al.* 1999b] have derived an expression for the steady state hysteresis loop of graded ferroelectrics. The spontaneous polarization P_s is linearly varied with position z:

$$P_s = \frac{\alpha P_{so}}{d_f} z + P_{so}\,, \tag{1.17}$$

where α is a constant, d_f and P_{so} represent the thickness of the ferroelectric film and the minimum polarization, respectively.

Thus, the charge density ρ can be obtained from Poisson's equation as:

$$\rho = \frac{-\alpha P_{so}}{d_f}. \tag{1.18}$$

The built-in potential due to the charge distribution is calculated as:

$$V_{bi} = -\frac{1}{C_f d_f}\int_0^{d_f} z\rho(z)dz = \frac{\alpha P_{so}}{2C_f}, \tag{1.19}$$

where C_f is the capacitance of the ferroelectric. The charge offset is then obtained from the built-in potential as:

$$\Delta Q = C_f V_{bi} = \frac{\alpha\kappa P_{soo} V_{\max}^{\gamma}}{2d_f^{\gamma}}. \tag{1.20}$$

where $P_{so} = \kappa P_{soo} E_{\max}^{\gamma}$, a relation suggested by Mohammed *et al.* [Mohammed *et al.*]. γ is typically, but not exclusively, in the range, $1 \le \gamma \le 2$.

In the above theoretical model proposed by Chen *et al.*, the authors have shown that the observed charge offsets are a direct result of the polarization gradient and their model is relatively easy to be handled. However the analysis is only performed by considering the equilibrium state and hence the proposed theory can not explain the continuous shifting process of the many observed charge offsets in experiments.

1.3.5 Pintilie *et al.*'s model for compositionally graded ferroelectics

Pintilie *et al.* developed a simple two-layer structure model for the built-in charge from simple energy considerations [Pintilie *et al.* 2003].

The dielectric permittivities are assumed to be the same while the absolute values of remanent polarization are assumed to be different within the two layers. Starting from the initial condition of no external applied field on the structure, the potentials in the two layers, due to different polarization, are obtained by solving the Laplace's equation in each layer with the boundary and continuity conditions. The built-in potential is derived from simple energy consideration as follows. First the energy density deposited in the ferroelectric capacitor during polarization reversal is calculated by the integral of the hysteresis loop:

$$w = \frac{1}{2}\int P(E)dE\,. \tag{1.21}$$

Considering that the total polarization is split in two parts then the total energy will be given by two components:

$$w = \frac{1}{2}\int P_{rev}(E)dE + w_{irev}\,. \tag{1.22}$$

The first term is due to that part of polarization that can still be reversed. The second term is due to the part of polarization that cannot be reversed which gives the displacement of the loop along the polarization. The second term in Eq. (1.22) is given by:

$$w_{irev} = \frac{1}{2\varepsilon}(P_1^2 + P_2^2) = \frac{Q_{bi}^2}{2AdC}\,. \tag{1.23}$$

Here $P_{1,2}$ refers to that part of polarization that cannot be reversed in each layer. A and d are the electrode area and the total thickness of the structure, respectively. $C = \varepsilon A/d$ is the capacitance and ε is the permittivity of the structure. A generalization of this procedure is then used to obtain an expression for the built-in potential V_{bi} as:

$$V_{bi} = \frac{d}{n}\sqrt{n\left(\sum_{i=1}^{n}\frac{1}{\varepsilon_i}\right)\left(\sum_{i=1}^{n}\frac{P_i^2}{\varepsilon_i}\right)}\,, \tag{1.24}$$

where n is the number of layers (herein $n=2$). The DC voltage on the graded structure is applied on the RC connection of the Sawyer-Tower circuit and given by:

$$V_{offset} = V_{bi}[1 - \exp(-t/\tau)]\,, \tag{1.25}$$

where τ is the time constant of the Sawyer-Tower configuration.

1.3.6 Bouregba *et al.*'s model for compositionally graded ferroelectics

Bouregba *et al.* suggested that probably the presence of asymmetrical leakage current in compositionally graded ferroelectrics might be the origin of the offsets often observed in these structures [Bouregba *et al.*, 2003].

The idea is demonstrated by setting a pair of diodes in parallel with a

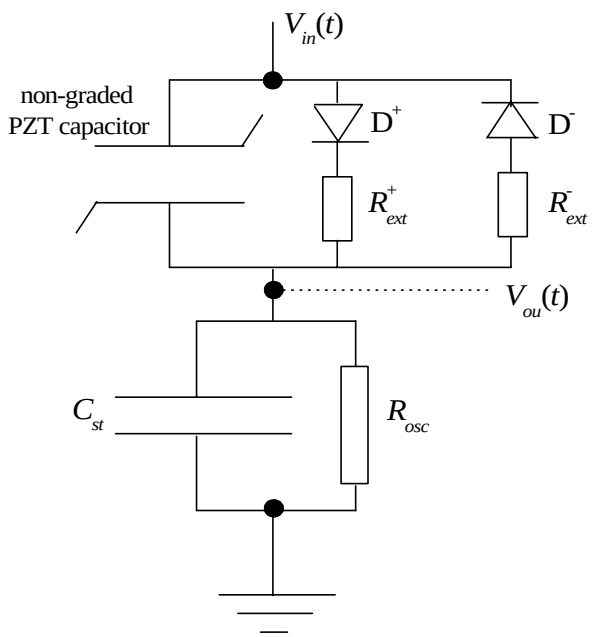

FIG. 1.4 Scheme of the Sawyer–Tower circuit with added elements allowing the observation of polarization offsets on a non-graded PZT capacitor.

non-graded structure. Each diode is in series with an external resistor of different values (R^+_{ext} and R^-_{ext}). When a sinusoidal voltage is applied, only one diode is conducting in each half cycle (see Fig. 1.4). The DC component of the offset voltage measured from the Sawyer-Tower circuit is:

$$V_{off} = \frac{1}{T}\left\{\tau_1 A_1\left(1-e^{-\frac{T}{2\tau_1}}\right)+\tau_2 A_2\left(1-e^{-\frac{T}{2\tau_2}}\right) - \frac{R_{osc}V_{inm}T}{\pi}\left[\frac{\cos\varphi_2}{(R_{osc}+R^-_{ext})\sqrt{1+(\omega\tau_2)^2}}-\frac{\cos\varphi_1}{(R_{osc}+R^+_{ext})\sqrt{1+(\omega\tau_1)^2}}\right]\right\}, \tag{1.26}$$

where

$$A_1 = \frac{R_{osc}V_{inm}}{e^{-\frac{T}{2\tau_2}}-e^{-\frac{T}{2\tau_1}}}\left[\frac{\sin\varphi_1}{(R_{osc}+R^-_{ext})\sqrt{1+(\omega\tau_1)^2}} - \frac{\sin\varphi_2}{(R_{osc}+R^-_{ext})\sqrt{1+(\omega\tau_2)^2}}\right]e^{\frac{T}{2\tau_1}}\left(1+e^{-\frac{T}{2\tau_2}}\right), \tag{1.27}$$

$$A_2 = A_1 e^{-\frac{T}{2\tau_1}} \frac{1+e^{\frac{T}{2\tau_1}}}{1+e^{-\frac{T}{2\tau_2}}}, \tag{1.28}$$

and

$$\tau_1 = \frac{R_{osc} R_{ext}^{+} C_{st}}{R_{osc} + R_{ext}^{+}}, \tag{1.29}$$

$$\tau_2 = \frac{R_{osc} R_{ext}^{-} C_{st}}{R_{osc} + R_{ext}^{-}}, \tag{1.30}$$

$$\varphi_1 = -atn(\omega\tau_1), \tag{1.31}$$

$$\varphi_2 = -atn(\omega\tau_2), \tag{1.32}$$

V_{inm} is the amplitude of the applied voltage, $\omega = 2\pi f$ is the pulsation of the input voltage and f =1/T is the measuring frequency.

In the above model, the authors have demonstrated that artificial but significant offsets can be observed on non graded $Pb(Zr_xTi_{1-x})O_3$ (PZT) capacitor during S-T hysteresis measurements. To the best of our knowledge, Bouregba and Poullain's group is the first to propose that the asymmetrical conduction currents which are the direct consequence of the graded nature of the polarization are fundamentally at the origin of the offsets of the hysteresis loops of graded ferroelectric films.

1.3.7 Bouregba and Poullain's model for lossy ferroelectric films

Bouregba and Poullain [Bouregba and Poullain, 2002] aimed to extract the true ferroelectric hysteresis loop from the hysteresis loop measured from a Sawyer-Tower circuit. The usually measured *D-E* loops may be subject to strong deformations, which may originate from the unavoidable presence of circuit elements and/or from the leaky character of the ferroelectric sample, preventing the accurate evaluation of remanent and spontaneous polarization and of the coercive field. Their numerical computation scheme would restore the true shape of the ferroelectric polarization and determine both the resistivity and the linear dielectric constant of a ferroelectric sample.

Later on, they [Bouregba and Poullain 2003] extended their model to include the

effect of the passive layers, in which a marked decrease of the linear dielectric constant and of remanent and maximum polarizations is observed, at the film interfaces. They derived the following mathematical expressions by which one can extract and plot correctly the true hysteresis loop of the ferroelectric layer from Sawyer-Tower hysteresis measurements:

$$P_{fe}(t)=\frac{\left(\frac{C_{st}}{A}+\frac{\varepsilon_{fe}}{(d_{fe}+d_{il})\alpha}\right)V_{ou}(t)-\frac{\varepsilon_{fe}}{(d_{fe}+d_{il})\alpha}V_{in}(t)+\gamma(t)}{1-\frac{\varepsilon_{fe}d_{il}}{(d_{fe}+d_{il})\varepsilon_{il}\alpha}}, \tag{1.33}$$

$$E_{fe}(t)=\frac{V_{in}(t)-V_{ou}(t)-d_{il}P_{sd}(t)/\varepsilon_{il}}{(d_{fe}+d_{il})\alpha}, \tag{1.34}$$

where

$$\alpha=1+\frac{d_{il}}{d_{fe}+d_{il}}(\frac{\varepsilon_{fe}}{\varepsilon_{il}}-1), \tag{1.35}$$

$$\gamma(t)=\int_{(t)}\left[\frac{V_{ou}(t)}{A}\left(\frac{1}{R_{fe}}+\frac{1}{R_{osc}}\right)\right]dt-\int_{(t)}\frac{V_{in}(t)}{AR_{fe}}dt, \tag{1.36}$$

Subscripts *fe* and *il* represent ferroelectric and passive layer respectively. $V_{in}(t)$ and $V_{ou}(t)$ are the driving alternating signal and output signal, respectively. C_{st} and R_{osc} are the capacitance of the reference capacitor and the input resistance of the oscilloscope, respectively. A and ε denote area and permittivity respectively.

1.3.8 Lü and Cao's model for asymmetic ferroelectric films

Lü and Cao used Ginzburg-Landau-Devonshire theory and took the structural difference between the surface layer and the bulk ferroelectric into account to study the behavior of ferroelectric thin film [Lü and Cao, 2002; 2003]. They used the model to study the effect of asymmetric boundary conditions and the horizontal shift of the hysteresis loop from the center point.

According to their theory, the inhomogeneous nature of the film near the surface region is described by the variation of "Curie temperature" with a space variable.

The generalized GLD free energy for unit area is given as follows:

$$G = G_0 + \int_{-L}^{+L} dz \left\{ \frac{A[T - T_b\varphi(z)]P^2}{2} + \frac{CP^4}{4} + \frac{DP^6}{6} + \frac{1}{2}K\left(\frac{dP}{dz}\right)^2 - \frac{1}{2}E_d P - \bar{E}_{ie}P - EP \right\}, \quad (1.37)$$

where A, C, D, and K are independent of temperature T and position z. T_b is the transition temperature of bulk material; E is the applied field along the z direction. $\bar{E}_{ie}$ is the average effective internal bias field which direction is parallel to the direction of the easy polarization of the asymmetry ferroelectric thin film. $\psi(z)$ represents the inhomogeneous nature of the surface layer. E_d is the depolarization field:

$$E_d = -\frac{1}{\varepsilon_0}(P - \bar{P}), \quad (1.38)$$

where ε_0 is the vacuum dielectric permittivity.

The Euler's equation for such a system is given by

$$K\frac{d^2P}{dz^2} = A\left[T - T_b\psi(z)\right]P + CP^3 + DP^5 - E_d - \bar{E}_{ie} - E, \quad (1.39)$$

with

$$\left.\frac{dP}{dz}\right|_{z=\pm L} = 0. \quad (1.40)$$

rather than the extrapolation length description widely adopted in the free energy formulation for thin films.

1.3.9 Abe *et al.*'s model for asymmetric ferroelectric films

Abe *et al.* [Abe *et al.* 2002] proposed a nonswitching layer model to explain voltage shift phenomena of hysteresis loops in ferroelectric thin films. A nonswitching layer, which has irreversible spontaneous polarization, was assumed to be present between the bulk ferroelectric layer and the bottom electrode.

In the ferroelectric layer, the Landau-Ginzburg free energy is:

$$G_F = \frac{1}{2}\chi_F P_F^2 + \frac{1}{4}\xi_F P_F^4 + \frac{1}{6}\varsigma_F P_F^6, \tag{1.41}$$

where χ_F, ξ_F, and ς_F are dielectric stiffness and stiffness coefficients for higher orders of the ferroelectric layer.

In the nonswitching layer, the free energy is calculated by:

$$G_N = \frac{1}{2}\chi_N (P_N - P_0)^2, \tag{1.42}$$

where χ_N is dielectric stiffness of the nonswitching layer. P_0 denotes the spontaneous polarization of the nonswitching layer.

The electric fields in the ferroelectric layer and nonswitching layer are derived from the free energy functions and are expressed as follows:

$$E_F = \chi_F P_F + \xi_F P_F^3 + \varsigma_F P_F^5, \tag{1.43}$$

and

$$E_N = \chi_N (P_N - P_0). \tag{1.44}$$

The free electric charge density at the interface between the two layers is:

$$q = D_N - D_F = \varepsilon_0 \varepsilon_N E_N + P_0 - \varepsilon_0 E_F - P_F, \tag{1.45}$$

where D_N and D_F are the electric displacement of the nonswitching layer and ferroelectric layer, respectively. ε_N is the permittivity of the nonswitching layer.

Thus, the applied voltage can be expressed as:

$$V = d_{eff} E_F + P_F / C_N + V_{shift} = (d_F + \frac{d_N}{\varepsilon_N})E_F + \frac{d_N}{\varepsilon_0 \varepsilon_F} P_F + \frac{d_N}{\varepsilon_0 \varepsilon_N}(q - P_0), \tag{1.46}$$

where d_F and d_N are the thicknesses of the ferroelectric and nonswitching layers. d_{eff} is the effective thickness of the ferroelectric thin film, C_N is capacitance per unit area of the nonswitching layer and V_{shift} is the voltage shift of the hysteresis loop in the thin film.

1.3.10 Nan *et al.*'s model for effective electrostriction of 0-3 composites

Nan *et al.* [Nan *et al.* 2000] developed an analytical approach for the effective electrostriction in inhomogeneous materials based on Green's function method. They gave explicit expressions for the effective electrostrictive coefficient of isotropic particulate composites containing randomly oriented spherical ferroelectric crystallites having cubic symmetry.

The coupled electromechanical interaction of an electrostrictive inhomogeneous material consisting of microcrystallites having a center of symmetry with perfectly bonded interface can be described by the following constitutive equations:

$$\sigma = \mathrm{C}\varepsilon - \mathrm{BEE}, \tag{1.47}$$

$$\mathrm{D} = \kappa\mathrm{E} + 2\mathrm{B}^T\varepsilon\mathrm{E}, \tag{1.48}$$

where σ, ε, D and E, are the stress, strain, electric displacement, and electric field, respectively. C is the elastic stiffness, and $\mathrm{B} = \mathrm{CM}$, where M is the electrostrictive coefficient tensor relating the strain to the electric field. B^T is the transpose of B, and κ is the permittivity.

The effective behavior of the inhomogeneous material is defined in terms of macroscopic average fields (denoted by $\langle\ \rangle$), namely,

$$\langle\sigma\rangle = \mathrm{C}^*\langle\varepsilon\rangle - \mathrm{B}^*\langle\mathrm{E}\rangle\langle\mathrm{E}\rangle, \tag{1.49}$$

$$\langle\mathrm{D}\rangle = \kappa^*\langle\mathrm{E}\rangle + 2\mathrm{B}^{T*}\langle\varepsilon\rangle\langle\mathrm{E}\rangle. \tag{1.50}$$

The electric-mechanical boundary conditions are:

$$u_i(S) = \varepsilon_{ij}^o x_j = u_i^o, \quad \psi(S) = -E_i^o x_i = \psi^o, \tag{1.51}$$

where S is the external surface of the material, u_i and ψ denote elastic displacement and electric potential, respectively.

Consider a state of static equilibrium in the absence of body forces and free electric charges, the nonlinearly coupled equilibrium equations are:

$$\sigma_{ij,j}(x) = 0, \quad D_{j,j}(x) = 0, \tag{1.52}$$

where the commas in the subscripts denote partial differentiation with respect to x_j.

From Eqs. (1.49)-(1.52), the effective properties of the material can be solved by means of the Green's function method:

$$\mathrm{C}^* = \left\langle \mathrm{CT}^{66} \right\rangle \left\langle \mathrm{T}^{66} \right\rangle^{-1}, \tag{1.53}$$

$$\kappa^* = \left\langle \kappa \mathrm{T}^{33} \right\rangle \left\langle \mathrm{T}^{33} \right\rangle^{-1}, \tag{1.54}$$

$$\mathrm{M}^* \left\langle \mathrm{T}^{33} \right\rangle \left\langle \mathrm{T}^{33} \right\rangle = \mathrm{C}^{*-1} \left\langle \left[(\mathrm{C}\text{-}\mathrm{C}^*)\mathrm{T}^{66}\mathrm{G}^u + \mathrm{I} \right] \mathrm{CMT}^{33}\mathrm{T}^{33} \right\rangle. \tag{1.55}$$

with

$$\mathrm{T}^{66} = (\mathrm{I} - \mathrm{G}^u \mathrm{C}')^{-1}, \quad \mathrm{T}^{33} = (\mathrm{I} - \mathrm{G}^{\psi} \kappa')^{-1}, \tag{1.56}$$

where I is the unit tensor. G^u and G^{ψ} are the modified displacement and electric potential Green's function for the homogeneous medium.

Eq. (1.55) directly yields the explicit effective-medium-like approximate results for the effective electrostrictive coefficients of a common isotropic two-phase composite consisting of randomly oriented, spherical relaxor ferroelectric crystallites having cubic symmetry:

$$M_h^* = \sum_{i=1}^{2} f_i (A_{11}^{(i)} + 2A_{12}^{(i)}) \left(\frac{3\kappa^*}{\kappa_i + 2\kappa^*} \right)^2, \tag{1.57}$$

$$M_{44}^* = \sum_{i=1}^{2} f_i \frac{4(A_{11}^{(i)} - A_{12}^{(i)}) + 6A_{44}^{(i)}}{5} \left(\frac{3\kappa^*}{\kappa_i + 2\kappa^*} \right)^2, \tag{1.58}$$

where M_h^* and M_{44}^* are the hydrostatic and shearlike electrostrictive coefficients, respectively. $A_{ij}^{(i)}$ are the components of the tensor $\mathrm{A} = \left[\mathrm{I} - \mathrm{G}^u (\mathrm{C} - \mathrm{C}^*) \right]^{-1} (\mathrm{C}^*)^{-1} \mathrm{CM}$ of the *i*th phase.

1.3.11 Armstrong's model for magnetostriction of particulate composites

Armstrong [Armstrong, 2000; 2002] presented a new theory of the nonlinear magnetoelastic behavior of magnetically dilute magnetostrictive particulate composites. The theory assumes a uniform external magnetic field is operating on a large number of well-distributed, crystallographically and shape parallel ellipsoidal magnetostrictive particles encased in an elastic, non-magnetic matrix [Fig. 1.5].

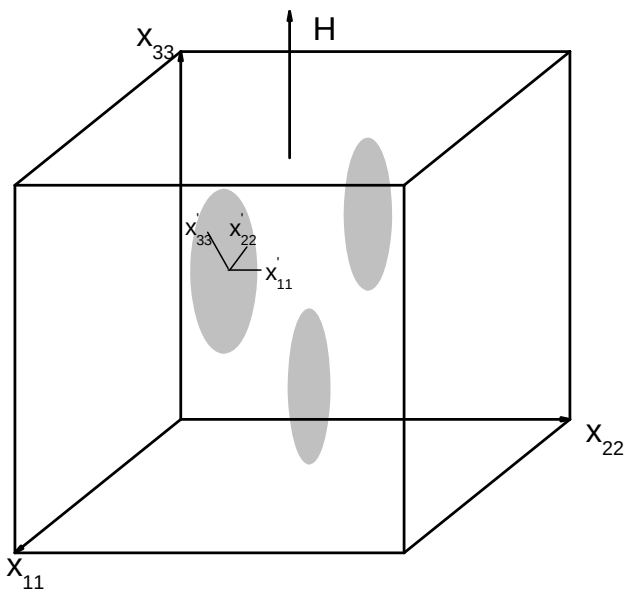

FIG. 1.5 Idealized composite geometry.

The magnetic free energy component due to the contribution of the magnetic field is given by:

$$E_{field} = -\mu_0 M_S H\{(\sin[\theta_m]\cos[\varphi_m])(\sin[\theta_f]\cos[\varphi_f]) + (\sin[\theta_m]\sin[\varphi_m])(\sin[\theta_f]\sin[\varphi_f]) + \cos[\varphi_m]\cos[\varphi_f]\}, \quad (1.59)$$

where H is the field strength, M_s is the magnetization, $[\theta_m, \varphi_m]$ is the magnetization direction in spherical polar coordinates and $[\theta_f, \varphi_f]$ is the applied field orientation.

The positive magnetocrystalline energy extracted as the magnetization vector rotates away from a “hard” direction to an “easy” direction is:

$$E_{an} = K_1\{(\sin[\theta_m]\cos[\varphi_m])^2(\sin[\theta_m]\sin[\varphi_m])^2 + (\sin[\theta_m]\sin[\varphi_m])^2\cos^2[\theta_m] + \cos^2[\theta_m](\sin[\theta_m]\cos[\varphi_m])^2\}, \quad (1.60)$$

where a negative value of K_1 results in minimal magnetocrystalline energies in the $\langle 111 \rangle$ family of directions.

The magnetic free energy due to the interaction of an applied stress with strains resulting from magnetic moment rotations is:

$$E_{\sigma'} = \Big\{-(2/3)\lambda_{100}\Big\{\sigma'_{11}\Big((\sin[\theta_m]\cos[\varphi_m])^2 - 1/3\Big) + \sigma'_{22}\Big((\sin[\theta_m]\sin[\varphi_m])^2 - 1/3\Big)$$

$$+\sigma_{33}^{'}(\cos^2[\theta_m]-1/3)\}-3\lambda_{111}\left\{\sigma_{12}^{'}(\sin[\theta_m]\cos[\varphi_m])(\sin[\theta_m]\sin[\varphi_m])\right.$$

$$\left.+\sigma_{23}^{'}(\sin[\theta_m]\sin[\varphi_m])\cos[\theta_m]+\sigma_{31}^{'}(\sin[\theta_m]\cos[\varphi_m])\cos[\theta_m]\right\}\Big\}, \qquad (1.61)$$

where λ_{100} and λ_{111} are the change in strain resulting from the rotation of a fully random magnetization state into a fully oriented $[100]$ or $[111]$ direction, respectively.

The total magnetic free energy is now the vector sum of the field, magnetocrystalline and magnetoelastic energies.

The magnetostriction λ in the direction of $[\theta_\lambda, \varphi_\lambda]$ is derived from the magnetic free energy in this direction as:

$$\lambda = \iint K \exp[-(E_{field}+E_{an}+E_{\sigma^{'}})/\omega]$$

$$\times\begin{Bmatrix} \frac{3}{2}\lambda_{100}C_{1122}-(\sin[\theta_m]\cos[\varphi_m])^2\frac{C_{1111}-C_{1122}}{C_{1111}+2C_{1122}} \\ \frac{3}{2}\lambda_{100}C_{1122}-(\sin[\theta_m]\sin[\varphi_m])^2\frac{C_{1111}-C_{1122}}{C_{1111}+2C_{1122}} \\ \frac{3}{2}\lambda_{100}C_{1122}-(\cos[\theta_m])^2\frac{C_{1111}-C_{1122}}{C_{1111}+2C_{1122}} \\ \frac{3}{2}\lambda_{111}(\sin[\theta_m]\cos[\theta_m])\sin[\theta_m]\sin[\varphi_m]) \\ \frac{3}{2}\lambda_{111}(\sin[\theta_m]\sin[\varphi_m])\cos[\theta_m] \\ \frac{3}{2}\lambda_{111}(\sin[\theta_m]\cos[\varphi_m])\cos[\theta_m] \end{Bmatrix}\sin[\theta_m]d\theta_m d\varphi_m, \qquad (1.62)$$

where K is a normalization factor evaluated at each applied field and stress condition, ω is the energy distribution parameter, the C_{ijkl} are the matrix elastic constants.

1.3.12 Nan *et al.*'s model for magnetoelectric effect of particulate composites

Nan *et al.* [Nan *et al.* 2001a; 2001b] suggested that the Terfenol-D-particle-filled P(VDF-TrFE) matrix composite may be a type of giant ME material due to the giant magnetostriction of Terfenol-D and large piezoelectric stress coefficients of the

P(VDF-TrFE) polymer. They derived the general solution to the ME effect of such magnetostrictive/piezoelectric composites by the Green's function technique.

The constitutive equations for a perfectly bonded Terfenol-D/P(VDF-TrFE) composite are:

$$\sigma = \mathrm{c}\varepsilon - \chi^T \mathrm{H}\mathrm{H}\,, \tag{1.63}$$

$$\mathrm{B} = \mu \mathrm{H} + \chi\varepsilon \mathrm{H}\,, \tag{1.64}$$

where σ, ε, B and H, are the stress tensor, strain tensor, magnetic induction, and magnetic field, respectively. c is the elastic stiffness, and χ is the magnetostrictive coefficient (χ^T is the transpose of χ). μ is the permeability.

The effective behavior of the inhomogeneous material is defined in terms of macroscopic average fields (denoted by $\langle\ \rangle$), namely,

$$\langle\sigma\rangle = \mathrm{c}^* \langle\varepsilon\rangle - \mathrm{e}^{T*} \langle\mathrm{E}\rangle - \mathrm{c}^* \varepsilon^{ms*}, \tag{1.65}$$

$$\langle\mathrm{D}\rangle = \mathrm{e}^* \langle\varepsilon\rangle + \kappa^* \langle\mathrm{E}\rangle + \alpha^* \langle\mathrm{H}\rangle, \tag{1.66}$$

where quantities with asterisks represent those of the composite, e is the piezoelectric coefficient tensor; κ and α denote the dielectric constant tensor at constant strain and the ME coefficient, respectively. ε^{ms} is the mangetostrictively induced strains.

They assume that the composite is subjected on its external surface S to the homogeneous mechanical-electric-magnetic boundary conditions:

$$u_i(S) = \varepsilon_{ij}^o x_j = u_i^o,\ \ \phi(S) = -E_i^o x_i = \phi^o,\ \ \psi(S) = -H_i^o x_i = \psi^o\,, \tag{1.67}$$

where u_i, ϕ, and ψ denote elastic displacement, electric potential, and magnetic potential respectively.

Consider a state of static equilibrium in the absence of body forces and free electric charges, the nonlinearly coupled equilibrium equations are:

$$\sigma_{ij,j}(x) = 0,\ \ D_{j,j}(x) = 0,\ \ B_{i,i}(x) = 0\,, \tag{1.68}$$

where the commas in the subscripts denote partial differentiation with respect to x_j.

The composite ME coefficient is obtained by solving the equilibrium equation (1.68) under the boundary conditions (1.67) by use of the Green's function technique:

$$\alpha^{*}\left\langle \mathrm{H}\right\rangle = f\ \mathrm{e}^{*}\left\langle \left[\mathrm{I}-\mathrm{G}^{u}(\mathrm{c}-\mathrm{c}^{o})\right]^{-1}\mathrm{G}^{u}\mathrm{c}\varepsilon^{ms}\right\rangle_{orient}, \tag{1.69}$$

$$\varepsilon^{ms*} = f(\mathrm{c}^{*})^{-1}\left\langle \left[(\mathrm{c}-\mathrm{c}^{*})\left[\mathrm{I}-\mathrm{G}^{u}(\mathrm{c}-\mathrm{c}^{o})\right]^{-1}\times\mathrm{G}^{u}+\mathrm{I}\right]\mathrm{c}\varepsilon^{ms}\right\rangle_{orient}, \tag{1.70}$$

where G^{u} is the modified displacement and, I is the unit tensor. f is the volume fraction. $\langle\ \rangle_{orient}$ denotes averaging over all possible orientations of the inclusion microcrystallites in the composite.

Although Nan's group has theoretically studied the magnetoelectric effect for 0-3 composites, they seldom directly compare with experimental observations. Their model has not taken the effect of conductivity into account, and hence cannot discuss the influence of the constituent's electrical conductivity on the ME effect.

Chapter 2 Effects of polarization and permittivity gradients and other parameters on polarization offset of graded ferroelectric thin films

2.1 Introduction

The "graded ferroelectrics" have attracted great research interest for many years because of its uncommon physical properties. The unconventional behavior presented by such heterogeneous ferroelectric systems is thought to arise from the polarization nonuniformity imposed by a composition, temperature or stress gradient [Schubring *et al.*, 1992; Alpay *et al.*, 2002; Mantese *et al.*, 2002]. One of the most notable phenomenon is the large polarization offset along the vertical axis found in the hysteresis loop measurements. Values as large as $420\mu C/cm^2$ were reported for the polarization offset in lead-zirconate-titanate (PZT) graded structures [Brazier *et al.*, 1998]. These offsets have been reported to have a strong temperature dependence giving rise to possible pyroelectric applications in addition to other potential sensor, actuator, and energy converter applications. On the other hand, recent results have shown the polarization offsets in graded PZT to be sensitive to the ambient oxygen concentration giving rise to possible oxygen sensor applications [Brazier *et al.*, 1999]. Theoretical models have played key roles in providing deeper insight, and different approaches have been proposed. The offset has been interpreted as a static polarization developed across the ferroelectric film under the

application of an alternating voltage. Recently it was suggested that very large offsets are unphysical and they have to be corrected with the ratio between the sample capacitance and that of the reference or loading capacitance. Another suggested origin of the polarization offset is the possible asymmetry in the leakage current which gives a sort of diode effect. Thus, although a number of distinct groups have reported on the anomalous hysteretic behavior of the graded ferroelectric structures, none of the suggested models can give a convenient explanation for the polarization offset occurrence.

On the other hand, it is widely reported that the offset magnitudes and directions are strongly dependent on the composition or temperature gradient. It is suggested that the polarization offsets are composition or temperature dependent through the polarization and dielectric constants of the graded materials [Pintilie *et al.*, 2003]. The offsets also display a dependence on the applied electric field. However, so far only very few experimental and theoretical investigations have been performed to study the interplay of the effects of ferroelectric, dielectric properties and other related parameters on the offset. We believe such investigations can furnish further insight into the mechanism.

In this chapter, we aim to gain a deeper understanding of the conditions under which sizeable polarization offset occurs by studying the various dependences of the polarization shift. We demonstrate that the vertical shift along the displacement axis is strongly dependent on the remanent polarization and permittivity gradients, charge mobilities and thickness in the graded ferroelectric thin film. Investigation on the

charge motions and the time development of charge offsets further supports our previous notion that electric conduction asymmetry accounts for the shift of the hysteresis loop along the polarization axis.

2.2 Theory

2.2.1 Landau-Khalatnikov kinetics of switching

The graded ferroelectric film is considered as a stacking of N thin layers, each of thickness $\Delta x = L/N$ where L is the film thickness. We take $x = 0$ at the interface between the ferroelectric film and top electrode so that the position of any layer inside the film is given by $x = i \cdot \Delta x$, where $1 \le i \le N$. The polarization and electric field at position x and time t are respectively denoted as $P(x,t)$ and $E(x,t)$, and are defined to be along the x direction. The dynamics of the dipoles is modeled by the Landau-Khalatnikov equation:

$$\gamma \frac{\partial P(x,t)}{\partial t} = -\alpha(x)P(x,t) - \beta(x)P(x,t)^3 + E(x,t) + \kappa(x)\frac{\partial^2 P(x,t)}{\partial x^2} \qquad (2.1)$$

where γ represents the viscosity that causes the delay in motion of dipole moments. $\alpha(x) < 0$ and $\beta(x) > 0$ are the corresponding Landau coefficients of the material at location x. The last term in Eq. (2.1) comes from energy associated with polarization gradients, where $\kappa(x)$ is the corresponding interaction coefficient between neighboring dipoles.

The kinetic equation above conforms to the equations used by a number of works, notedly [Baudry and Tournier, 2001; Baudry, 1999; Lo, 2003], which is obtained by minimizing the free energy of the film under applied electric field. It should be noted that $E(x,t)$ in Eq. (2.1) denotes the local electric field instead of external electric field. With this approach, the explicit consideration of the depolarization field is subsumed in the formulation. In particular, Baudry and Tournier [Baudry

and Tournier, 2001] has given an excellent discussion on this point, incorporating implications due to the presence of charge carriers and non-uniformity of polarization.

A more complete expression for Eq. (2.1) should include the corresponding terms from the elastic energy in the free energy of the system as is done in Ban *et al.*'s paper [Ban *et al.*, 2003]. However, for the case of composition graded film investigated in the present work, the contribution of the elastic energy is found to be quite insignificant by following a calculation based on the relevant equations derived in Ban *et al.*'s paper [Ban *et al.*, 2003]. Therefore we neglected the elastic energy term in this work for simplicity.

The variables in Eq. (2.1) are then normalized to dimensionless variables by the following relations:

$$\begin{aligned} &P^* = \frac{P}{P_S}, \qquad t^* = \frac{t}{\tau}, \qquad x^* = \frac{x}{\Delta x} \\ &\alpha^* = \frac{\tau\alpha}{\gamma}, \qquad \beta^* = \frac{\tau P_S^2 \beta}{\gamma}, \qquad E^* = \frac{\tau E}{\gamma P_S}, \qquad \kappa^* = \frac{\tau\kappa}{\gamma} \end{aligned} \tag{2.2}$$

where P_S is the spontaneous polarization of the ferroelectric thin film and τ is a characteristic relaxation time for the system. With normalized polarization and time parameters, Eq. (2.1) becomes

$$\begin{aligned} \frac{dP^*(x^*,t^*)}{dt^*} &= -\alpha^*(x^*)P^*(x^*,t^*) - \beta^*(x^*)P^*(x^*,t^*)^3 \\ &\quad + E^*(x^*,t^*) + \kappa^*(x^*)[(P^*(x^*+1,t^*) + P(x^*-1,t^*) - 2P^*(x^*,t^*)] \end{aligned} \tag{2.3}$$

2.2.2 Electric conduction

In general, if there are inhomogeneities inside the ferroelectric film, the electric displacement $D(x,t) = \varepsilon(x)E(x,t) + P(x,t)$ may not be spatially uniform.

According to Gauss' law, there should be the presence of free space charges and the corresponding effect on electrical conduction has to be taken into account. In our previous study of compositionally graded ferroelectric films [Chan *et al.*, 2004], we derived the following formula for the time-dependent conductivity associated with space charges and named it 'time-dependent space-charge-limited conduction' (TDSCL):

$$\sigma(x,t) = \frac{\mu_p - \mu_n}{2}\frac{\partial D(x,t)}{\partial x} + \sqrt{[\frac{\mu_p + \mu_n}{2}\frac{\partial D(x,t)}{\partial x}]^2 + \sigma_0(x)^2} \qquad (2.4)$$

$\sigma_0(x)$ is the intrinsic (Ohmic) conductivity; μ_p and μ_n are respectively the mobilities ($\mu_p, \mu_n > 0$) of p- and n- type free carriers, which we simply assume to be spatially invariant. Versus the Ohmic conductivity $\sigma_0(x)$ which can be spatially dependent, the above $\sigma(x,t)$ expression contains a time-dependent $\partial D(x,t)/\partial x$ quantity, thus $\sigma(x,t)$ is a "time-dependent" conductivity. Eq. (2.4) was derived by borrowing the law of mass action from semiconductor physics [Chan *et al.*, 2004]; we will here give further justification to the application of this law for ferroelectric materials that are more or less insulators. We will also illustrate that Eq. (2.4) is reducible to the well-known Mott's equation for steady-state (time-independent) space-charge-limited conduction ($J \sim V^2$), which is derived for linear dielectrics with a single carrier type [Coelho, 1979]. Eq. (2.4) is therefore a more general formula for conduction involving space charges. For detailed derivation of Eq. (2.4), please refer to section II of the original paper [Chan *et al.*, 2004].

The law of mass action in semiconductor physics states that the product of the concentrations of p- and n- type carriers is a constant. It is derived from (a) the

equilibrium Fermi distribution of carriers in the absence of electric field, as well as (b) the assumption that the distance of each band edge from the Fermi level is much larger than $k_B T$, where k_B is the Boltzmann constant and T the temperature [Hook and Hall, 1974]. In the strictest sense, this law should not be applied in the presence of an electric field because the carriers no longer obey the Fermi distribution function. In our case, the justifications for applying this law lie on the facts that (a) ferroelectric materials are essentially insulators and that (b) the frequency of the applied voltage is not very high (about $1\ kHz$). An insulator can be regarded as a wide-band-gap semiconductor and we may assume that the band gap is wide enough so that the distance of each band edge from the Fermi level is much larger than $k_B T$. Because it is an insulator, we may also assume that the system only undergoes a very small and negligible deviation from the equilibrium Fermi distribution. Furthermore, since the frequency of the applied voltage is not very high, any non-steady-state effect resulting from the time variation of electric field may be ignored.

To illustrate how Eq. (2.4) can be reduced to Mott's equation $J \sim V^2$, we recall that Eq. (2.4) was derived from the following definition of conductivity [Chan *et al.*, 2004]:

$$\sigma(x,t) = q\mu_n\left[C_{in}(x) + \Delta n(x,t)\right] + q\mu_p\left[C_{in}(x) + \Delta p(x,t)\right] \tag{2.5}$$

with the intrinsic (Ohmic) conductivity given by

$$\sigma_0(x) = q \cdot [\mu_n + \mu_p] \cdot C_{in}(x) \tag{2.6}$$

For $\sigma_0(x) \to 0$ but $\sigma(x,t)$ being non-zero, we must have $C_{in}(x) \to 0$ and at least either μ_n or μ_p remaining finite. Since the carrier concentrations

$\left[C_{in}(x)+\Delta n(x,t)\right]$ and $\left[C_{in}(x)+\Delta p(x,t)\right]$ are non-negative, for $C_{in}(x)\to 0$ we must have $\Delta n(x,t)\geq 0$ and $\Delta p(x,t)\geq 0$, as well as respectively equal to the n- and p-type carrier concentrations. Because $C_{in}(x)\to 0$, Eqs. (8) and (9) of the original paper [Chan *et al.*, 2004] are reduced to

$$\Delta n(x,t)^2+\Delta n(x,t)\left[\frac{1}{q}\frac{\partial D(x,t)}{\partial x}\right]\approx 0 \tag{2.7}$$

$$\Delta p(x,t)^2+\Delta p(x,t)\left[-\frac{1}{q}\frac{\partial D(x,t)}{\partial x}\right]\approx 0 \tag{2.8}$$

so that

$$\Delta n(x,t)\approx 0 \quad \text{or} \quad \Delta n(x,t)\approx -\frac{1}{q}\frac{\partial D(x,t)}{\partial x} \tag{2.9}$$

$$\Delta p(x,t)\approx 0 \quad \text{or} \quad \Delta p(x,t)\approx \frac{1}{q}\frac{\partial D(x,t)}{\partial x} \tag{2.10}$$

The definition of space charge reads

$$\frac{\partial D(x,t)}{\partial x}=q\left[\Delta p(x,t)-\Delta n(x,t)\right] \tag{2.11}$$

From Eqs. (2.9), (2.10) and (2.11), it can be seen that only the following combinations of solutions are allowed:

$$\Delta n(x,t)\approx -\frac{1}{q}\frac{\partial D(x,t)}{\partial x} \quad \text{and} \quad \Delta p(x,t)\approx 0 \tag{2.12}$$

$$\Delta p(x,t)\approx \frac{1}{q}\frac{\partial D(x,t)}{\partial x} \quad \text{and} \quad \Delta n(x,t)\approx 0 \tag{2.13}$$

Thus, in the limit of zero intrinsic conductivity, we can only have the presence of predominantly either carrier type. The p- and n-type carriers are mutually exclusive and it automatically reduces to a single-carrier condition. Since both $\Delta n(x,t)$ and $\Delta p(x,t)$ are non-negative, it can be seen from Eqs. (2.12) and (2.13)

that $\partial D(x,t)/\partial x > 0$ necessarily implies the presence of only p-type carriers and $\partial D(x,t)/\partial x < 0$ the presence of only n-type carriers.

In the limit $\sigma_0(x) \to 0$, Eq. (2.4) becomes:

$$\sigma(x,t) \approx \frac{\mu_p - \mu_n}{2}\frac{\partial D(x,t)}{\partial x} + \frac{\mu_p + \mu_n}{2}\left|\frac{\partial D(x,t)}{\partial x}\right| \tag{2.14}$$

If $\partial D(x,t)/\partial x > 0$, it is

$$\sigma(x,t) \approx \frac{\mu_p - \mu_n}{2}\frac{\partial D(x,t)}{\partial x} + \frac{\mu_p + \mu_n}{2}\frac{\partial D(x,t)}{\partial x} = \mu_p \frac{\partial D(x,t)}{\partial x} \tag{2.15}$$

And if $\partial D(x,t)/\partial x < 0$, it is

$$\sigma(x,t) \approx \frac{\mu_p - \mu_n}{2}\frac{\partial D(x,t)}{\partial x} - \frac{\mu_p + \mu_n}{2}\frac{\partial D(x,t)}{\partial x} = -\mu_n \frac{\partial D(x,t)}{\partial x} \tag{2.16}$$

which are the original conditions from which Mott's result $J \sim V^2$ is derived, if we remove their time dependence [Coelho, 1979]. It should be noted that, in the derivation of Eqs. (2.15) and (2.16), the mobility of the absent carrier type automatically disappears, hence need not be deliberately suppressed. This puts our previous suggestion in section II of ref. [Chan *et al.*, 2004] in a more general context.

The total current $J(t)$ across the circuit is constitutive of the conduction and displacement currents:

$$J(t) = j_c(x,t) + j_d(x,t) = \sigma(x,t)E(x,t) + \frac{\partial}{\partial t}D(x,t) \tag{2.17}$$

where subscripts c and d denote the conduction and displacement currents, respectively. The circuit condition is given by:

$$\int_0^L E(x,t)dx = V_o(t) \tag{2.18}$$

where L is film thickness and $V_o(t) = V_{amp} sin(\omega t)$ is the applied sinusoidal voltage.

The measured charge density (accumulated on an ideal reference capacitor in a Sawyer-Tower circuit or by use of the charge integration technique) at a certain time t_0 is given by the integration of total current density across the film:

$$Q(t_0) = \int_0^{t_0} J(t)dt \tag{2.19}$$

The above variables are converted into dimensionless variables in the simulation by Eq. (2.2) together with the following relations:

$$\begin{aligned} &D^* = \frac{D}{P_S}, \quad \varepsilon^* = \frac{\gamma\varepsilon}{\tau}, \qquad j^* = \frac{\tau j}{P_S}, \qquad \mathrm{V}^* = \frac{\tau V}{\gamma \Delta x P_S} \\ &\sigma^* = \gamma\sigma, \quad \mu_p{}^* = \frac{P_S \gamma \mu_p}{2\Delta x}, \quad \mu_n{}^* = \frac{P_S \gamma \mu_n}{2\Delta x}, \quad Q^* = \frac{Q}{P_S} \end{aligned} \tag{2.20}$$

Eqs. (2.4) and (2.17) become

$$\sigma^*(x^*,t^*) = (\mu_p^* - \mu_n^*)\frac{\partial D^*(x^*,t^*)}{\partial x^*} + \sqrt{[(\mu_p^* + \mu_n^*)\frac{\partial D^*(x^*,t^*)}{\partial x^*}]^2 + \sigma_0{}^*(x^*)^2} \tag{2.21}$$

$$J^*(t^*) = j_c^*(x^*,t^*) + j_d^*(x^*,t^*) = \sigma^*(x^*,t^*)E^*(x^*,t^*) + \frac{\partial}{\partial t^*}D^*(x^*,t^*) \tag{2.22}$$

Also the form of Eqs. (2.18) and (2.19) does not change if written in terms of the dimensionless variables.

We have chosen the following values of the parameters: $f^* = 0.02$ and $E_{amp}^* = 1.5$ (which e.g. correspond to $f = 1\ kHz$ and $E_{amp} = 150\ kV/cm$ for graded PZT thin film) for the calculations, where $E_{amp}^* = \frac{V_{amp}^*}{L^*}$ is the normalized applied electric field amplitude, while $L^* = \frac{L}{\Delta x}$ is the normalized film thickness. Unless stated otherwise, these values have been retained for obtaining all of the results presented in this chapter. Also, it is found through calculation that the effects of $\kappa(x)$ on the results are quite limited. Hence we have neglected $\kappa(x)$ in the

simulation. All the modeled results are picked from the application time to the sixth cycle of the external ac field to examine the shift effect.

2.3 Results and discussion

The purpose of this chapter is to gain a deeper understanding of the conditions under which large polarization offset occurs or otherwise. The selection of parameters in fitting a particular experiment is based on the relations in Eqs. (2.2) and (2.20). The parameters used in our modeling are listed in Table 2.1, where ε_0 is the permittivity of vacuum. Due to the highly nonlinear nature of the equations, numerical calculation has to be employed. In the calculation, the corresponding smallest Δx should not be too small (not smaller than the characteristic length scale of the material, which is of the order of several nm) so that the Landau continuum theory could still be applied.

TABLE 2.1 The dimensionless parameters used in our calculations.

Fig.	P_r^*	E_c^*	$\varepsilon^*/\varepsilon_0$ (10^{-2})	σ_0^* (10^{-4})	L^*	μ_p^* (10^{-3})	μ_n^*
1	$0.3+0.04x$	0.2	$2.6+0.033x$	1	30	0.01	0.1
2(a)	$0.3+0.04x$	0.3	$2.6+0.033x$	2	30	0.01	0.1
2(b)	$1.5-0.04x$	0.3	$3.6-0.033x$	2	30	0.01	0.1
2(c)	$0.3+0.04x$	0.3	$3.6-0.7x+0.0222x^2$	2	30	0.01	0.1
2(d)	$1.5-0.04x$	0.3	$2.6-1.3x+0.0444x^2$	2	30	0.01	0.1
3(a)	$0.3+0.04x$	0.3	$2.6+0.033x$	2	30	0.01	0.5
3(b)	$0.3+0.04x$	0.3	$2.6+0.033x$	2	30	0.01	0.01
4(a)	$0.3+0.04x$	0.3	$2.6+0.033x$	2	20	0.01	0.1
4(b)	$0.3+0.04x$	0.3	$2.6+0.033x$	2	100	0.01	0.1
5	$0.3+0.04x$	0.3	$2.6+0.033x$	2	30	0.01	0.1

2.3.1 Effect of polarization and permittivity gradients

The anomalous vertical offset of hysteresis loops are usually observed in graded ferroelectric films (e.g., temperature or compositionally graded). For these kinds of materials, the ferroelectric, dielectric and electric properties may vary across the thickness due to the composition gradient or to any other stimulus (temperature, mechanical stress, etc.). Investigation of the critical variables which have to be graded to lead to the offsets can help to understand the rather complicated anomalous shift mechanism. Fig. 2.1 shows the downward shifting loops when only P_r^* and ε^* are linearly increasing across the film thickness direction. Our simulations show that the remanent polarization and permittivity gradients are already sufficient to demonstrate the shift phenomenon. Fig. 2.2 (*a*) is obtained with the same P_r^* and ε^* gradients but different E_c^* and σ_0^* as in Fig. 2.1. Further, it is found that E_c^* and σ_0^* gradients (e.g. we have tried 0.1-2 for both E_c^* and σ_0^* gradients) do not impose any significant effects on the final results. It is also found that only graded either in ε^* or P_r^* is not sufficient to lead to the vertical offset.

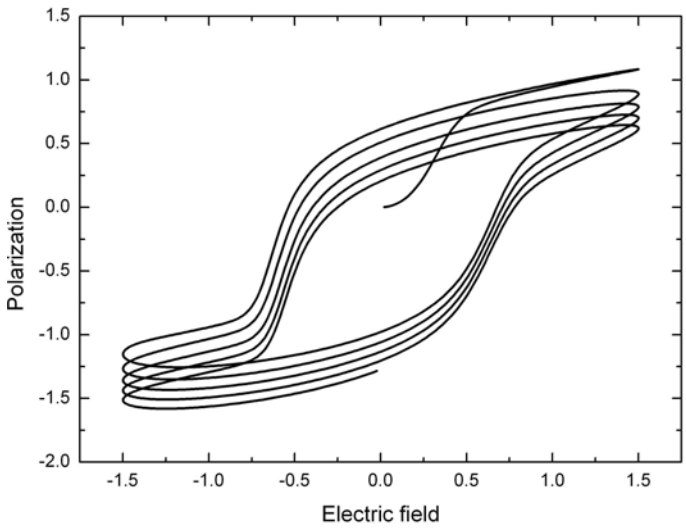

FIG. 2.1 The shifting of hysteresis loops when only P_r^* and ε^* are linearly increasing with x^*.

Since we have numerically validated that E_c^* and σ_0^* gradients do not lead to nor sensitively affect offsets, we therefore assume E_c^* and σ_0^* to be constant in the following calculations for simplicity. On inverting the P_r^* and ε^* gradient directions (decreasing with x^*), it is found that the vertical shifting is in the upward direction as shown in Fig. 2.2 (*b*). The vertical shifting effect will become more notable for larger gradients of P_r^* and ε^*. Interestingly, we have tried several different values (i.e., $P_r^* = 0.3 + 0.04x$, $\varepsilon^* / \varepsilon_0 = 0.036 - 0.00033x$; $P_r^* = 1.5 - 0.04x$, $\varepsilon^* / \varepsilon_0 = 0.026 + 0.00033x$; $P_r^* = 2 - 0.03x$, $\varepsilon^* / \varepsilon_0 = 0.038 + 0.0004x$) for the uniform gradients of remanent polarization and permittivity and it is found there is no shifting effect at all if the gradients are in opposite directions. The loops will only display a vertical shift with nonlinear permittivity variation across the thickness direction for this opposing gradients case. Here we used a simple quadratic function to describe the permittivity profile (Table 2.1). Fig. 2.2 (*c*) shows the downward shifting loops with linearly increasing P_r^* but nonlinearly decreasing ε^* along film thickness direction. Similarly, the simulated upward shifting hysteresis loops shown in Fig. 2.2 (d) are calculated with linearly decreasing P_r^* but nonlinearly increasing ε^* along film thickness direction. From the above simulation results, we can see that the shifting direction is mostly determined by the gradient direction of P_r^*. The polarization offset is positive (negative) with negative (positive) P_r^* gradient. This point is validated by experimental results reported in the literature [Brazier *et al.*, 1998; Bao *et al.*, 2001; Bouregba *et al.*, 2003].

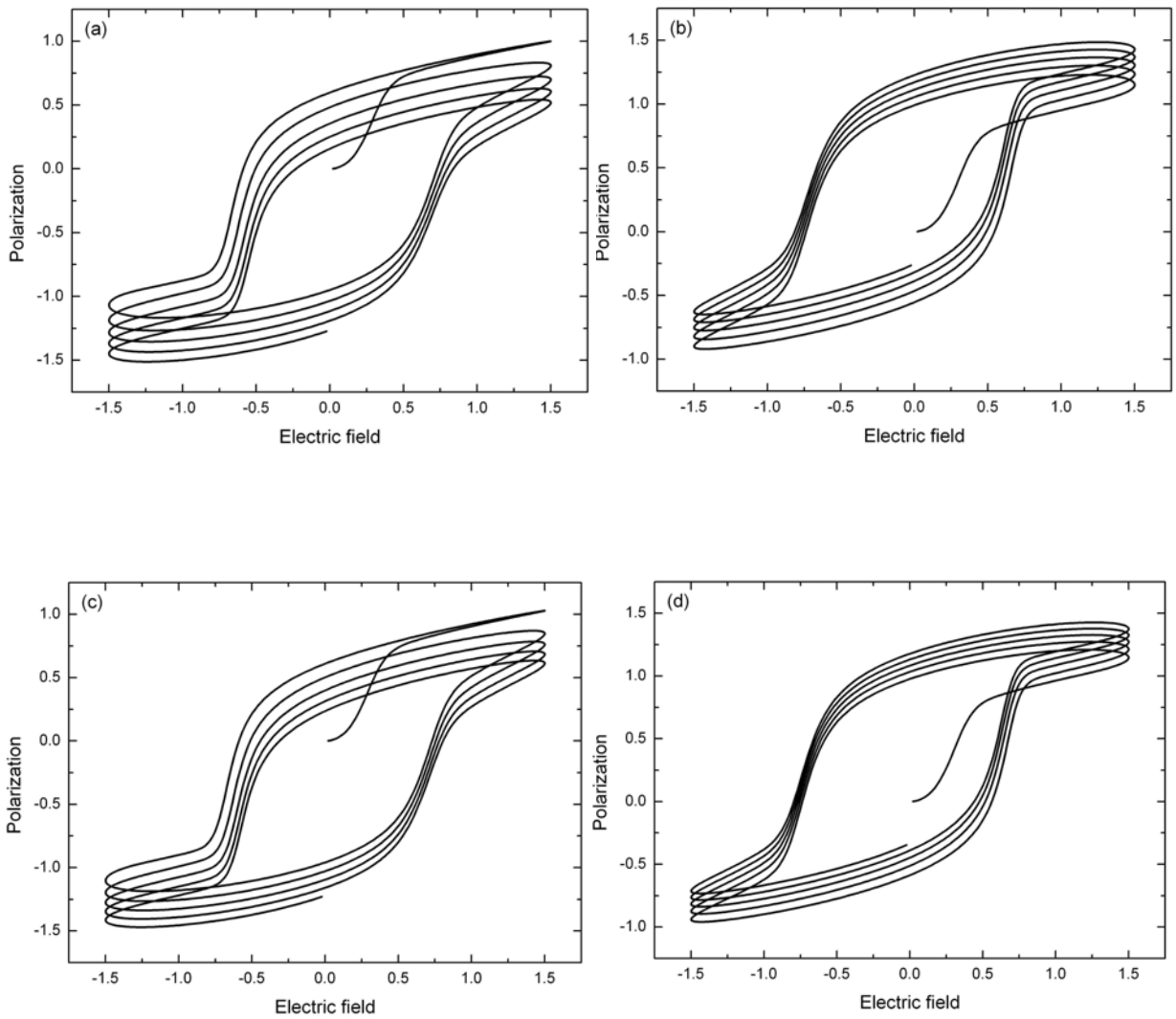

FIG. 2.2 The shifting of hysteresis loops: (*a*) with linearly increasing P_r^* and ε^* gradients; (*b*) with linearly decreasing P_r^* and ε^* gradients; (*c*) with linearly increasing P_r^* gradient but nonlinearly decreasing ε^* gradient; (*d*) with linearly decreasing P_r^* gradient but nonlinearly increasing ε^* gradient along film thickness direction.

2.3.2 Effect of charge carrier mobilities and film thickness

The phenomena of asymmetric leakage current have been observed in many thin film materials, and it has been theoretically demonstrated that space charges are likely responsible for the occurrence of polarization offsets in graded ferroelectrics. The

purpose of this section is to investigate the effects of free charge carrier mobilities and film thickness on the anomalous hysteretic behavior in graded thin films. In this calculation, the remanent polarization and permittivity are assumed linearly varying with x in the same direction. Figs. 2.3 (*a*) and (*b*) show the simulated hysteresis loops by adopting different negative charge carrier mobilities. As μ_n^* decreases, the vertical "shift" decreases. It is interesting to note that the modeled hysteresis loop is very symmetrical and centered at the origin of the axes when the mobility is small enough (e.g. $\mu_n^* = 0.01$). It is also found that when μ_p^* is smaller than μ_n^* by an order, an almost maximum vertical "shift" is observed. Any further reduction in μ_p^* will have little effect in the vertical shift. When the values for μ_p^* and μ_n^* are interchanged, the hysteresis loop shifts to the opposite direction with an almost unchanged shift magnitude after a certain number of cycles.

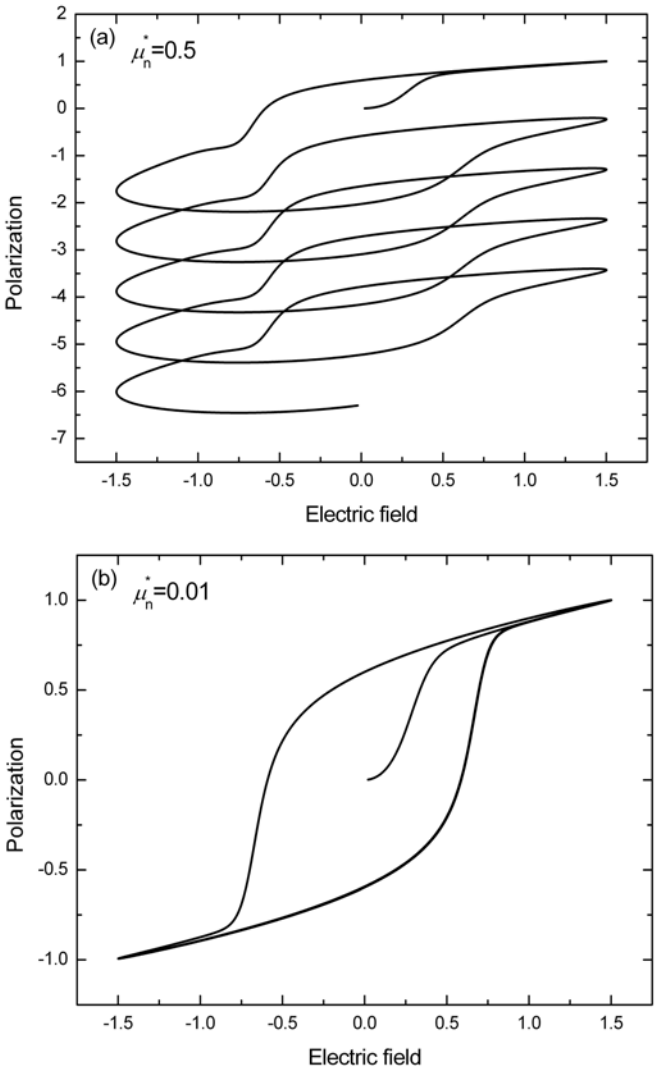

FIG. 2.3 The simulated hysteresis loops: (*a*) when $\mu_n^* = 0.5$; (*b*) when $\mu_n^* = 0.01$.

Fig. 2.4 shows the effect of film thickness on the hysteresis loops. As the thickness increases, the vertical "shift" decreases. There is almost no vertical shift when the film is thick enough (e.g. $L^* = 100$). In fact, it is found that there will be notable polarization offset only when the thickness lies between 10 *nm* to 3 μm by modeling the compositionally graded PZT thin film. This is also the range of experimental measurements where notable vertical shifts of hysteresis loop are

reported in the literature [Brazier *et al.*, 1998; Bao *et al.*, 2001; Bouregba et al., 2003; Brazier *et al.*, 1999].

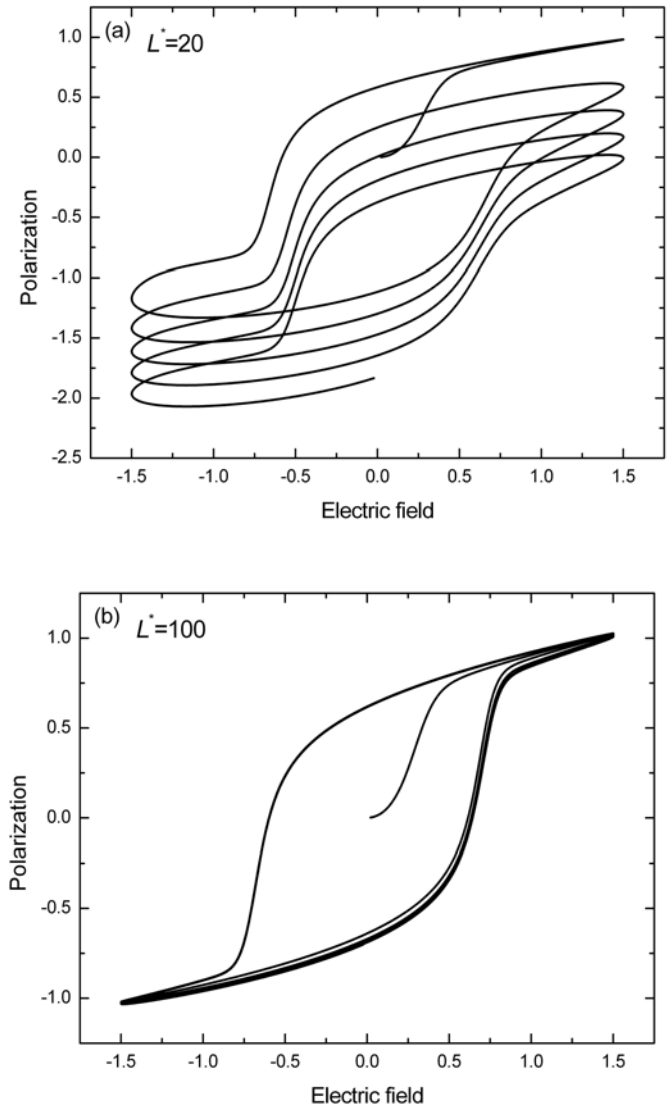

FIG. 2.4 Effect of thickness of ferroelectric thin film on the simulated hysteresis loops: (*a*) when $L^* = 20$; (*b*) when $L^* = 100$.

In our previous study of compositionally graded ferroelectric films, we have already demonstrated that polarization gradient across a ferroelectric film can lead to asymmetric conduction, which we believe provides a mechanism for the polarization

offset phenomenon. Now it is worth further examining the asymmetric conduction current. From Eqs. (2.17) and (2.19), we can see that the charge offset $Q^*(t^*)$ should come from either or both of the two parts: one is the conduction current induced charge accumulation $Q_c^*(x^*,t^*)=\int_0^{t^*} j_c^*(x^*,t^*)dt^*$; the other is the displacement current induced charge accumulation $Q_d^*(x^*,t^*)=\int_0^{t^*} j_d^*(x^*,t^*)dt^*$. Fig. 2.5 shows the time development of Q_c^*, Q_d^* and total Q^*. From the figure, it is evident that the displacement current accumulated charge Q_d^* repeats itself quite well in successive field cycles while the conduction current induced charge Q_c^* develops to larger negative values with time. It is therefore obvious that the charge offset come mostly from the conduction current induced charge accumulation Q_c^*. Hence the simulation results confirm our previous notion that the asymmetric electric conduction mechanism is a major contributor to the polarization offsets observed in experiments.

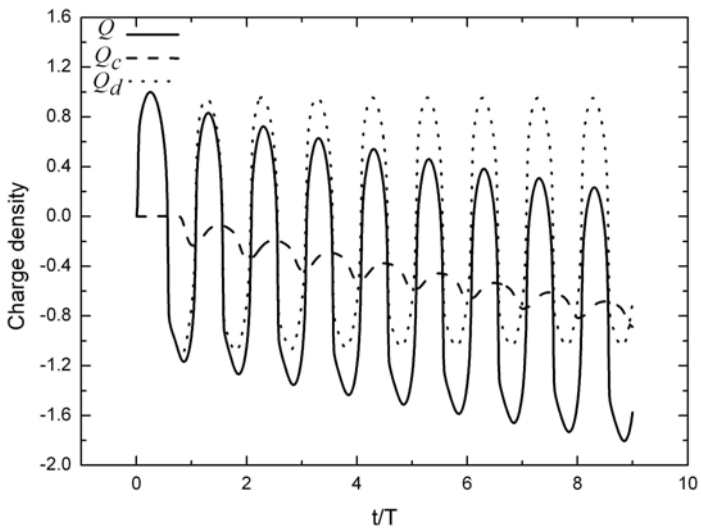

FIG. 2.5 Time development of charge densities induced by conduction current, displacement and total currents.

Chapter 3 Mechanisms of imprint effect in ferroelectric thin films

3.1 Introduction

In the previous chapter, we have discussed the effects of polarization and permittivity gradients and other parameters on polarization offset of compositionally graded ferroelectric thin films. On the other hand, even in non-graded ferroelectric (FE) thin films, some abnormal phenomena or failures, such as fatigue and imprint have been widely observed. It is important to understand the physical mechanisms behind these phenomena, in order to further advance ferroelectric materials into the memory market and provide a carefully directed improvement of these materials. Currently, three major failure mechanisms are believed to be limiting the lifetime of ferroelectric memory devices (FMD): fatigue, retention loss, and imprint. In this chapter, we aim to provide a better understanding of the physical origin of imprint, which is commonly believed to be a result of some kind of asymmetric polarization behaviour due to the preference of a certain polarization state over the other in ferroelectric bistable states and eventually leads to a failure when retrieving stored data [Nagasawa *et al.*, 1999; Liu *et al.*, 2001; Dey *et al.*, 1995; Robels *et al.*, 1995; Abe *et al.*, 2002]. The imprint effect manifests itself in a horizontal shift of the measured hysteresis loops. Because of its influence in data storage, various efforts have been made to understand the origin of imprint.

Warren *et al.* [Warren *et al.* 1996] attributed the occurrence of imprint to defect

dipoles related to oxygen vacancies. Abe *et al.* assumed a non-switching layer between the ferroelectric layer and bottom electrode, which is possibly formed by relaxation of lattice misfit strain in the heteroepitaxial ferroelectric thin film [Abe *et al.*, 2002; Abe *et al.*, 1997; Abe *et al.*, 1995]. Other explanations include domain pinning [Nagasawa *et al.*, 1999; Liu *et al.*, 2002] and presence of surface layers [Robels *et al.*, 1995; Abe *et al.*, 2002; Lü *et al.*, 2003]. However, all these mechanisms suggested have not been fully examined by accurate physical models or simulations, and there has not been a general agreement on a definitive mechanism for imprint. On the other hand, asymmetric polarization switching (different up- and down-switching processes) has also been investigated, for it is believed to be a likely origin of imprint. Wang *et al.* [Wang *et al.*, 1999] phenomenologically modeled the asymmetric behavior of polarization switching by including an odd-power term in the expression of Landau free energy. However, the physical origin of such asymmetry in polarization switching has yet not been identified. Hong *et al.* used a high resolution AFM to investigate the domain nucleation and growth during polarization switching in sol–gel prepared PZT thin films, and revealed that the forward domain growth is the rate limiting mechanism [Hong *et al.*, 1999]. Baudry used a lattice model to simulate the shifting of hysteresis loops and took into account the effects of non-uniform space charge by introducing a doping layer in the ferroelectric film near the electrode [Baudry and Tournier, 2001]. Lee *et al.* modeled shifted hysteresis loops by considering asymmetric electrode materials [Lee *et al.*, 2002]. Lo and Chen demonstrated that effects of space charge and Schottky barrier heights in

electrode materials could be the origin of horizontal shifting of measured hysteresis loops [Lo and Chen, 2002]. Recently, Lü and Cao introduced asymmetric surface layers to represent the case of one easy polarization direction; the modeled asymmetry in the hysteresis loop is due to the presence of non-screened depolarization field [Lü and Cao, 2003]. However, almost all the modeled hysteresis loops mentioned above did not shift as much as those observed in experiments.

We have developed a model in which the polarizations near the bottom electrode are much harder to reverse than the others under the applied alternating voltage, which leads to horizontal shifting of measured D-E loops. Warren *et al.* have already demonstrated that ionic defects, such as oxygen vacancies produced by reducing treatment, are responsible for ferroelectric domain pinning and formation of non-switching layers, which shifts the hysteresis loops horizontally [Warren *et al.*, 1996]. We propose that non-switching layers may be formed by lattice misfit stress or by electronic charge trapping at domain boundaries, leading to the occurrence of imprint. By treating some layers near the bottom electrode as graded surface layers induced by some degradation mechanisms, our simulation successfully reproduced the large horizontal shifting of hysteresis loops observed in experiments. Our results demonstrate clearly that irreversible layers near the electrode induced by stress or by trapped defects are likely to be the origin of imprint failure. In general, our model shows a good agreement with experimental results in the literature.

3.2 Theoretical considerations and numerical calculation

3.2.1 Review of the Landau model for switching

A ferroelectric film, placed in a Sawyer-Tower circuit [Sawyer and Tower, 1935], is modeled as a stacking of N thin layers; each layer has a thickness $\Delta x = L / N$ where L is the film thickness. We take $x = 0$ at the interface between the ferroelectric film and top electrode (Fig. 3.1) so that the position of any layer inside the film is given by $x = i \cdot \Delta x$, where $1 \le i \le N$. The polarization and electric field at position x and time t are respectively denoted as $P(x,t)$ and $E(x,t)$, and are defined to be along the positive x direction.

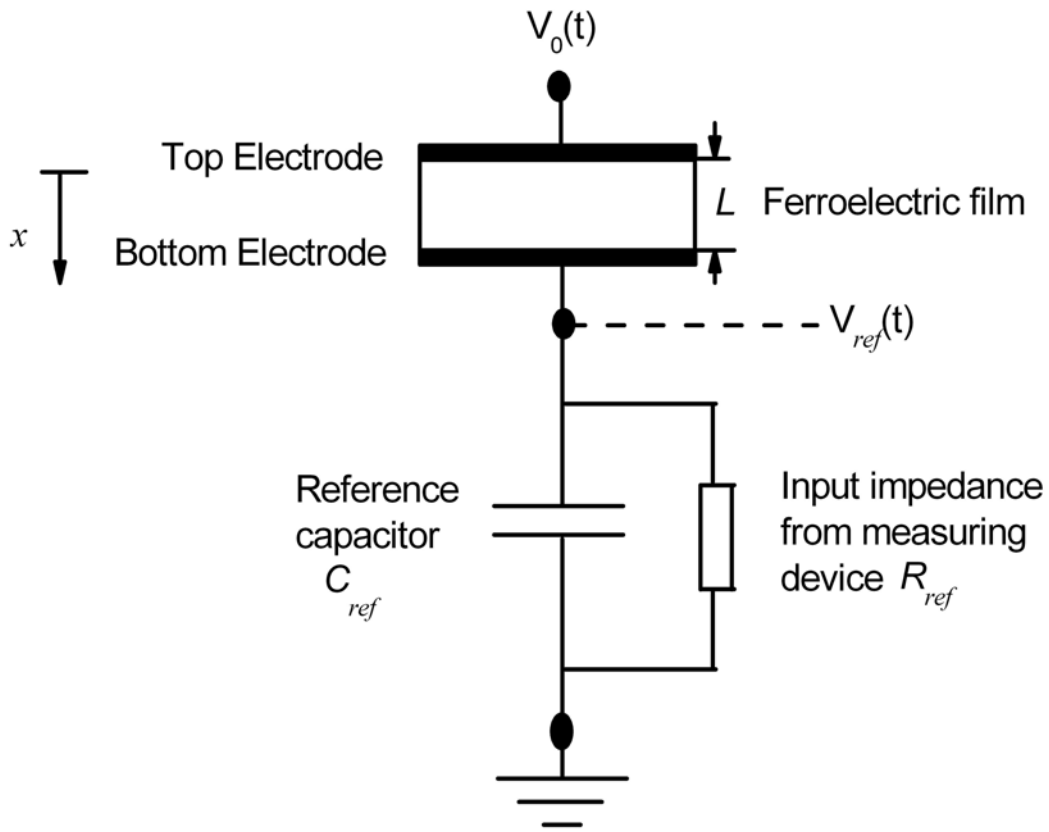

FIG. 3.1 Schematic diagram of the Sawyer–Tower circuit.

The dynamics of dipoles is modeled using the Landau–Khalatnikov kinetic equation, which is a phenomenological equation of motion:

$$\gamma \frac{\partial P(x,t)}{\partial t} = -\frac{\partial F(t)}{\partial P(x,t)} = -\alpha(x)P(x,t) - \beta(x)P(x,t)^3 + E(x,t)$$

$$+ \kappa(x)\left[P(x+\Delta x,t) + P(x-\Delta x,t) - 2P(x,t)\right] \qquad (3.1)$$

where $\alpha(x) < 0$ and $\beta(x) > 0$ are the corresponding Landau coefficients at x. $\alpha(x)$ is temperature dependent: $\alpha(x) = a(x)(T - T_c)$, where $a(x)$ is a positive constant and the temperature T is smaller than the Curie temperature T_c. $\kappa(x)$ is the corresponding interaction coefficient between neighboring atoms. According to Landau's theory, the remanent polarization $P_r(x)$ and coercive field $E_c(x)$ are related to $\alpha(x)$ and $\beta(x)$ as

$$P_r(x) = \sqrt{-\frac{\alpha(x)}{\beta(x)}} \qquad (3.2)$$

$$E_c(x) = -\frac{2\alpha(x)}{3\sqrt{3}}\sqrt{-\frac{\alpha(x)}{\beta(x)}} \qquad (3.3)$$

The coefficient γ represents the viscosity that causes the delay in motion of individual dipole moments.

3.2.2 Time-dependent space-charge-limited conduction

In our previous study of compositionally graded ferroelectric films [Chan *et al.*, 2004], we derived the following formula for the time-dependent conductivity associated with space charges and named it 'time-dependent space-charge-limited conduction' (TDSCL):

$$\sigma(x,t)=\frac{\mu_p-\mu_n}{2}\frac{\partial D(x,t)}{\partial x}+\sqrt{[\frac{\mu_p+\mu_n}{2}\frac{\partial D(x,t)}{\partial x}]^2+\sigma_0(x)^2} \tag{3.4}$$

where $D(x,t)=\varepsilon(x)E(x,t)+P(x,t)$ is the electric displacement at position *x*, $\sigma_0(x)$ is the intrinsic conductivity, μ_p and $-\mu_n$ (μ_p, $\mu_n>0$) are the positive and negative charge carrier mobilities, respectively. Here we also employ the same conduction mechanism as described in Chan *et al.*'s paper [Chan *et al.*, 2004].

3.2.3 Method of numerical simulation

In real hysteresis-loop measurement, the voltage $V_{ref}(t)$ of the reference capacitor is recorded against the average electric field $E_{ave}(t)=$ $[V_o(t)-V_{ref}(t)]/L$ of the ferroelectric film (Fig. 3.1). The conservation of charge gives the continuity of the total current $J(t)$ across the circuit:

$$J(t)=\sigma(x,t)E(x,t)+\frac{\partial D(x,t)}{\partial t}=\frac{V_{ref}(t)}{R_{ref}A_{ferro}}+\frac{C_{ref}}{A_{ferro}}\frac{dV_{ref}(t)}{dt} \tag{3.5}$$

with the electric displacement $D(x,t)=\varepsilon(x)E(x,t)+P(x,t)$ and the time-dependent conductivity given by Eq. (3.4). $\varepsilon(x)$ and A_{ferro} are respectively the dielectric permittivity and cross-sectional area of the ferroelectric film. C_{ref} and R_{ref} are respectively the capacitance of the reference capacitor and the input impedance of the measuring device. The conservation of energy gives the vanishing of voltage sum across the circuit:

$$\int_0^L E(x,t)dx+V_{ref}(t)-V_o(t)=0 \tag{3.6}$$

The initial conditions at time $t=0$ are $P(x,0)=0$, $E(x,0)=0$, and correspondingly from Eq. (3.1), the derivative $[\partial P(x,t)/\partial t]_{t=0}=0$ for all x inside

the film. Having a sinusoidal applied voltage $V_o(t) = V_{o\max}\sin(\omega t)$ such that $V_0(0) = 0$, it follows from Eq. (3.6) that the initial voltage $V_{ref}(0)$ must also be zero. With all the above initial conditions specified, the values of every quantity at subsequent time steps can be computed by the forward-Euler method.

The derivatives $\partial E(x,t)/\partial t$ and $dV_{ref}(t)/dt$ at time t can be determined from the following equations, which follow directly from Eqs. (3.5) and (3.6):

$$\frac{\partial E(x,t)}{\partial t} = \frac{\dfrac{V_{ref}(t)}{R_{ref}A_{ferro}} + \dfrac{C_{ref}}{A_{ferro}}\dfrac{dV_{ref}(t)}{dt} - J_c(x,t) - \dfrac{\partial P(x,t)}{\partial t}}{\varepsilon(x)} \tag{3.7}$$

$$\frac{dV_{ref}(t)}{dt} = \frac{\dfrac{dV_o(t)}{dt} + \displaystyle\int_0^L \frac{J_c(x,t) + \dfrac{\partial P(x,t)}{\partial t}}{\varepsilon(x)}dx - \dfrac{\displaystyle\int_0^L \frac{1}{\varepsilon(x)}dx}{R_{ref}A_{ferro}}V_{ref}}{\dfrac{C_{ref}}{A_{ferro}}\displaystyle\int_0^L \frac{1}{\varepsilon(x)}dx + 1} \tag{3.8}$$

so that the electric field and capacitor voltage at a later time $t + dt$ can be determined:

$$E(x,t+dt) = E(x,t) + \frac{\partial E(x,t)}{\partial t}dt \tag{3.9}$$

$$V_{ref}(t+dt) = V_{ref}(t) + \frac{dV_{ref}(t)}{dt}dt \tag{3.10}$$

By determining $\partial P(x,t)/\partial t$ from $E(x,t)$ and $P(x,t)$ using Eq. (3.1) (Landau-Khalatnikov), the polarization at $t + dt$ can also be determined:

$$P(x,t+dt) = P(x,t) + \frac{\partial P(x,t)}{\partial t}dt \tag{3.11}$$

The foregoing formulation is employed in the investigation of the imprint effect discussed earlier. Except especially defined, the values of the parameters which we use in the calculation are listed as follows:

$\mu_p = 0.25\times10^{-8}\ \ cm^2V^{-1}s^{-1}$, $\mu_n = 0.25\times10^{-5}\ \ cm^2V^{-1}s^{-1}$, $C_{ref} = 2.2\times10^{-8}\ \ F$, $A_{ferro} = 6.25\times10^{-8}\ \ m^2$, $R_{ref} = 10^2\ \ M\Omega$, $\kappa = 1\ \ kV.cm/\mu C$, $N = 200$, $dt = 10^{-9}\ \ s$, $\gamma = 1.0\ \ kVms.cm^4/\mu C$, $f = \omega/2\pi = 1\ kHz$, $L = 800\ \ nm$.

Also, except especially emphasized, all the simulated loops shown in this chapter have already reached their steady states.

3.3 Results and discussion

Stress, oxygen-vancancy-induced domain pinning, and film-electrode surface layers characterized by degradation of film properties have been suggested as possible origins of the imprint [Nagasawa *et al.*, 1999; Liu *et al*, 2001; Robels *et al.*, 1995; Abe *et al.*, 2002; Abe *et al.*, 1997; Abe and Komatsu, 1995; Lü and Cao, 2003], and therefore have become the subject of our present investigation. Table 3.1 shows all the adopted values for the properties of the bulk and surface layers, as well as the applied field parameters, for our calculation in each figure.

TABLE 3.1 The properties of the ferroelectric thin film and some related parameters used in our calculations.

Fig.	P_{rf} (μC cm^{-2})	E_{cf} (kV cm^{-1})	$\varepsilon_f / \varepsilon_0$	σ_{of} (10^{-11} Ω^{-1} m^{-1})	P_{rd} (μC cm^{-2})	E_{cd} (kV cm^{-1})	$\varepsilon_d / \varepsilon_0$	V_{omax} (V)	ν
2	55	50	260	2.86	Nil	Nil	Nil	8.8	Nil
4	55	50	260	2.86	55	2000	260	20	0.1
5	55	50	260	2.86	55	2000	260	20	0.1
6	55	50	260	2.86	55	2000	260	13	Varied
8	55	50	260	2.86	Varied	50	Varied	20	0.1
9	55	50	260	2.86	Varied	50	Varied	20	Varied
10	55	50	260	2.86	Varied	50	Varied	20	0.1
11	55	50	260	2.86	Varied	50	Varied	20	0.1

3.3.1 Effect of stress

In heteroepitaxial films, the crystal structure may usually deviate from the

original structure to a large extent [Abe *et al.*, 1997]. As a result of clamping-induced electrode-film interaction [Saya *et al.*, 2000; Li *et al.*, 2002] and the corresponding thermal or lattice mismatch [Grossman *et al.*, 2002], interfacial stress is always present at the surface. Müller and Thomas investigated the thickness dependence of early-stage stress development in two-dimensional solid film growth and obtained the following exponential stress distribution function: $\sigma^{'}(x') = \sigma_0^{'} e^{-x'/\alpha_t} = [\sigma^{'}_0 e^{-L/\alpha_t}] e^{x/\alpha_t}$, where $x' = L - x$ and $\sigma_0^{'}$ is the film / bottom electrode interfacial stress [Müller and Thomas, 2000]. $\sigma_0^{'} > 0$ and $\sigma_0^{'} < 0$ represent the presence of tensile and compressive stress, respectively, and α_t is a parameter that describes the physics of long-range interactions between the deposited layers.

In the presence of stress, the Landau–Khalatnikov equation should become

$$\gamma \frac{dP_i}{dt} = -\frac{\partial F}{\partial P_i} = -\alpha P_i - \beta P_i^3 + E_i + \kappa(P_{i+1} + P_{i-1} - 2P_i) - Q\sigma_i^{'} P_i \qquad (3.12)$$

where Q is the electrostrictive coefficient. In our simulation, we use $\sigma_0^{'} = -1.5\times10^9 \ Pa$ and $Q = 6.6\times10^{-2} \ m^4/C^2$. Fig. 3.2 shows the simulated D-E loop by using the modeling approach discussed in section 3.2.3, which is similar to the experimental loops reported in the literature [Abe *et al.*, 1997; Abe and Komatsu, 1995; Park *et al.*, 1997; Dey *et al.*, 1995; Park *et al.*, 1998; Xu *et al.*, 1990; Wu *et al.*, 2000] and therefore suggests that film-electrode lattice mismatch may be one possible origin of imprint.

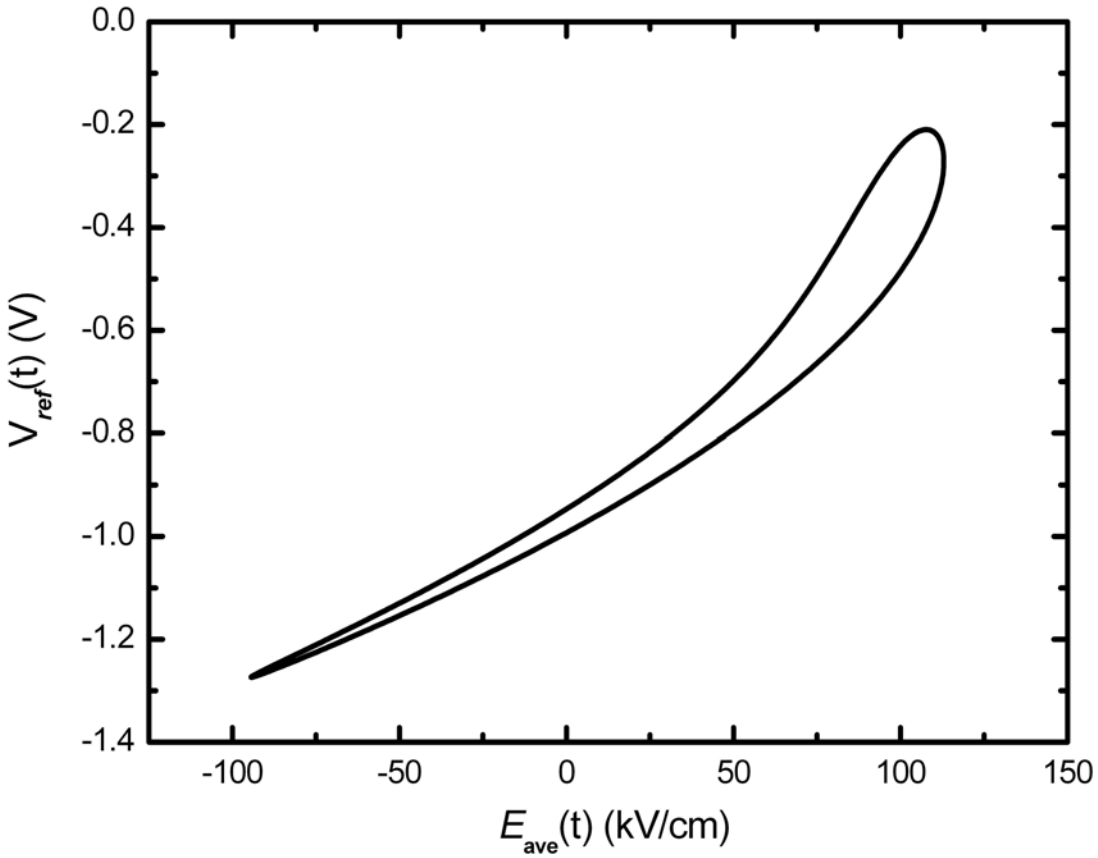

FIG. 3.2 Simulated D-E loop under the influence of compressive stress.

Effects of stress on film properties have previously been investigated, where significant changes in hysteresis loop behavior have been observed [Desu *et al.*, 1993; Kumazawa *et al.*, 1998]. Both experimental and theoretical results show that the coercive field E_c increases when the film is compressively stressed [Spierings *et al.*, 1995; Song *et al.*, 2003]. From the abovementioned exponential stress distribution function, we know that the stress is maximum at the film / bottom electrode interface. The coercive field near the bottom electrode is thus likely to be larger than elsewhere so that the polarization in this region is much harder to reverse, inducing a pseudo non-switching layer that is probably the ultimate origin of imprint.

3.3.2 Effect of domain pinning

Experimental results in the literature show that domain pinning near film/electrode interfaces [Wu *et al.*, 2000; Pike *et al*., 1995] is mainly caused by the presence of oxygen vacancies. Warren *et al.* proposed that electron trapping is a result of the alignment of defect-dipole complexes [Al-Shareef *et al.*, 1997]. In particular, interface-trapped charges will lead to the pinning of dipoles which can be regarded as the preference of one polarization state over the other. Such pinning phenomena have been reported for PZT and $BaTiO_3$ by Dimos *et al.* [Sadashivan *et al.*, 1998; Dimos *et al.*, 1996]. They showed that the occurrence of imprint can be attributed primarily to domain wall pinning due to charge trapping [Dimos *et al.*, 1996]. He *et al.* investigated the interaction between oxygen vacancies and domain walls using density-functional theory and then conducted a first-principle investigation of oxygen-vacancy pinning of domain walls in $PbTiO_3$ [He and Vanderbilt, 2003].

We assume that a pseudo non-switching surface layer is formed at either film/electrode interface (Fig. 3.3). Compared with the bulk, we assume this surface layer has a much larger coercive field but roughly the same remanent polarization. In fact, it has been experimentally observed that the presence of defects or damage vacancies will induce a larger coercive field but smaller remanent polarization [Stoilichnov et al., 2000; Li et al., 2001; Shimizu et al., 2002; Robels et al., 1995; Loloee and Crimp, 2002], making the polarization harder to reverse and producing a

pseudo domain pinning effect in the surface layer.

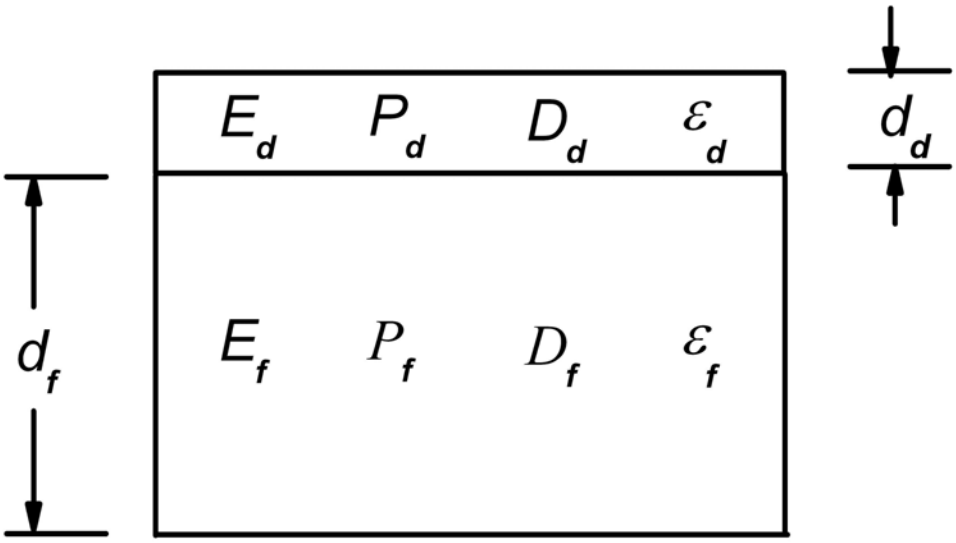

FIG. 3.3 Schematic diagram of a ferroelectric thin film consisting of two phases.

The electric displacements across the ferroelectric layer, D_f, and across the surface layer, D_d, are given by the following equations:

$$D_f = \varepsilon_f E_f + P_f \tag{3.13}$$

$$D_d = \varepsilon_d E_d + P_d \tag{3.14}$$

where E denotes electric field and P polarization, while the subscripts f and d denote the normal ferroelectric region and non-switching surface layer, respectively. The average field across the thin film is calculated as

$$E_{ave} = (1-\nu)E_f + \nu E_d \tag{3.15}$$

where ν represents the thickness fraction of the non-switching layer in the film. Taking into account the surface non-switching layer, the continuity of total current can be expressed as

$$J(t) = \sigma_f(x,t)E_f(x,t) + \varepsilon_f(x)\frac{\partial E_f(x,t)}{\partial t} + \frac{\partial P_f(x,t)}{\partial t}$$

$$= \sigma_d(x,t)E_d(x,t) + \varepsilon_d(x)\frac{\partial E_d(x,t)}{\partial t} + \frac{\partial P_d(x,t)}{\partial t} \qquad (3.16)$$

where $\sigma(x,t)$ and $\varepsilon(x)$ are the time-dependent space-charge-limited conductivity mentioned in section 3.2.2 and permittivity, respectively.

Fig. 3.4 (*a*) shows the simulated results of the D-E hysteresis loop for a ferroelectric thin film with a pseudo non-switching layer. The modeled P-E relations of the ferroelectric and non-switching layer are respectively shown in Figs. 3.4 (*b*) and 3.4 (*c*). It can be seen that the hysteresis loop of the ferroelectric layer is completely cycled, while the polarization of the non-switching layer only stays in the lower part of its P-E loop so that polarization switching cannot occur. The simulated D-E loop shown in Fig. 3.4 (*a*) has a large horizontal shift to the right side, giving evidence that domain pinning within the surface layer could lead to imprint. Loops with negative-susceptibility like those depicted in Fig 4(b) have already been reported in a paper describing the ferroelectric behaviour of some barium titanate poled ceramics [Baerwald and Berlincourt, 1953], and Ricinschi *et al.* have discussed the physical meaning of the negative-susceptibility regions in hysteresis loops [Ricinschi *et al.*, 1998]. Fig. 3.4 is obtained when we apply a sinusoidal wave without any initial phase. If there exists an initial phase π such that $V_0(t) = V_{0\max}\sin(\omega t + \pi)$, all the abovementioned D-E and P-E relations only change by a 180° flip about the x- and y-axes, as shown in Fig. 3.5. It is because in the non-switching layer the polarization stays in the upper part of the loop instead of the lower part, as shown in Fig. 3.5 (c). It should be noted that the type of 'long-tail' hysteresis loops

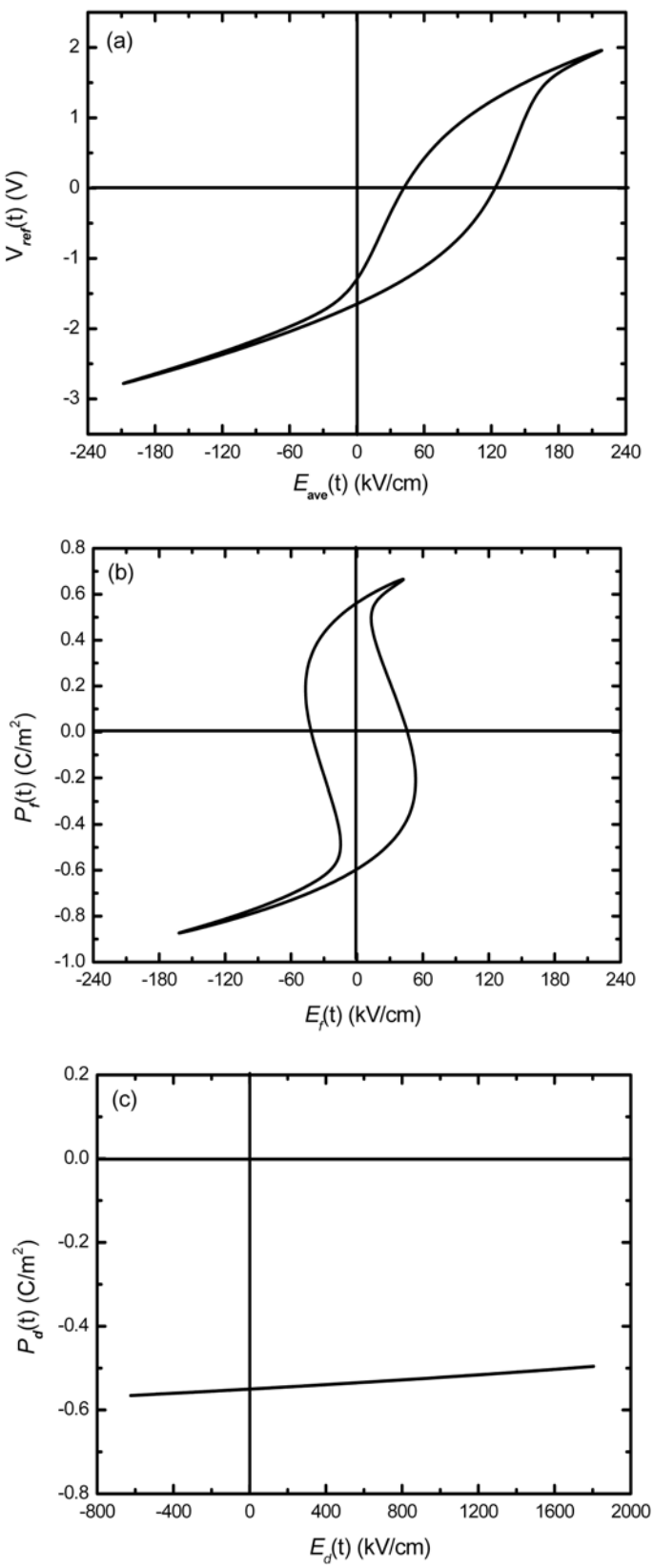

FIG. 3.4 When the polarization of the non-switching layer only stays in the lower part of the P-E loop: (*a*) D-E hysteresis loop for ferroelectric thin films; (*b*) Modeled P-E relations of the ferroelectric layer; (*c*) Modeled P-E relations of the non-switching layer.

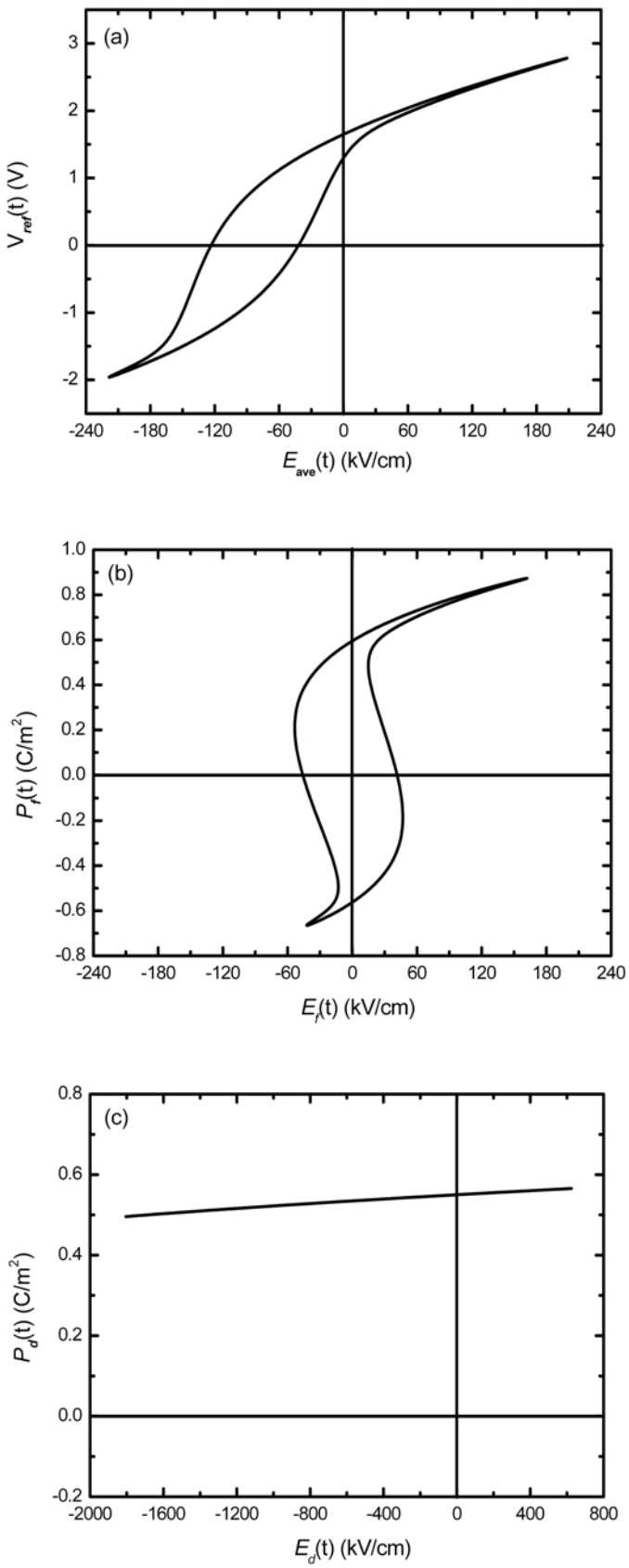

FIG. 3.5 When the polarization of the non-switching layer only stays in the upper part of the P-E loop: (*a*) D-E hysteresis loop for ferroelectric thin films; (*b*) Modeled P-E relations of the

ferroelectric layer; (*c*) Modeled P-E relations of the non-switching layer.

shown in Fig. 3.4 (*a*) and Fig. 3.5 (*a*) exhibit a striking similarity with those observed in experiments [Dey *et al.*, 1995; Abe *et al.*, 1997; Abe and Komatsu, 1995; Park *et al.*, 1998; Wu *et al.*, 2000], thus justifying the validity of our model that includes a pseudo non-switching surface layer. Fig. 3.6 shows the effect of thickness ratio of the non-switching layer on the hysteresis loop. When $\nu = 0.01$, the simulated loop almost centers at the origin and no notable horizontal shift is observed. With ν increasing, the magnitude of horizontal shift increases. Therefore, our model should be confined to the study of thin ferroelectric films where the surface layer has an appreciable thickness fraction.

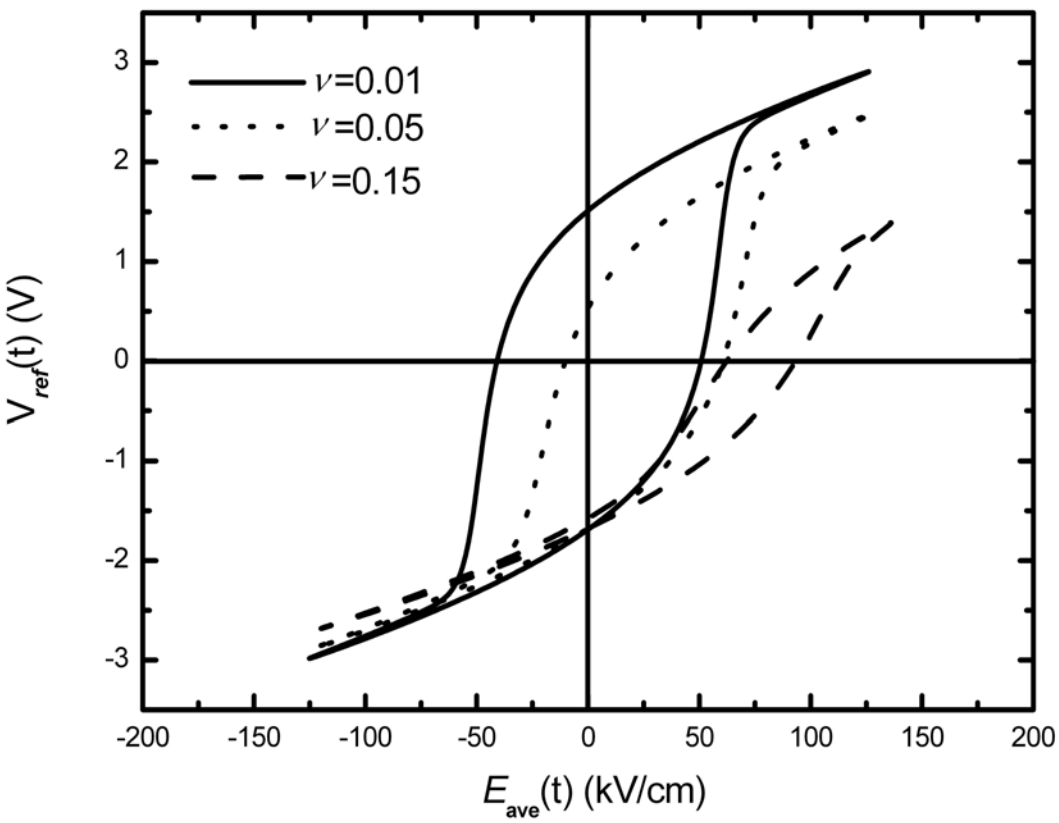

FIG. 3.6 Effect of thickness ratio of the non-switching layer on the hysteresis loop.

We have used a double-layer model with an abrupt interface to model the imprint effect under the influence of domain pinning near the film/electrode interface. Similar results are obtained if the interface is replaced by a smoother one with gradual variation in properties. We have also calculated the shift effect by assuming Ohmic conductivity alone, i.e. assuming $\sigma(x,t) \approx \sigma_0$ and not using the full TDSCL conductivity expression in Eq. (3.4). It is found that a shift also exists and that the shift magnitudes are about one third to one half of the shift magnitudes from TDSCL conduction calculations for some typical σ_0 values of ferroelectric thin film [Chan *et al.*, 2004]. We therefore suggest that the TDSCL conduction is likely one of the dominating factors even in the presence of domain pinning for the occurrence of large imprint effects observed in experiments.

3.3.3 Effect of graded surface layer

It has been known experimentally that ferroelectric properties of surface layers such as remanent polarization and permittivity are weaker than those of the bulk region [Sakashita *et al.*, 1993; Hase *et al.*, 1993; Tagantsev *et al.*, 1995]. Such degradation of ferroelectric properties [Saya *et al.*, 2000] has been suggested to occur for reasons such as: (a) interdiffusion between a ferroelectric thin film and electrode [Nakamura *et al.*, 1994], (b) insufficient flatness of bottom electrode and film, (c) vacancies of Pb and/or oxygen [Lee *et al.*, 1992]. It is justifiable to model the surface layer as a graded one in which the permittivity and remanent polarization decrease gradually from the bulk values (Fig. 3.7).

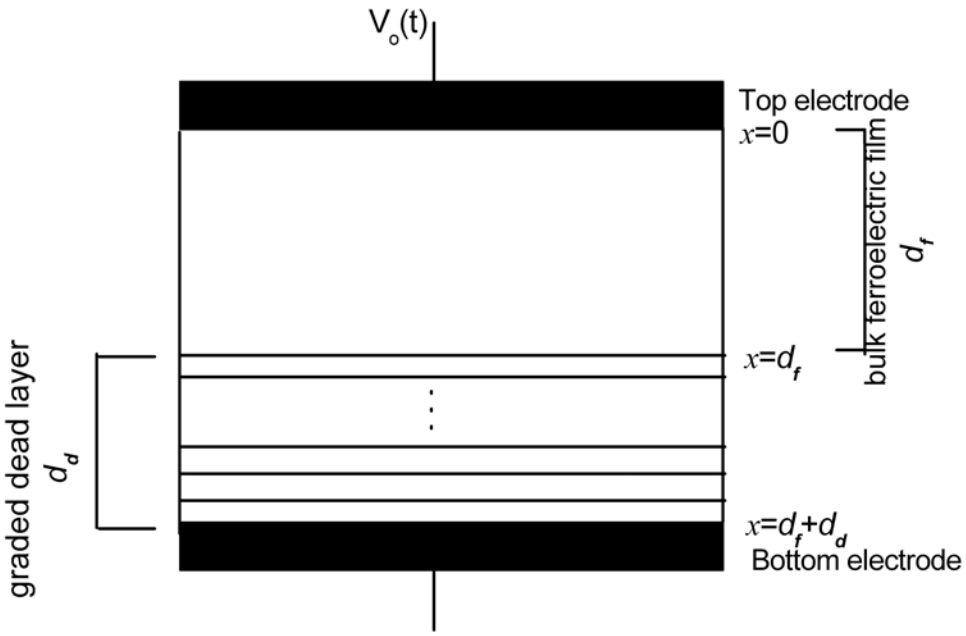

FIG. 3.7 Ferroelectric thin film consisting of bulk ferroelectric and graded surface layer whose thickness are respectively d_f and d_d.

Fig. 3.8 shows the D-E loop simulated from our model incorporating a graded surface layer near the bottom electrode, for which a large horizontal shift is produced (see Table 3.2 for related parameters). Note that this type of hysteresis loop can be found in related experimental measurements [Warren *et al.*, 1996]. Fig. 3.9 shows the effect of thickness ratio of the graded layer on the hysteresis loop; the magnitude of horizontal shift increases with the fraction of graded layer. Fig. 3.10 (a) illustrates two cases where only Ohmic conductivity is considered and where the

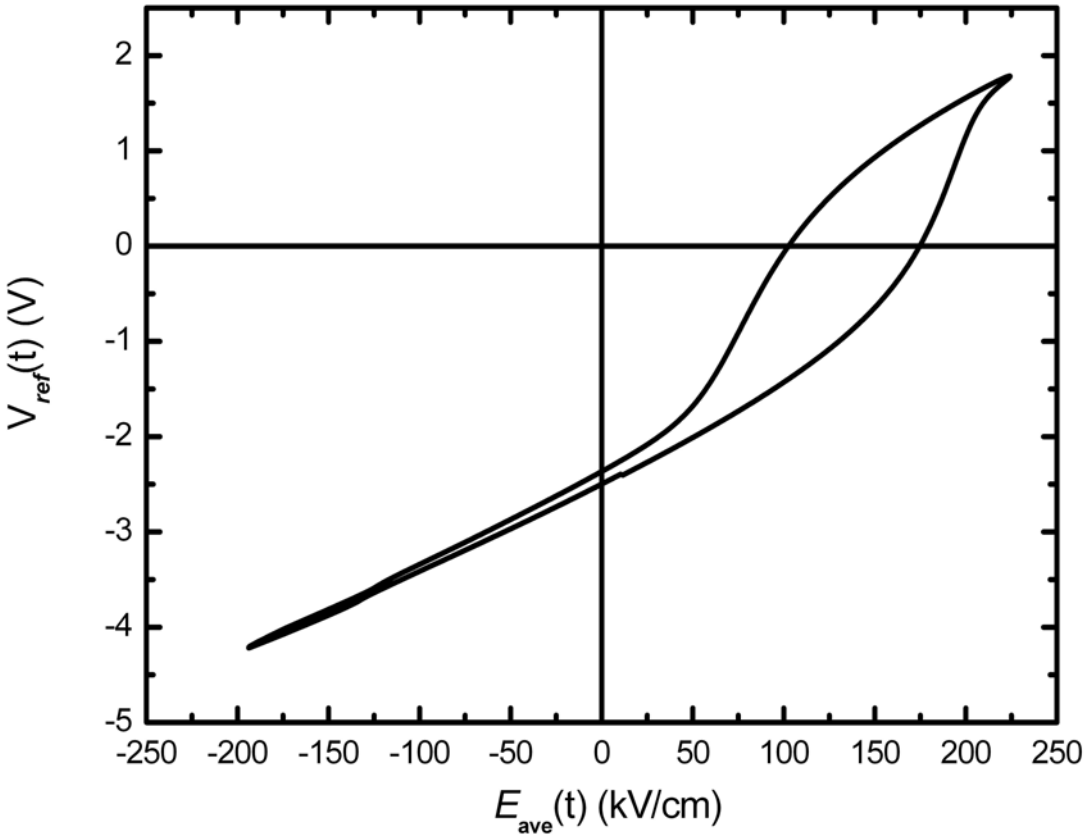

FIG. 3.8 D-E loop simulated from our model with a graded surface layer near the bottom electrode.

TABLE 3.2 The variations of remanent polarization and permittivity of the graded surface layer with *x*.

$\frac{x-d_f}{d_d}$	$P_r(x)$ (μC cm^{-2})	$\varepsilon_d(x) / \varepsilon_0$
0	55	260
0.25	26.4	210
0.5	11.8	160
0.75	5.4	110
1	1.2	60

effect of TDSCL conduction is taken into account. There is almost no horizontal shift when only Ohmic conductivity is considered but a notable horizontal shift is observed when TDSCL conduction is taken into account. Fig. 3.10 (b) shows the time evolution of interfacial charge ($= D_d - D_f$) for, respectively, the consideration and neglect of TDSCL conduction. It is interesting to see that there is averagely positive interfacial charge accumulated when TDSCL conduction is taken into account while there is almost no interfacial charge accumulation for the case of only Ohmic conduction.

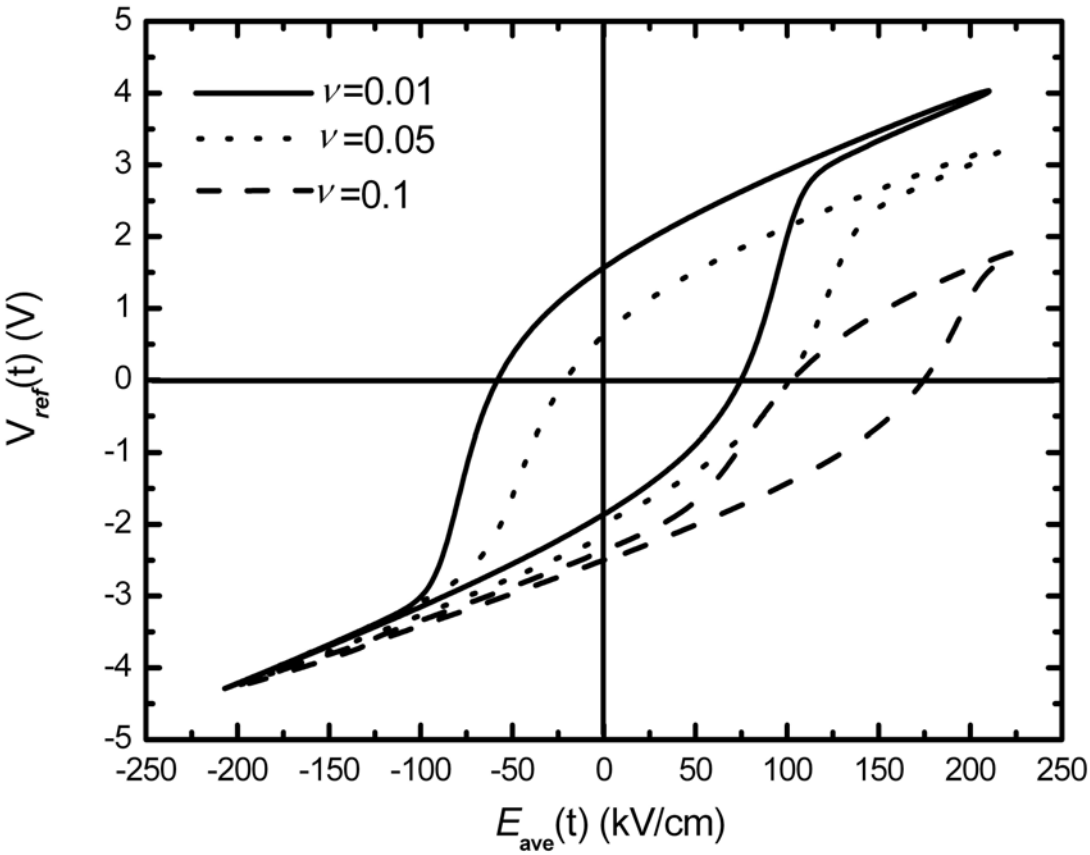

FIG. 3.9 Effect of thickness ratio of the graded layer on the hysteresis loop.

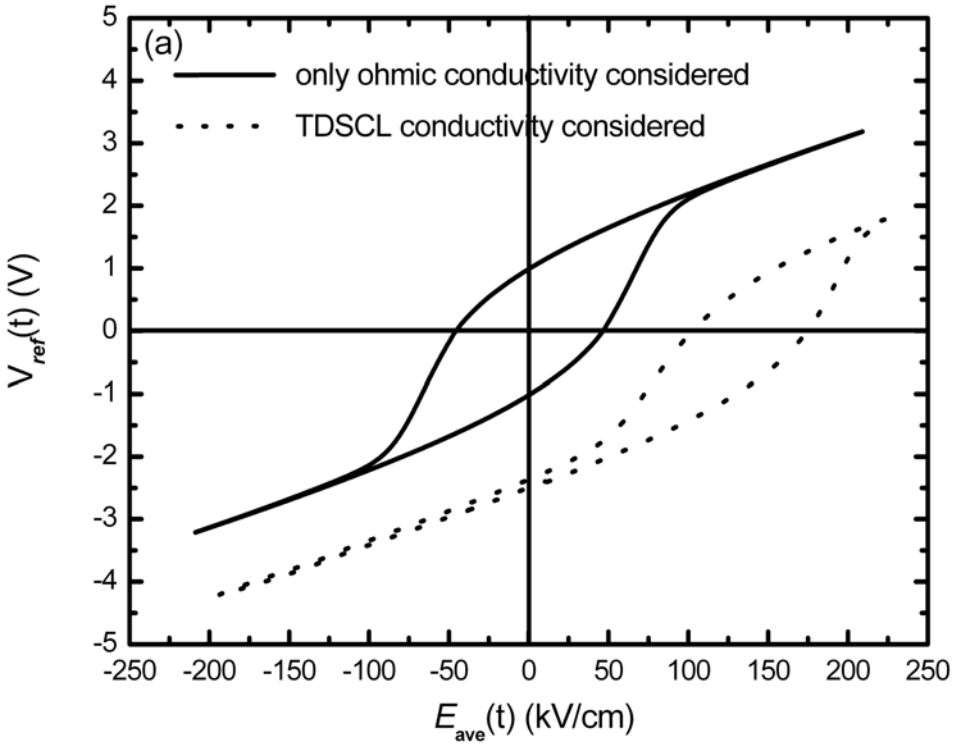

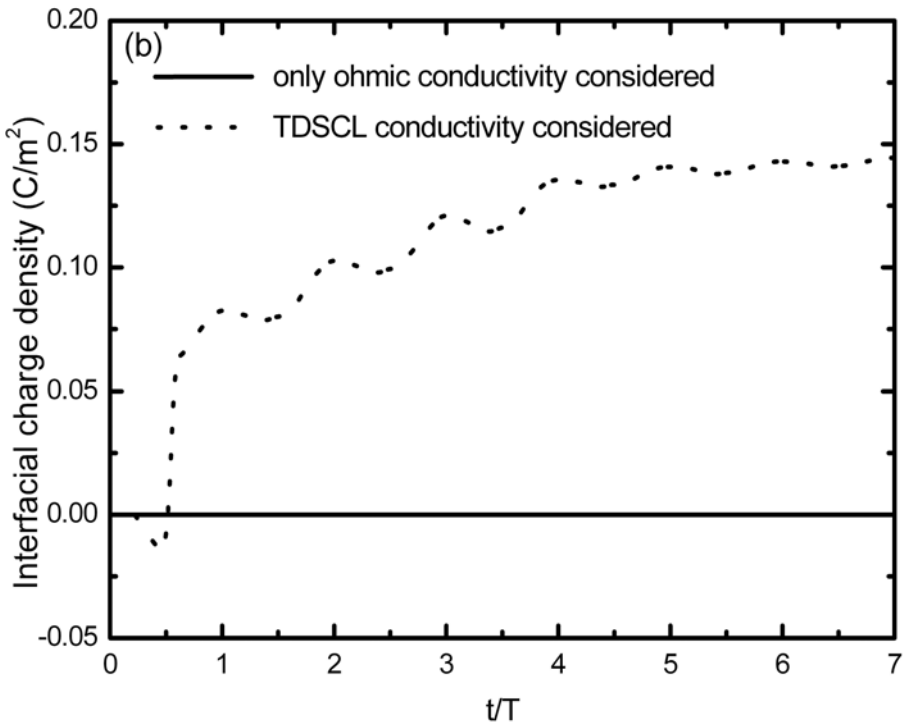

FIG. 3.10 Effects of TDSCL and Ohmic conductivities: (a) on the simulated D-E loop; (*b*) on the time evolution of interfacial charge densities.

Fig. 3.11 shows the time development of electric fields in the bulk ferroelectric

layer (E_f) and the graded surface layer (E_d); a large positive DC bias has accumulated in the graded surface layer while a much smaller negative DC bias in the bulk layer. On the other hand, the electric-field distributions inside the bulk and graded surface layers are both non-uniform. The electric field tends to be concentrated within the graded surface layer, possibly because this region has reduced permittivity and tends to acquire a strong field for polarization reversal [Abe *et al.*, 1997]. It is found that the measured D-E loop shifts to the opposite side when the graded surface layer is placed adjacent to the top electrode instead of the bottom one, where the gradient of the surface layer is reversed, i.e. the direction of horizontal shift is determined by the gradient of the surface layer.

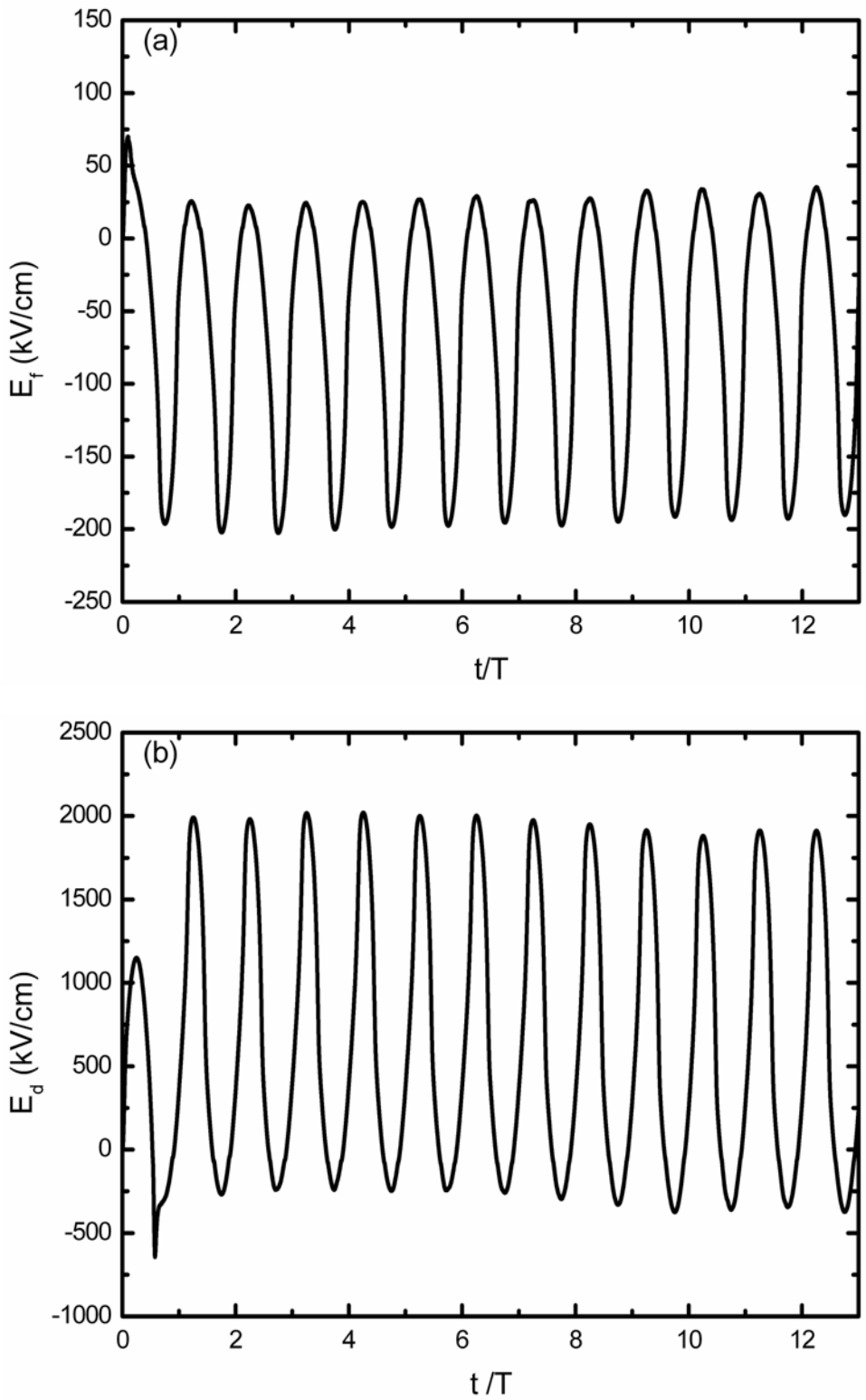

FIG. 3.11 Time development of electric fields: (*a*) in the bulk ferroelectric layer; (*b*) in the graded surface layer.

Summing up, we have taken the TDSCL into account to investigate the effects of

stress, domain pinning and graded surface layer on the hysteresis loops. In the first and third cases, the consideration of TDSCL is necessary to lead to the horizontally shifted hysteresis loops; while Ohmic conduction is also able to give a horizontal shift behavior when considering domain pinning, but it is unable to produce large shift magnitudes observed in some ferroelectric thin film systems. On the other hand, imprint is a very complicated issue and may also be explained by charge injected from the electrodes and trapped at interfacial states. In addition, imprint effect is also very often in part attributed to the role of oxygen vacancy-related defect dipoles throughout the film [Al-Shareef *et al.*, 1997]. Therefore, although the cases discussed here are not exhaustive and the mechanisms investigated herein are not exclusive, the consideration of TDSCL is likely to be one of the possible origins for the occurrence of imprint where large shifts of hysteresis loops are observed in experiments.

In general, the qualitative similarity between published experimental results and our simulation shows that stress, domain pinning induced by e.g. oxygen vacancies, and graded surface layer or their multiple effects are likely to be responsible for the widely observed imprint phenomena. In addition, our graded dead layer model may well be extended to study the polarization behaviour in step-graded or multilayered ferroelectric structures. In fact, by adopting the interfacial coupling coefficient to account for the intrinsic interaction across the interface between neighboring constituents, our model is extended to study the unconventional ferroelectric and dielectric properties in ferroelectric superlattices in the next chapter.

Chapter 4 Enhancement of dielectric and ferroelectric properties in ferroelectric superlattices

4.1 Introduction

Ferroelectric multilayer/superlattices have attracted great research interest recently [Erbil *et al.*, 1996; Shimuta *et al.*, 2002; Pontes *et al.*, 2004]. These kinds of structures have been identified as possessing functional physical properties more superior than their single-phase films, offering opportunities for potential application in dynamic random access memories and ferroelectric memories which require a large remanent polarization or a high dielectric constant in small size. Experimentally, elevated remanent polarization is one of the most important features of ferroelectric superlattices. Lee *et al.* reported a strong polarization enhancement in asymmetric three-component ferroelectric superlattices [Lee *et al.*, 2005]. Shimuta *et al.* reported the largest remanent polarization $2P_r$ of 46 $\mu C/cm^2$, which is about three times that of the $BaTiO_3$ single-phase film, in asymmetric epitaxial $BaTiO_3/SrTiO_3$ (BTO/STO) strained superlattice structures [Shimuta *et al.*, 2002]. On the other hand, the enhancement in the dielectric constant is also a commonly observed phenomenon in ferroelectric multilayer/superlattices. Wang *et al.* reported the enhancement of the dielectric constant in multilayered $Pb(Zr_{0.8}Ti_{0.2})O_3/Pb(Zr_{0.2}Ti_{0.8})O_3$ thin films prepared by rf magnetron sputtering [Wang *et al.*, 2003]. Erbil *et al.* observed the giant relative permittivity as high as 420000 in the epitaxial heterostructure composed of $PbTiO_3/Pb_{1-x}La_xTiO_3$ [Erbil *et al.*, 1996].

In addition, recent results have shown the ferroelectric and dielectric properties are sensitively dependent on various macroscopic geometrical parameters such as layer thickness, layering sequence and individual layer thickness ratio [Shimuta *et al.*, 2002; Wang *et al.*, 2003].

Although there has been an emphasis on the practical development of such superlattices, theoretical understanding of their anomalous behaviour is rather limited. It is believed that the interfacial coupling between the constituent layers should play an important role and hence must be taken into consideration [Sepliarsky *et al*., 2002; Qu *et al.*, 1997]. The strong interfacial coupling between individual polar layers are proposed as mechanisms leading to the observed behavior that cannot be explained simply in terms of those measured on single films of the constituent materials in epitaxial $SrTiO_3/BaTiO_3$ superlattices [Christen *et al.*, 2003]. The enhancement of dielectric properties of $Pb(Zr,Ti)O_3$ films with tetragonal/rhombohedral multilayered structure is attributed to the presence of interfaces between the tetragonal and the rhombohedral phase layer [Pontes *et al.*, 2004; Wang *et al.*, 2003]. On the other hand, it has been demonstrated that electrical conductivity in ferroelectrics can induce new phenomena or modify known physical phenomena, which may be difficult to understand if the materials are regarded as perfectly insulating [Chan *et al.*, 2003; Wong and Shin, 2005]. In particular, the time-dependent space-charge-limited (TDSCL) conduction has been demonstrated to be a possible origin leading to the abnormal polarization offset along the polarization axis widely observed in the compositionally graded ferroelectric thin films [Chan *et al.*, 2003]. It is also

suggested that the dramatically elevated dielectric constants may be obtainable by increasing the conductivity of the ferroelectric superlattices through impurity doping [Erbil *et al.*, 1996]. However, so far only very few theoretical investigations have been performed to study the interplay of the effects of interfacial coupling and electrical conductivity on the ferroelectric and dielectric properties of multilayer/superlattices. We believe such investigations can furnish further insight into the mechanism.

Taking the hint that electrical conductivity may play a non-trivial role behind the many anomalous phenomenon observed in ferroelectric thin films and composite structures [Erbil et al., 1996; Chan et al., 2003; Wong and Shin, 2005], we aim in the present work to study to what extent the consideration of electrical conductivity can account for the enhancement of ferroelectric and dielectric properties in the interface-coupled ferroelectric superlattices. For illustration purposes, recent experimental observations on the enhancement of remanent polarization and dielectric constant in $BaTiO_3/SrTiO_3$ superlattices and heterolayered PZT thin films [Shimuta *et al.*, 2002; Pontes *et al.*, 2004] are compared with our model calculations.

4.2 Theory and modeling

4.2.1 Landau-Khalatnikov kinetics of switching

Consider an infinite ferroelectric superlattice formed from alternating layers of two different materials A and B. A typical repeating unit (a period) of this structure is a bilayer of A and B. Periodic boundary conditions are applied to the top and bottom surfaces of this bilayer unit so as to describe the infinite ferroelectric superlattice. This suggests that we only have to consider a one-period superlattice structure. Further, each layer A or B in the superlattice interacts with its neighboring layers via some interfacial coupling mechanism to be elaborated later on.

We assume that all spatial variation takes place along the *x*-direction. The dynamics of the dipoles of A and B are modeled by the Landau-Khalatnikov equation:

$$\begin{cases} \gamma_A \dfrac{\partial P_A(x,t)}{\partial t} = -\alpha_A P_A(x,t) - \beta_A P_A(x,t)^3 - \nu_A P_A(x,t)^5 + E_A(x,t) + \kappa_A \dfrac{\partial^2 P_A(x,t)}{\partial x^2} \\ \gamma_B \dfrac{\partial P_B(x,t)}{\partial t} = -\alpha_B P_B(x,t) - \beta_B P_B(x,t)^3 - \nu_B P_B(x,t)^5 + E_B(x,t) + \kappa_B \dfrac{\partial^2 P_B(x,t)}{\partial x^2} \end{cases} \quad (4.1)$$

where γ represents the viscosity that causes the delay in motion of dipole moments. α, β and ν are the corresponding Landau coefficients of the material. The last term in each of the above equations comes from energy associated with polarization gradients, where κ is the corresponding interaction coefficient between neighboring dipoles.

The form of the kinetic equations above conforms to the equations used by a number of works, notedly [Baudry and Tournier, 2001; Boudry, 1999], which is obtained by minimizing the free energy of the film under applied electric field. It

should be noted that $E(x,t)$ in Eq. (4.1) denotes the local electric field instead of external electric field. With this approach, the explicit consideration of the depolarization field is subsumed in the formulation. In particular, Baudry and Tournier [Baudry and Tournier, 2001] has given an excellent discussion on this point, incorporating implications due to the presence of charge carriers and non-uniformity of polarization.

The boundary conditions for the polarizations at the interface x=0 are

$$\begin{cases} \kappa_A \left.\dfrac{dP_A}{dx}\right|_{x=0} - \lambda(P_{A0} - P_{B0}) = 0 \\ \kappa_B \left.\dfrac{dP_B}{dx}\right|_{x=0} + \lambda(P_{A0} - P_{B0}) = 0 \end{cases} \tag{4.2}$$

and the periodic boundary conditions for the polarizations of an infinite superlattice structure can be described by

$$\begin{cases} \kappa_A \left.\dfrac{dP_A}{dx}\right|_{x=-d_A} - \lambda(P_A\big|_{x=-d_A} - P_B\big|_{x=-d_A}) = 0 \\ \kappa_B \left.\dfrac{dP_B}{dx}\right|_{x=d_B} - \lambda(P_A\big|_{x=d_B} - P_B\big|_{x=d_B}) = 0 \end{cases} \tag{4.3}$$

where d_A and d_B are the layer thicknesses of a bilayer unit.

The boundary condition equations above are obtained by including an interfacial coupling energy term into the free energy and then minimizing the free energy of the interface structure under applied electric field. The parameter λ describes the strength of the interfacial coupling between the constituents A and B. The detailed discussion about the interfacial coupling can be found in Refs. [Tsang *et al.*, 2004 and Chew *et al.*, 2005].

4.2.2 Electric conduction

In our previous study of compositionally graded ferroelectric films [Chan *et al.*, 2003; Zhou *et al.*, 2005], we used the following 'time-dependent space-charge-limited conduction' (TDSCL) formula for the time-dependent conductivity associated with space charges:

$$\sigma(x,t) = \frac{\mu_p - \mu_n}{2}\frac{\partial D(x,t)}{\partial x} + \sqrt{[\frac{\mu_p + \mu_n}{2}\frac{\partial D(x,t)}{\partial x}]^2 + \sigma_0(x)^2} \tag{4.4}$$

where $D(x,t) = \varepsilon(x)E(x,t) + P(x,t)$ is the electric displacement at position x and time t, $\sigma_0(x)$ is the intrinsic conductivity, μ_p and $-\mu_n$ (μ_p, $\mu_n > 0$) are the positive and negative charge carrier mobilities, respectively. Here we also employ the same conduction mechanism for the present problem. The total current $J(t)$ across the superlattice structure consists of the conduction and displacement currents:

$$J(t) = j_c(x,t) + j_d(x,t) = \sigma(x,t)E(x,t) + \frac{\partial}{\partial t}D(x,t) \tag{4.5}$$

where subscripts *c* and *d* denote "conduction" and "displacement", respectively. The circuit condition is given by:

$$\int_{-d_A}^{d_B} E(x,t)dx = E(t)L \tag{4.6}$$

where $L = d_A + d_B$ is the period thickness and $E(t) = E_{amp}sin(\omega t)$ is the applied electric field across the superlattice. It is noted that the applied field amplitude E_{amp} should be sufficiently small so that polarization switching will not occur within the ferroelectric superlattice when measuring permittivity. The measured electric displacement of the superlattice at a certain time t is given by the integration of total current density across the circuit:

$$D(t) = \int_0^t J(t)dt \tag{4.7}$$

The relative dielectric constant of the superlattice is calculated by:

$$\varepsilon = \frac{\{D(t)\}_{\sin \omega t}}{E_{amp}}, \tag{4.8}$$

where $\{\ \}_{\sin \omega t}$ is the $\sin(\omega t)$ – Fourier component of the function within the bracket.

4.3 Results and disccusion

To verify our model, we perform numerical calculations for $BaTiO_3/SrTiO_3$ superlattices and multilayered $Pb(Zr,Ti)O_3$ films reported in [Shimuta *et al.*, 2002] and [Pontes *et al.*, 2004] and compare with experimental data therein. The properties of the constituent phases used for calculations are obtained by slightly fine-tuning/interpolating the physical parameters found in the existing literature and are given in Table 4.1 [Sepliarsky *et al.*, 2002; Qu *et al.*, 1997; Christen *et al.*, 2003; Fong *et al.*, 2004; Foster *et al.*, 1997; Ban *et al.*, 2003]. The mobility values are taken as $\mu_p = 1\times10^{-9} m^2V^{-1}s^{-1}$, $\mu_n = 1\times10^{-12} m^2V^{-1}s^{-1}$ following Ref. [Chan *et al.*, 2003] values in order of magnitude. The following nominal interfacial coupling coefficient value is used: $\lambda = 1/\varepsilon_0$, where ε_0 is the vacuum permittivity. Unless stated otherwise, all the above-mentioned parameters are retained for all the calculations.

TABLE 4.1 The physical parameters for BTO/STO and PZT60/PZT40 superlattices used in our calculations (all the values are in SI units).

Parameter	$BaTiO_3$	$SrTiO_3$	$Pb(Zr_{0.6}Ti_{0.4})O_3$	$Pb(Zr_{0.4}Ti_{0.6})O_3$
α	-6.18×10^{7}	3.92×10^{8}	-3.3×10^{8}	-1.87×10^{8}
β	1.26×10^{10}	8.4×10^{9}	5.3×10^{10}	5.5×10^{9}
ν	3.96×10^{10}	0	2.8×10^{-10}	2.8×10^{-10}
κ	1×10^{-11}	1×10^{-11}	1×10^{-10}	1×10^{-10}
σ_0	1×10^{-10}	1×10^{-11}	1.4×10^{-11}	2.3×10^{-11}

4.3.1 Enhancement of remanent polarization in $BaTiO_3/SrTiO_3$ superlattices

Barium titanate ($BaTiO_3$) is one of the most important ferroelectric perovskites. However, its ferroelectric properties, particularly remanent polarization, are not as superior as those of $Pb(Zr,Ti)O_3$. Therefore, various efforts have been dedicated to enhance the ferroelectric properties of $BaTiO_3$. Experimentally, $BaTiO_3/SrTiO_3$ (BTO/STO) superlattices were fabricated by metal-organic vapour deposition, pulsed laser deposition and the sol-gel method [Qu *et al.*, 1997]. The thickness ratio of BTO and STO was usually chosen to be one in most of the BTO/STO superlattices. Recently, Shimuta and coworkers reported the enhancement of remanent polarization in asymmetric $BaTiO_3/SrTiO_3$ strained superlattices with unequal BTO and STO layer thickness within each stacking periodicity [Shimuta *et al.*, 2002]. In their work, both symmetric and asymmetric BTO/STO superlattices have been fabricated by a pulsed-laser deposition technique. The superlattice with 15 unit cells of BTO and 3 unit cells of STO in one period showed the largest remanent polarization $2P_r$ of $26\mu C/cm^2$, which is more than three times that of single-phase BTO thin film, and approaching that of bulk BTO. The layer thickness dependence of remanent polarization calculated by our model is shown in Fig. 4.1. Note that herein the BTO layer thickness is equal to that of STO in each period of the superlattice. It can be seen from Fig. 4.1 that the remanent polarization increases when the layer thickness decreases. The experimental data of symmetric superlattices with 3/3, 5/5, 10/10 and 65/65 (*n*/*m* denotes *n* unit cells of BTO and *m* unit cells of STO in each

periodicity) are also shown in Fig. 4.1. It is seen that our results are in good agreement with the experiments. Interestingly, the remanent polarization of the superlattice exceeds that of the BT single-phase film ($2P_r = 14\mu C/cm^2$) when the layer thickness is smaller than 1.5 nm, which is also validated by the experimental results.

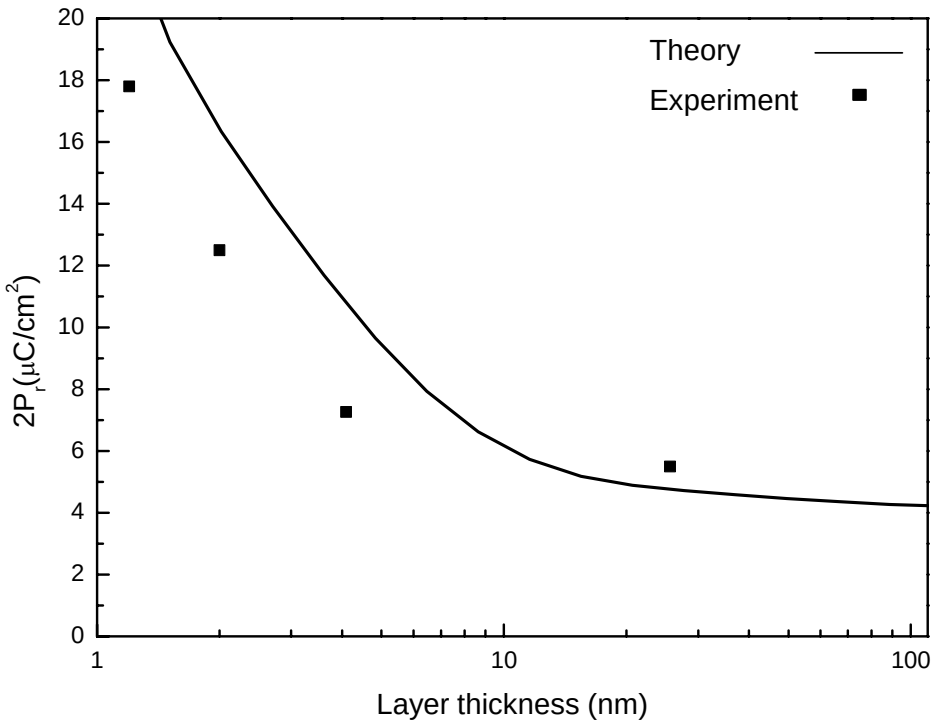

FIG. 4.1 Calculated and experimental results of remanent polarization $2P_r$ as a function of layer thickness in the BTO/STO symmetric superlattices.

Fig. 4.2 shows the P-E hysteresis loops of the superlattice with the stacking periodicity of 15/3 and the BTO single-phase thin film. The simulated P-E loop of

the superlattice with the stacking periodicity of 15/3 is much more inflated than that of BTO thin film. The remanent polarization $2P_r$ is about three times that of the single phase BTO thin film. It is also noted that the shapes of the simulated P-E loops are strikingly similar with the experiments, which is partly a manifestation of the electrical conductivity of the superlattices.

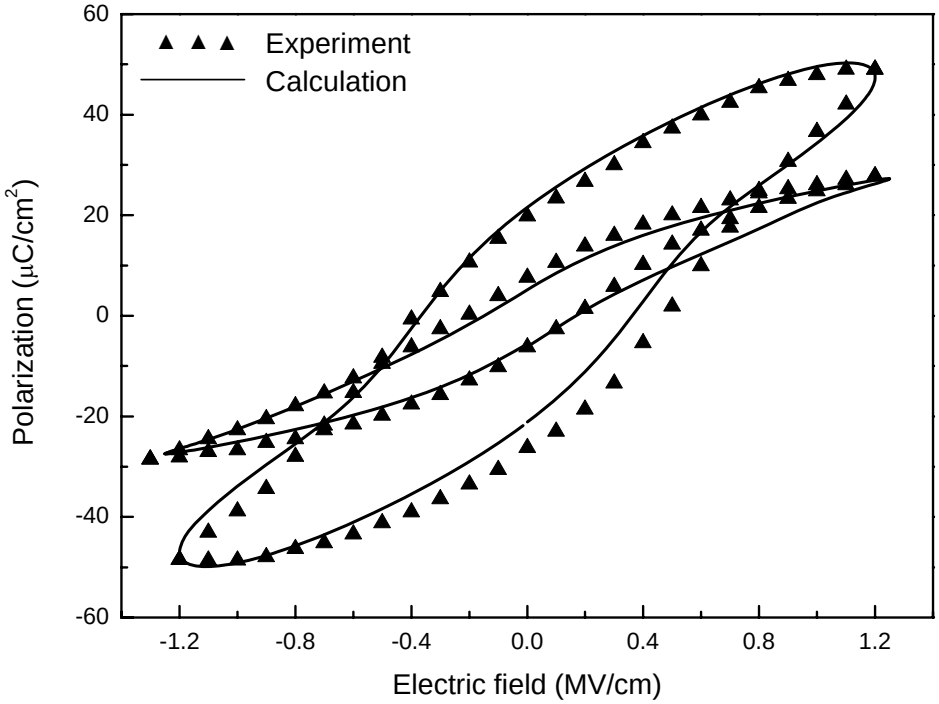

FIG 4.2 Calculated and experimental P-E hysteresis loops of BTO/STO superlattice with the stacking periodicity of 15/3 and BTO single-phase film.

4.3.2 Enhancement of P_r and ε properties of heterolayered PZT

Recently, considerable experimental efforts have been dedicated to the fabrication of $Pb(Zr,Ti)O_3$ (PZT) multilayered films because their ferroelectric

properties and dielectric permittivity can be easily modulated by adjusting the Zr:Ti ratio near a rhombohedral-tetragonal morphotropic phase boundary (MPB). In a recent paper [Pontes *et al.*, 2004], Pontes *et al.* reported the enhancement of both dielectric and ferroelectric properties of heterolayered PZT film, which consisted of six alternating $Pb(Zr_{0.6}Ti_{0.4})O_3$ (PZT60) and $Pb(Zr_{0.4}Ti_{0.6})O_3$ (PZT40) layers, fabricated by a chemical solution deposition. In their work, a dielectric constant of 701 at 100 kHz was observed for the heterolayered PZT40/PZT60 film. The dielectric constant of the heterolayered PZT film can not be explained by the capacitor series model, according to which the PZT multilayer structure is regarded as a series connection of PZT60 and PZT40 layers, thus the effective dielectric constant can be expressed theoretically as:

$$\frac{1}{\varepsilon_{eff}} = \left(\frac{t_1}{\varepsilon_{PZT60}} + \frac{t_2}{\varepsilon_{PZT40}} + \frac{t_3}{\varepsilon_{PZT60}} + \frac{t_4}{\varepsilon_{PZT40}} + \frac{t_5}{\varepsilon_{PZT60}} + \frac{t_6}{\varepsilon_{PZT40}} \right) / (t_1 + t_2 + t_3 + t_4 + t_5 + t_6) \quad (4.9)$$

where t_1, t_3, and t_5 are the thickness of PZT60 and t_2, t_4, and t_6 are the thickness of PZT40. Considering that the dielectric constants of PZT60 and PZT40 are 452 and 512 [Pontes *et al.*, 2004], ε_{eff} was calculated to be about 481. However, the measured dielectric constant value (□ 701) was much higher. On the other hand, it has been theoretically demonstrated that the permittivity of ferroelectric composites can be significantly enhanced by electrical conductivity [Wong and Shin, 2005]. It is also suggested that the measured permittivity will dramatically increase by increasing the conductivity of the ferroelectric superlattices [Erbil *et al.*, 1996]. Interestingly, our calculation gives a value of 698 for the permittivity of heterolayered PZT film at the frequency of 100 kHz. The frequency dependence of dielectric

constant is shown in Fig. 4.3. Although there is some deviation in dielectric constant magnitudes at low frequencies, i.e. $10^3 - 10^4 Hz$, our calculation gives the same trend, namely, the calculated ε_{eff} decreases with increasing frequency *f*, having similar permittivity magnitudes as experimentally observed.

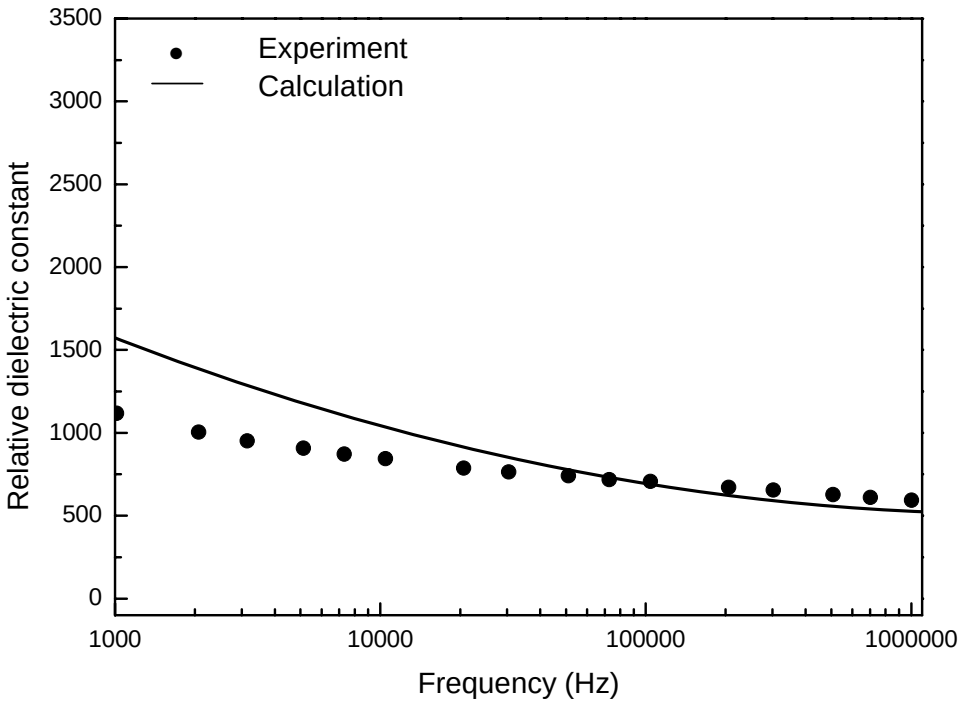

FIG 4.3 Calculated and experimental dielectric constant as a function of applied frequency of multilayered PZT thin films.

Fig. 4.4 shows the hysteresis loop of PZT60, PZT40, and PZT multilayered thin film. Interesting to note, the P-E hysteresis loop of the PZT multilayered film is much inflated compared with that of single-phase PZT films, the same feature also observed in BTO/STO superlattices as discussed in 4.3.1. The remanent polarization $2P_r$ of the hysteresis loop of single-layer PZT60 and PZT40 thin films are about

$19\mu C/cm^2$ and $39\mu C/cm^2$, while the heterolayered PZT thin film exhibited a much larger remanent polarization value of $2P_r \approx 50\mu C/cm^2$.

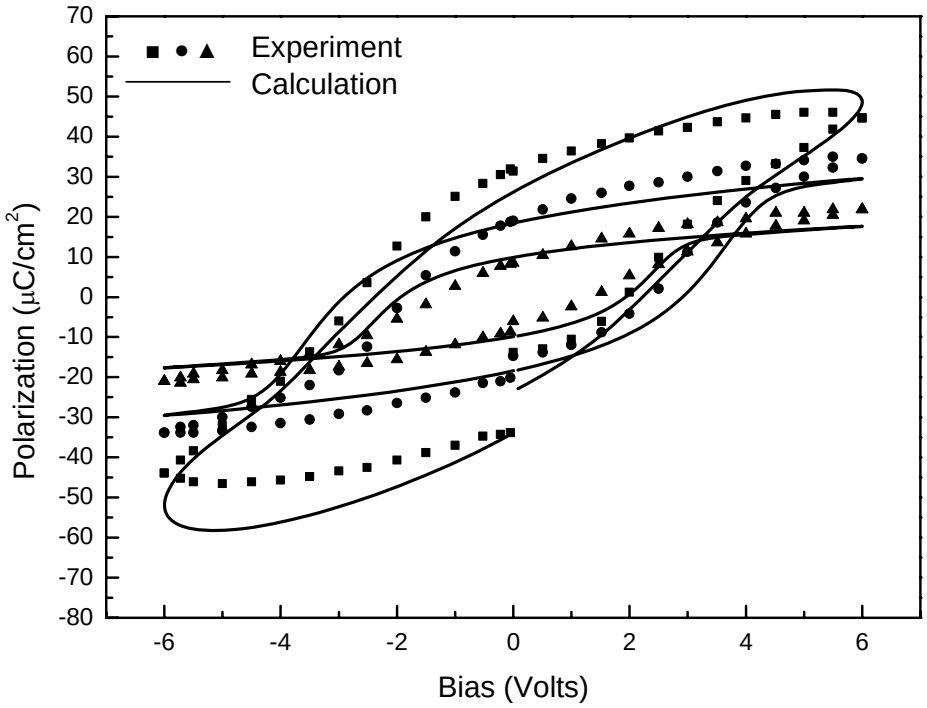

FIG 4.4 Calculated and experimental P-E hysteresis loops of PZT60 (▲), PZT40 (●), and multilayered PZT (■) thin films.

Summing up, a detailed discussion of the remanent polarization and dielectric permittivity of two typical ferroelectric superlattice systems: $BaTiO_3/SrTiO_3$ superlattice and multilayered $Pb(Zr,Ti)O_3$ thin films are given. For BTO/STO superlattices, the remanent polarization is found to be sensitively dependent on the macroscopic geometrical size (layer thickness) dimensions; the heterolayered PZT thin films made from alternating layers of PZT60 and PZT40 exhibit quite different

ferroelectric and dielectric properties compared with their single-phase thin films. Both ferroelectric superlattices show much larger remanent polarization values than their single-phase thin films, which can not be satisfactorily explained by traditional theoretical models. In addition, a remarkable enhancement of dielectric constant of PZT multilayered films is also given by our calculation.

In all, our theory is able to reproduce some key experimental features of BTO/STO superlattices and multilayered PZT thin films by taking the electrical conductivity into account. In addition, our model can be easily extended to study the temperature dependence of ferroelectric and dielectric properties of ferroelectric superlattices. However, further efforts are required to understand the dramatic improvement of dielectric properties found in some superlattice structures, which can be one or even several orders larger than the single-phase films of the constituent materials [Erbil *et al.*, 1996; Wang *et al.*, 2003].

Chapter 5 Electrostriction and magnetostriction of 0-3 composites

5.1 Introduction

It is shown in the previous chapters that electrical conductivity in ferroelectric thin films may lead to various anomalous phenomena which are difficult to understand by assuming perfectly insulating ferroelectrics. In fact, the considerations of electrical conductivity have also been demonstrated to be important to study the dielectric, pyroelectric and piezoelectric properties of ferroelectric 0-3 composites [Srinivasan *et al.*, 2004; Sakamoto *et al.*, 2002; Wong *et al.*, 2002]. In this chapter, we will show that electric conductivity also plays an important role in determining electrostriction strain characteristics of ferroelectric 0-3 composite systems. On the other hand, if we apply a magnetic field on the magnetostrictive composites, the magnetostrictive inclusion particles will deform under the applied magnetic field, thus giving a large magnetostriction effect. Therefore it is quite natural to extend our electrostriction model to study the 0-3 composites containing highly magnetostrictive inclusion particles. For convenience, following discussion of the electrostriction problem in each section (subsection) of this chapter, we extend our discussion to magnetostriction, which is very similar to the electrostriction model, to study the magnetostriction behavior for particulate composites of magnetostrictive polycrystalline inclusions in elastically isotropic matrices.

5.1.1 Electrostriction of 0-3 composites

Electrostriction is the effect of electric-field-induced strain in dielectric materials. It is distinguished from the inverse piezoelectric effect in that electrostrictive strain is proportional to the square of the applied electric field and occurs in all dielectric materials irrespective of the crystal symmetry. From a practical point of view, the mechanisms causing this effect include contributions from the electrostatic attraction between the electrodes and space charges injected from the electrodes as well as from the field-induced molecular structural change. The deformation can be exploited for devices such as actuators, microrobots, or other electromechanical transducers.

In the past, the electrostriction in polymeric materials has not attracted much attention due to their relatively low electrostrictive strains (0.01%) as well as their low strain energy density. However, in recent years, several polymers with large electrostrictive strain ($>3\%$) have been identified which include the thermoplastic elastomer polyurethane (PU) [Zhengyl *et al.*, 1994], the rubber polychloroprene [Ma, and Reneker, 1996], and the electron-irradiated ferroelectric copolymer poly(vinylidene fluoride-trifluoroethylene) P(VDF-TrFE) [Zhang *et al.*, 1998]. As far as is known, PU is a block copolymer composed of flexible long chain polyols and rigid diisocyanate components. The molecular chains are predominantly linear with the soft and hard segments distributed alternately. Phase separation usually occurs in the synthesis process. The hard segments segregate to form microphases dispersed in the nonpolar and flexible matrix. This two-phase feature with one phase in the microdomain structure has been regarded as being responsible for the large

electrostriction of PU. Nevertheless, due to the compliance of polymers, the electromechanical stress produced is not competitive with the ceramic counterpart. Thus the ceramic/polymer composites appear as a good alternative. A combination of two electroactive materials will result in composites that benefit from the advantages of both materials. In fact, the composites of lead zirconate titanate PZT/PVDF [Das-Gupta, 1991] and PZT/PU [Sakamoto *et al.*, 1999] had been studied extensively, in particular the latter one exhibits significantly large pyroelectric effect as well [Lam *et al.*, 2004]. It is obvious that there is still much research work toward clarifying the electromechanical mechanisms leading to the large strains and other interesting properties that may evolve from the electroactive ceramic/polymer composites.

In this chapter, we elucidate a method to account for the electrostriction strain of a 0-3 composite comprising ferroelectric ceramic particles embedded in a polymer matrix. The theory to be developed should be able to give a strain-electric field loop of a butterfly shape as observed in experiment, and in particular showing a smaller switching field and coercive field when the ceramic content increases.

5.1.2 Magnetostriction of 0-3 composites

Magnetostrictive composites containing highly magnetostrictive micro/nano particles have been a focus of sensor and actuator studies for a number of years [Sandlund *et al.*, 1994]. The addition of a matrix can provide increased mechanical strength and extend the high frequency application range. Although there is an

increasing emphasis on the practical development of such kinds of composites, further fundamental understanding of their magnetostrictive behavior is desirable. An often cited theoretical approach for the magnetostriction of such composites is the single-sphere model proposed by Herbst *et al* [Herbst *et al.*, 1997]. However, this simple model yields an incorrect prediction in the limit of only a single magnetostrictive phase. Recently, Nan and coworkers [Nan *et al.*, 1998; Nan and Weng, 1999] have developed a more rigorous but necessarily more complicated treatment for the effective magnetostriction of the magnetostrictive composites based on Green's function technique. More recently, a few simple expressions have been given based on simplified Reuss and Voigt type average approximations to describe the measured saturation magnetostriction of the composites [Chen *et al.*, 1999; Guo *et al.*, 2002].

Part of the objective of the present chapter is to develop a conceptually simple and convenient approach to model magnetostriction behavior for particulate composites of magnetostrictive polycrystalline inclusions in elastically isotropic matrices. For illustrative purposes, we calculate the magnetostriction responses of composites containing Terfenol-D and nickel. Through numerical calculation, we have obtained the macroscopic longitudinal strains parallel to the applied magnetic field for Terfenol-D/glass composite [Chen *et al.*, 1999] and both longitudinal and transverse strains for the nickel/epoxy composite [Nersessian *et al.*, 2004]. Detailed modeling procedures and comparison with experimental results are included in this chapter.

5.2 Theory

5.2.1 Our model on electrostriction strains of 0-3 composites

It is assumed that the 0-3 composites under consideration do not possess high ceramic loading so that the theory may be kept sufficiently simple. Our previous work [Wong *et al.*, 2002] has demonstrated that considerations of the effect of accumulated charge at the matrix-inclusion interface are essential to understanding some characteristics of ferroelectric 0-3 composites. Here we also employ the same conduction mechanism as described in Wong's paper [Wong *et al.*, 2002]. In addition, the composite is assumed to be free from external mechanical stresses. Since particles are assumed to be well dispersed within the matrix, we start by considering a single inclusion problem as depicted in Fig. 5.1.

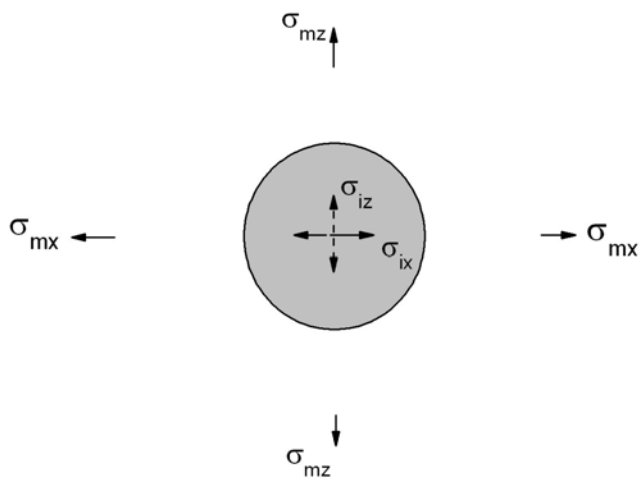

FIG. 5.1 Schematic diagram to show a single inclusion in the matrix under stresses in the x, y, and z directions. The y-direction stress not shown in the graph is perpendicular to the paper.

The ceramic particles are surrounded by the matrix medium in which asymptotic

uniform stresses σ_{mx}, σ_{my}, σ_{mz} act in the *x*, *y*, *z* directions, respectively. Within the particle, the corresponding stresses $\sigma_{ix,}$ $\sigma_{iy,}$ σ_{iz} are uniform. In the region close to the particle the stresses in the matrix become non-uniform due to the presence of the particle [Goodier, 1933]. The stresses and deformation in the matrix and in the inclusion have to be matched at the matrix-inclusion interface. Since both the elasticity equations and the interface conditions are linear equations involving stresses and deformation, it is therefore possible to relate the asymptotic matrix stresses and strains to the uniform stresses and strains in the inclusion. A similar approach but in a dielectric context has been employed in previous works [Landau and Lifshitz, 1960; Wong *et al.*, 2001]. Thus

$$\sigma_{ix} - \sigma_{mx} = A \times (e_{ix} - e_{mx}) + B \times (e_{iy} - e_{my}) + B \times (e_{iz} - e_{mz}) \tag{5.1}$$

$$\sigma_{iy} - \sigma_{my} = B \times (e_{ix} - e_{mx}) + A \times (e_{iy} - e_{my}) + B \times (e_{iz} - e_{mz}) \tag{5.2}$$

$$\sigma_{iz} - \sigma_{mz} = B \times (e_{ix} - e_{mx}) + B \times (e_{iy} - e_{my}) + A \times (e_{iz} - e_{mz}) \tag{5.3}$$

where e_k $(k = x, y, z)$ is strain, *i* and *m* denote inclusion and matrix, respectively. The constants *A* and *B* may be solved by employing Eqs.(5.1), (5.2) and (5.3) in special cases such as hydrostatic compression [Chew *et al.*, 2003], pure shear [Christensen, 1979] and simple tension [Goodier, 1933]. After some manipulation, we get the coefficients *A* and *B* which depend on the matrix elastic properties only [Appendix A]:

$$A = \frac{10}{9}\mu_m(-3 + \frac{2\mu_m}{k_m + 2\mu_m}) \tag{5.4}$$

$$B = \frac{1}{9}\mu_m(-3 - \frac{10\mu_m}{k_m + 2\mu_m}) \tag{5.5}$$

where k_m and μ_m are the bulk modulus and shear modulus, respectively.

The results of the single inclusion problem are now extended to a composite with a dilute suspension of inclusion particles to allow the electrostriction strain to be solved in terms of the dielectric and elastic properties of its constituents. Since we assume the composite is subjected to an electric field in the z direction in our problem, we only need to be concerned with the variables in the z direction and (say) x direction due to the transverse isotropy since $\sigma_{ix} = \sigma_{iy}$, $\sigma_{mx} = \sigma_{my}$, $e_{ix} = e_{iy}$ and $e_{mx} = e_{my}$. Thus:

$$\sigma_{ix} - \sigma_{mx} = (A + B) \times (e_{ix} - e_{mx}) + B \times (e_{iz} - e_{mz}) \tag{5.6}$$

$$\sigma_{iz} - \sigma_{mz} = 2B \times (e_{ix} - e_{mx}) + A \times (e_{iz} - e_{mz}) \tag{5.7}$$

The constitutive equations including electrostriction effect for the two materials are given by:

$$\sigma_{ix} = (2k_i + \frac{2}{3}\mu_i)e_{ix} + (k_i - \frac{2}{3}\mu_i)e_{iz} - f_{ix}(E_i) \tag{5.8}$$

$$\sigma_{mx} = (2k_m + \frac{2}{3}\mu_m)e_{mx} + (k_m - \frac{2}{3}\mu_m)e_{mz} - f_{mx}(E_m) \tag{5.9}$$

$$\sigma_{iz} = (2k_i - \frac{4}{3}\mu_i)e_{ix} + (k_i + \frac{4}{3}\mu_i)e_{iz} - f_{iz}(E_i) \tag{5.10}$$

$$\sigma_{mz} = (2k_m - \frac{4}{3}\mu_m)e_{mx} + (k_m + \frac{4}{3}\mu_m)e_{mz} - f_{mz}(E_m) \tag{5.11}$$

where $f_x(E)$ and $f_z(E)$ denote the electric field induced stresses perpendicular and parallel to the applied field direction, respectively. For a given material the form of the function $f(E)$ may be determined from experiment, usually for the case of zero external stress, i.e. $\sigma = 0$. Since the composite in our problem is assumed to be free from external mechanical stresses, we get:

$$\phi\sigma_{ix} + (1-\phi)\sigma_{mx} = 0 \tag{5.12}$$

$$\phi\sigma_{iz} + (1-\phi)\sigma_{mz} = 0 \tag{5.13}$$

The strain of the composite in the z-direction is calculated by:

$$\phi e_{iz} + (1-\phi)e_{mz} = e_z \tag{5.14}$$

where ϕ denotes the inclusion volume fraction.

Since our previous work has shown that electrical conductivity is essential to understanding the behavior of ferroelectric composites, we also need to include its effect in our present model. Hence the time evolution of E_i is written as [Wong *et al.*, 2002]:

$$\frac{\partial E_i}{\partial t} + \frac{E_i}{\tau} = \frac{3[\zeta_m E + \varepsilon_m \partial E/\partial t] - (1-\phi)\partial[P_i - P_m]/\partial t}{\phi 3\varepsilon_m + (1-\phi)(\varepsilon_i + 2\varepsilon_m)} \tag{5.15}$$

where

$$\tau = \frac{\phi 3\varepsilon_m + (1-\phi)(\varepsilon_i + 2\varepsilon_m)}{\phi 3\zeta_m + (1-\phi)(\zeta_i + 2\zeta_m)} \tag{5.16}$$

and ζ is the electric conductivity.

5.2.2 Magnetostriction model

Consider elastically isotropic magnetostrictive spherical inclusion particles embedded in an infinite, elastically isotropic, nonmagnetostrictive matrix, with a uniform magnetic field H applied along the z direction sufficiently far away from the inclusion. Young's modulus and Poisson's ratio for the inclusion (matrix) are $Y_i(Y_m)$ and $\nu_i(\nu_m)$, respectively. Bulk and shear moduli for the inclusion (matrix) are k_i (k_m) and μ_i (μ_m), respectively. The magnetic permeabilities of the inclusion and matrix are ξ_i and ξ_m, respectively. Since the matrix is

nonmagnetostrictive, ξ_m is assumed to be ξ_0 (the vacuum magnetic permeability) in the following calculations. The volumetric averaging of quantities (such as magnetic flux density *B*) is defined by:

$$\langle B_{gl} \rangle = \frac{1}{V} \int_V B_{gl} dV \ , \tag{5.17}$$

where the subscript $l = x, y, z$ refers to the three directions and *V* is the volume; $g = i, m$ denote inclusion and matrix, respectively.

The constitutive magnetostatic equations are:

$$\langle B_{iz} \rangle = \xi_0 \langle H_{iz} \rangle + \langle M_{iz} \rangle \ , \tag{5.18}$$

$$\langle B_{mz} \rangle = \xi_m \langle H_{mz} \rangle \ , \tag{5.19}$$

where $\langle M \rangle$ is the volumetric averaged magnetization.

The volumetric averaged magnetic field of the composite is calculated by:

$$\langle H_z \rangle = \phi \langle H_{iz} \rangle + (1-\phi) \langle H_{mz} \rangle \ , \tag{5.20}$$

where ϕ denotes the inclusion volume fraction.

The boundary conditions for the single inclusion problem give the following equation (Appendix B):

$$\langle B_{iz} \rangle - \langle B_{mz} \rangle = -2\xi_m (\langle H_{iz} \rangle - \langle H_{mz} \rangle) \ . \tag{5.21}$$

We assume that the induction field experienced by a single particulate in a composite is the sum of two parts: one due to the pure medium and the other due to the magnetization of the particulates embedded in the medium. A similar approach but in a dielectric context has been employed in a previous work [Poon and Shin, 2004]. Thus Eq. (5.21) becomes:

$$\langle B_{iz} \rangle - \langle B_{mz} \rangle' = -2\xi_m (\langle H_{iz} \rangle - \langle H_{mz} \rangle) \ , \tag{5.22}$$

where

$$\langle B_{mz}\rangle' = \langle B_{mz}\rangle + \phi(\langle B_{iz}\rangle - \xi_m \langle H_{iz}\rangle) \ . \tag{5.23}$$

From (5.18)-(5.23), (note that $\xi_m = \xi_0$, because we have assumed that the pure matrix material is nonmagnetic), we get

$$\langle H_z\rangle - \langle H_{iz}\rangle = \frac{(1-\phi)^2}{3\xi_0}\langle M_{iz}\rangle \ , \tag{5.24}$$

which relates the inclusion magnetic field to the applied magnetic field.

Here, for the elasticity part of the composite problem, the results of the elastic part of our electrostriction model as shown in Eqs. (5.1-5.7) are now employed to find the effective elastic properties of the 0-3 composite, but bearing in mind that we need to extend the theory to make it applicable up to high volume fraction of inclusions. For this we assume that the inclusion particles are surrounded by a “matrix” material which has the same effective elastic properties as the whole composite material. Thus Eqs. (5.6-5.7) become

$$\langle \sigma_{ix}\rangle - \langle \sigma_x\rangle = (A+B)\times(\langle e_{ix}\rangle - \langle e_x\rangle) + B\times(\langle e_{iz}\rangle - \langle e_z\rangle) \ , \tag{5.25}$$

$$\langle \sigma_{iz}\rangle - \langle \sigma_z\rangle = 2B\times(\langle e_{ix}\rangle - \langle e_x\rangle) + A\times(\langle e_{iz}\rangle - \langle e_z\rangle) \ , \tag{5.26}$$

and the coefficients A and B are replaced by:

$$A = \frac{10}{9}\mu(-3 + \frac{2\mu}{k+2\mu}) \ , \tag{5.27}$$

$$B = \frac{1}{9}\mu(-3 - \frac{10\mu}{k+2\mu}) \ , \tag{5.28}$$

where k and μ denote the effective bulk and shear moduli of the composite, respectively.

The following “self-consistent” equations for k and μ are derivable from

(5.25)-(5.28) [Appendix C]:

$$\frac{3}{3k+4\mu}=\frac{3\phi}{3k_i+4\mu}+\frac{3(1-\phi)}{3k_m+4\mu}\ , \tag{5.29}$$

$$\frac{3\phi k_i}{3k_i+4\mu}+\frac{3(1-\phi)k_m}{3k_m+4\mu}+5[\frac{\phi\mu_m}{\mu-\mu_m}+\frac{(1-\phi)\mu_i}{\mu-\mu_i}]+2=0\ , \tag{5.30}$$

which are the same with Hill's equations [Hill, 1965].

The constitutive equations including magnetostriction effect for the two materials are given by:

$$\langle\sigma_{ix}\rangle=(2k_i+\frac{2}{3}\mu_i)\langle e_{ix}\rangle+(k_i-\frac{2}{3}\mu_i)\langle e_{iz}\rangle-f_x(H_i)\ , \tag{5.31}$$

$$\langle\sigma_{mx}\rangle=(2k_m+\frac{2}{3}\mu_m)\langle e_{mx}\rangle+(k_m-\frac{2}{3}\mu_m)\langle e_{mz}\rangle\ , \tag{5.32}$$

$$\langle\sigma_{iz}\rangle=(2k_i-\frac{4}{3}\mu_i)\langle e_{ix}\rangle+(k_i+\frac{4}{3}\mu_i)\langle e_{iz}\rangle-f_z(H_i)\ , \tag{5.33}$$

$$\langle\sigma_{mz}\rangle=(2k_m-\frac{4}{3}\mu_m)\langle e_{mx}\rangle+(k_m+\frac{4}{3}\mu_m)\langle e_{mz}\rangle\ , \tag{5.34}$$

where $f_x(H_i)$ and $f_z(H_i)$ denote the magnetic field induced stresses perpendicular and parallel to the applied field (assumed to point in z direction) in the magnetostrictive inclusions, respectively. Since the composite in our problem is assumed to be free from external mechanical stresses, although it may be subjected to an external magnetic field, we get:

$$\phi\langle\sigma_{ix}\rangle+(1-\phi)\langle\sigma_{mx}\rangle=0\ , \tag{5.35}$$

$$\phi\langle\sigma_{iz}\rangle+(1-\phi)\langle\sigma_{mz}\rangle=0\ . \tag{5.36}$$

The strain of the composite in the z-direction is calculated by:

$$\phi\langle e_{iz}\rangle+(1-\phi)\langle e_{mz}\rangle=\langle e_z\rangle\ . \tag{5.37}$$

To use (5.31) and (5.33), the magnetostriction response functions $f(H_i)$'s for the inclusion material have to be determined. First, we use (5.24) to calculate the

inclusion magnetic field from the applied magnetic field. Herein, the magnetization-field relationship should be known or determined from experimental measurements. Then we can determine $f(H_i)$'s by comparing with measured longitudinal and transverse strains of the pure material, usually under zero external stresses, ie. $\sigma_x = \sigma_y = \sigma_z = 0$. Once the magnetostriction response functions $f(H_i)$'s are obtained, the magnetostrictive strains of the composites $\langle e_z \rangle$ under an applied magnetic field can be calculated from (5.25) to (5.37) for a given composite system.

5.3 Results and discussion

5.3.1 Modeling parameters and simulation results for electrostriction

To verify our electrostriction model, we study the electrostriction behaviour of particulate PZT/PU composites in which the volume fraction of PZT ranges from 5%, 13%, 18%, 26%, and 30%. TABLE 5.1 shows the permittivities, conductivities, ferroelectrics and elastic properties for the constituents used in this computation.

TABLE 5.1 Properties of constituents for PZT/PU 0-3 composites

	ε	$\zeta(\Omega^{-1}m^{-1})$	$P_r(C/m^2)$	$P_s(C/m^2)$	$E_c(MV/m)$	$Y(Gpa)$	ν
PZT	1800^a	5×10^{-12c}	0.35^b	0.4^b	0.667^b	36^e	0.3^e
PU	6.8^b	9×10^{-10d}	–	–	–	0.03^e	0.495^e

[a]Tai, L.S., *M. Phil. Thesis*, The Hong Kong Polytechnic University, (2001).

[b]Wong, Y.W., Liu, C.X., Tai, L.S. and Shin F.G., *Proceeding of The International Society for Optical Engineering*, Vol. 4329, pp. 516-519 (2001).

[d]Chan, H.L.W., Chen, Y. and Choy, C.L. *Integrated Ferroelectrics*, Vol. 9, pp. 207-214 (1995).

[d]Mark, J.E. *Polymer Data Handbook*, Oxford, New York, pp. 874 (1999).

[e]Furukawa, T., Fujino, K. and Fukada, E. *Japanese Journal of Applied Physics*, Vol. 15, pp. 2119-2129 (1976).

In our calculation, $P_m = 0$ because PU is not ferroelectric while P_i is generally not a simple function of E_i. We assume that the PZT particles are fully polarized initially, i.e, $P_i(t=0) = -P_{r,i}$ where r denotes "remanent". The model for a saturated hysteresis loop of a ferroelectric adopted in this calculation is [Miller *et al.*, 1990]:

$$P_i = P_{s,i} \tanh[\frac{E_i - E_{c,i}}{2E_{c,i}} ln(\frac{1+P_{r,i}/P_{s,i}}{1-P_{r,i}/P_{s,i}})] \tag{5.38}$$

when Eq. (5.38) is substituted into Eq. (5.15), the relation $\frac{\partial P_i}{\partial t} = \frac{\partial P_i}{\partial E_i}\frac{\partial E_i}{\partial t}$ is employed. To use Eqs. (5.8) to (5.11), the electrostriction functions $f(E)'s$ have to be determined. This is ideally done by comparing with measured longitudinal and transverse strains of the pure materials subjected to electric fields, usually under zero external stresses, ie. $\sigma_x = \sigma_y = \sigma_z = 0$. Experimental data on the transverse electrostrictive strain responses of PU and PZT are not readily available in the literature. Therefore, in the present study the ratios of the transverse strain to longitudinal strain of PU and PZT in the range -0.1 to -10 were tried in Eqs. (5.8) to (5.11) for fitting the experimental longitudinal strains. It is found that the calculated results actually do not depend on the ratio very sensitively (only differ a little in the final electrostrictive strain response magnitudes).

Fig. 5.2 shows the experimental (a) and calculated (b) strain-electric field curves of PZT/PU composites with different volume fractions of PZT. Our simulation gives a strain-electric field loop of a butterfly shape as observed in experiment. From Fig. 5.2 (b) we can see that the switching fields of the composites under applied electric fields decrease while the electrostriction strain magnitudes increase with increasing PZT volume fraction, which is in good agreement with the experiment. Although differing a little in strain magnitudes and shapes especially for $\phi = 0.13$, our simulation results show the key experimental features.

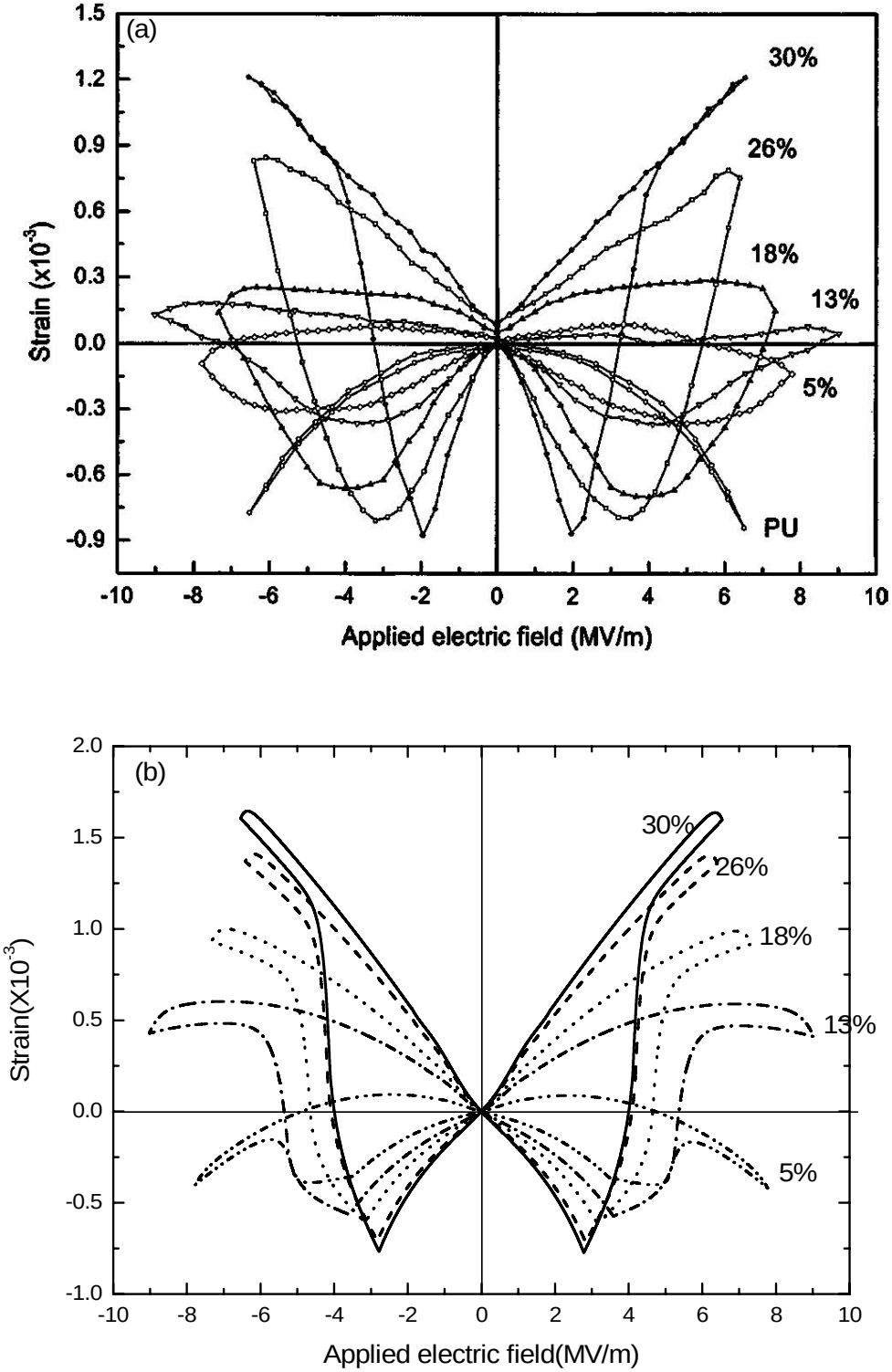

FIG. 5.2 The experimental (a) and calculated (b) curves for the electrostrictive strains of PZT/PU composites of various PZT volume fractions.

5.3.2 Comparison with experimental data of magnetostriction

To verify our magnetostriction model, we perform numerical calculations for the magnetostrictive composites of Terfenol-D/glass and nickel/epoxy reported in [Chen *et al.*, 1999a] and [Nersessian *et al.*, 2004] and compare with experimental data therein. The properties of the constituent phases used for calculations are given in Table 5.2. To find bulk and shear moduli from Y and ν, use is made of the following equations: $\mu = \dfrac{Y}{2(1+\nu)}$ and $k = \dfrac{Y}{3(1-\nu)}$.

TABLE 5.2 Properties of Terfenol-D and nickel magnetostrictive polycrystallites, and of glass and epoxy matrices used in the present numerical calculations

	Terfenol-D[a,b]	glass[b]	nickel[c]	epoxy[a]
Y (GPa)	30	50	210	2.8
ν	0.3	0.2	0.31	0.4
ξ/ξ_0	5	1	250	1

[a]Armstrong, W.D. *Journal of Intelligent Materials Systems and Instructures*, vol. 13, pp. 137-141, (2002).

[b]Chen, Y. Snyder, J.E., Schwichtenberg, C.R., Dennis, K.W., Falzgraf, D.K., McCallum, R.W. and Jiles, D.C. *Applied Physics Letters*, vol. 74, pp. 1159-1161, (1999).

[c] Bozorth, R.M. *Ferromagnetism*, Princeton, New Jersey, USA: Van Nostrand, pp. 269-275 (1968).

According to [Chen *et al.*, 1999a], Terfenol-D/glass composites were prepared by blending Terfenol-D and glass powder in a prescribed ratio. Then the powder was pressed and heated under argon atmosphere. At the end, the material was cooled to ambient temperature while maintaining the argon atmosphere. In another related reference [Nersessian *et al.*, 2004], the nickel/epoxy composite was fabricated by combining solid nickel microspheres with viny1 ester epoxy resin. However, the authors did not mention about any porosity in both cases, so when we use their data

we take the volume fraction values as reported without correcting for porosity.

The relevant magnetostriction response functions $f(H_i)$'s for each case have to be determined. Fig. 5.3 (a) shows the longitudinal magnetostriction of pure Terfenol-D (assumed polycrystalline) deduced from the experimental data of the composite having 60% volume fraction of Terfenol-D in [Chen *et al.*, 1999a]. Data on the transverse magnetostrictive strain responses of polycrystalline Terfenol-D are not readily available in the literature although some relevant information is contained in e.g. [Dong *et al.*, 2004] and [Duenas *et al.*, 2000]; we have therefore tried using the ratio of transverse strain to longitudinal strain of Terfenol-D in the range -0.1 to -10 in Eqs. (5.31) and (5.33) to calculate the longitudinal strain of Terfenol-D/glass composite, and found that the calculated results actually do not depend on the ratio sensitively (only differ a little in the final longitudinal magnetostrictive response magnitudes). Fig. 5.3 (b) shows a comparison between the calculations and reported experimental data [Chen *et al.*, 1999a] for the magnetostriction of elastically isotropic Terfenol-D/glass composite. Good agreement up to 80% volume fraction of Terfenol-D with the experimental data is obtained: most data points fall on the predicted lines, even for the composite with highest Terfenol-D content. Note that we have also tried to deduce from [Chen *et al.*, 1999a] the longitudinal magnetostriction of pure Terfenol-D from the experimental curve corresponding to other volume fractions of Terfenol-D, and found that the calculated results are equally satisfactory.

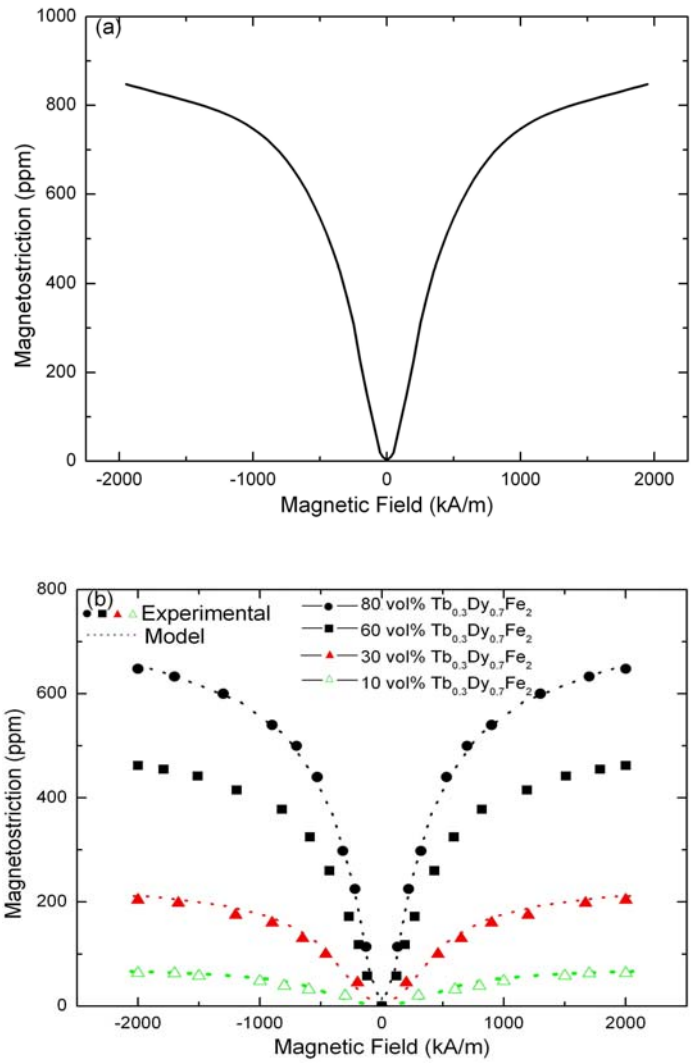

FIG. 5.3 (a) The longitudinal magnetostriction of pure Terfenol-D deduced from the experimental data of the composite having 60% volume fraction of Terfenol-D; (b) Measured and modeled results for longitudinal magnetostriction of several composites with different volume fractions of $Tb_{0.3}Dy_{0.7}Fe_2$ in glass matrix material.

For the nickel/epoxy composite of [Nersessian et al., 2004], the experimental longitudinal and transverse strains of nickel subjected to magnetic fields under zero external stresses are taken from [Bozorth, 1968] and shown in Fig. 5.4 (a). Hence the magnetostriction functions $f(H_i)$'s can be determined from Eqs. (5.31) and (5.33). Fig. 5.4 (b) shows a comparison of our theory prediction with experimental

data [Nersessian et al., 2004] for the nickel/epoxy composite containing 35% volume fraction of nickel particles. Our predicted longitudinal and transverse strain magnitudes are a little larger for small magnetic field ($\leq 75kA/m$) as well as a little smaller for large field than the experimental results. However, the magnitudes as well as the trends of the predicted lines are in fairly good agreement with the measured values for both longitudinal and transverse strains of this nickel/epoxy composite.

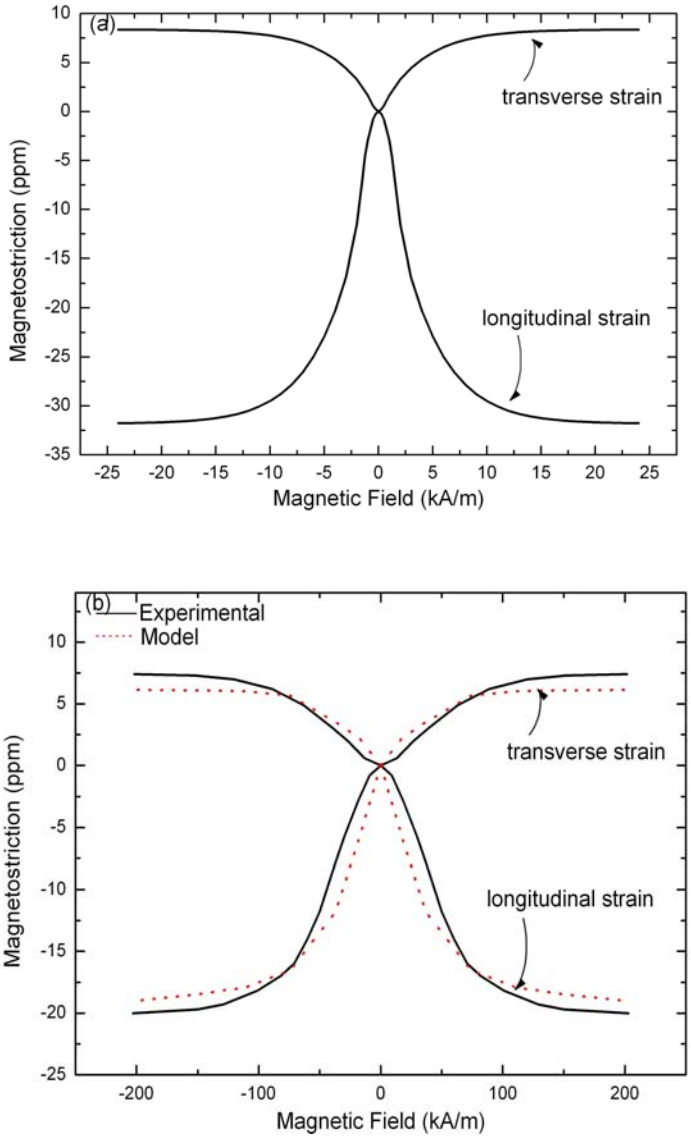

FIG. 5.4 (a) The experimental longitudinal and transverse strains of nickel subjected to magnetic fields under zero external stresses; (b) Measured and modeled results for longitudinal and transverse magnetostrictive strains as a function of magnetic field for nickel/epoxy composite.

The foregoing satisfactory comparison of theory with experiment shows that basically our treatment of the magnetostriction of a composite is quite adequate and that all the key physical concepts are already incorporated into the theoretical consideration. The next chapter uses a similar treatment on the magnetostriction of a composite, but there the matrix is piezoelectric, to investigate the magnetoelectric effect.

Chapter 6 Magnetoelectric effect of mildly conducting magnetostrictive/piezoelectric particulate composites

6.1 Introduction

The magnetostriction model proposed in the previous chapter (chapter 5) is now extended to study magnetoelectric (ME) effect of mildly conducting magnetostrictive/piezoelectric 0-3 composites in this chapter. The magnetoelectric (ME) effect is characterized by the appearance of dielectric polarization in a material under an applied magnetic field, which can be used in various applications such as magnetic-electric sensors and microwave electronics [Bracke and Vanvliet, 1981]. Several magnetoelectric single phase materials have been discovered since the first experimental observation of linear ME effect in the antiferromagnetic Cr_2O_3 crystal in 1960 [Folen *et al.*, 1961]. However, these single phase materials have not found much technological uses currently due to the fact that they mostly exhibit a very weak ME effect, and most of them have Neel or Curie temperature far below room temperature. Recently, magnetostrictive-piezoelectric layered and bulk composites have attracted much interest because they can exhibit a much stronger ME effect in a wide temperature range. Interestingly, at low frequencies and away from the resonance values, it was found that the measured ME effects strongly depended on the conductivity of the inclusion/matrix materials or, alternatively, on the applied frequency. Srinivasan *et al.* reported an enhancement in the strength of ME effect by adding cobalt oxide to the nickel ferrite that resulted in orders of magnitude increase

in the resistivity of the bulk nickel ferrite and barium lead zirconate titanate (BLZT) composites [Laletin and Srinivasan, 2002; Srinivasan *et al.*, 2004]. Nan *et al.* observed an increase in magnetoelectric voltage coefficient of bulk composites of NFO/PZT with increasing frequency in the whole range of 1-500 kHz [Zeng et al., 2004; Zhai *et al.*, 2004]. However, to the best of our knowledge, most of the theoretical investigations of magnetoelectric effect are rather focused on layered structures than particulate composites. In addition, none of the suggested models have explicitly taken the effect of conductivity into account, and hence cannot discuss the influence of the constituent's electrical conductivity on the ME effect.

In this chapter, we propose a relatively simple model to study the ME effect and its dependence on the conductivities of both inclusion and matrix phases of dilute 0-3 particulate composites in which the size of the inclusion particles are not too small as to cause complicated interfacial effects. For illustration the ME voltage coefficients of NFO/PZT are calculated and compared with experimental results reported in [Zhai *et al.*, 2004]. The present model is also applicable to other magnetoelectric particulate composite systems such as bulk composites of cobalt ferrite (CFO) and PZT.

6.2 Theory

Consider the magnetostrictive spherical inclusion particles embedded in piezoelectric matrix, with a uniform magnetic field H applied along the z direction. Bulk and shear moduli for the inclusion (matrix) are k_i (k_m) and μ_i (μ_m), respectively. The magnetic permeabilities of the inclusion and matrix material are ξ_i and ξ_0 (the vacuum magnetic permeability), respectively. The volumetric averaging of quantities (such as magnetic flux density B) is defined by:

$$\langle B_{gl} \rangle = \frac{1}{V}\int_V B_{gl} dV \ , \tag{6.1}$$

where $g = i, m$ denote inclusion and matrix, respectively; the subscript $l = x, y, z$ refers to the three coordinate directions and V is the volume. The constitutive magnetostatic equations are:

$$\langle B_{iz} \rangle = \xi_i \langle H_{iz} \rangle + \langle M_{iz} \rangle \ , \tag{6.2a}$$

$$\langle B_{mz} \rangle = \xi_0 \langle H_{mz} \rangle \ , \tag{6.2b}$$

where $\langle H \rangle$, $\langle M \rangle$ and $\langle B \rangle$ are the volumetric averaged magnetic field, magnetization, and flux density.

The volumetric averaged magnetic field and flux density of the composite are calculated by:

$$\langle H_z \rangle = \phi \langle H_{iz} \rangle + (1-\phi) \langle H_{mz} \rangle \ , \tag{6.3a}$$

$$\langle B_z \rangle = \phi \langle B_{iz} \rangle + (1-\phi) \langle B_{mz} \rangle \ , \tag{6.3b}$$

where ϕ denotes the inclusion volume fraction.

The boundary value problem gives the following equation [Zhou and Shin, 2005]:

$$\langle B_{iz}\rangle - \langle B_{mz}\rangle = -2\xi_0(\langle H_{iz}\rangle - \langle H_{mz}\rangle) \ . \tag{6.4}$$

From Eqs. (6.2)-(6.4), we get

$$\left[2+\phi+\xi_i(1-\phi)/\xi_0\right]\langle H_{iz}\rangle + (1-\phi)\langle M_{iz}\rangle = 3\langle H_z\rangle \ , \tag{6.5}$$

which relates the inclusion magnetic field to the applied magnetic field.

The magnetostrictive inclusion particles will deform under the application of external magnetic field, thus exerting forces on the piezoelectric matrix material, giving a piezoelectric signal. The strain-stress relationships can be solved by employing elastic theory in the inclusion and matrix, and matching boundary conditions at the interface. Since we assume the composite is subjected to a magnetic field in the z direction in our problem, we only need to be concerned with the variables in the z direction and (say) x direction due to the transverse isotropy since $T_{ix} = T_{iy}, T_{mx} = T_{my}, e_{ix} = e_{iy}$ and $e_{mx} = e_{my}$, where T and e are the stress and strain, respectively. The constitutive equations including magnetostriction effect for the two materials are given by [Zhou and Shin, 2005]:

$$\langle T_{gl}\rangle = (k_g - \frac{2}{3}\mu_g)\langle 2e_{gx} + e_{gz}\rangle + 2\mu_g\langle e_{gl}\rangle - f_{gl}(H_g) \ , \tag{6.6}$$

where $f_{gl}(H_g)$ denotes the magnetic field induced stresses perpendicular (l=x) and parallel (l=z) to the applied field in the magnetostrictive inclusions if g=i; $f_{gl}(H_g)$ is assumed to be zero for g=m since we have assumed that the pure matrix material is nonmagnetostrictive.

The elasticity equations are:

$$\langle T_{ix}\rangle - \langle T_{mx}\rangle = (A+B)\times(\langle e_{ix}\rangle - \langle e_{mx}\rangle) + B\times(\langle e_{iz}\rangle - \langle e_{mz}\rangle) \ , \tag{6.7a}$$

$$\langle T_{iz}\rangle - \langle T_{mz}\rangle = 2B\times(\langle e_{ix}\rangle - \langle e_{mx}\rangle) + A\times(\langle e_{iz}\rangle - \langle e_{mz}\rangle) \ , \tag{6.7b}$$

and the coefficients A and B are given by [Zhou and Shin, 2005]:

$$A = \frac{10}{9}\mu_m(-3 + \frac{2\mu_m}{k_m + 2\mu_m}) , \tag{6.8a}$$

$$B = \frac{1}{9}\mu_m(-3 - \frac{10\mu_m}{k_m + 2\mu_m}) . \tag{6.8b}$$

Since the composite in our ME effect problem is assumed to be free from external mechanical stresses, although it may be subjected to an external magnetic field, we also have:

$$\phi\langle T_{il}\rangle + (1-\phi)\langle T_{ml}\rangle = 0 . \tag{6.9}$$

As mentioned earlier there are experimental indications that electrical conductivity may play a subtle role in the ME effect of magnetoelectric composites, we therefore include conductivity effects in our present model. Hence the time evolution of E_i is written as [Wong *et al.*, 2002]:

$$\frac{\partial\langle E_i\rangle}{\partial t} = \frac{3[\sigma_m\langle E\rangle + \varepsilon_m\partial\langle E\rangle/\partial t] + (1-\phi)\partial\langle P_m\rangle/\partial t - [\phi 3\sigma_m + (1-\phi)(\sigma_i + 2\sigma_m)]\langle E_i\rangle}{\phi 3\varepsilon_m + (1-\phi)(\varepsilon_i + 2\varepsilon_m)} \tag{6.10}$$

where σ is electric conductivity and $\langle P_m\rangle = d_{33}\langle T_{mz}\rangle + 2d_{31}\langle T_{mx}\rangle$ is the electric polarization induced by stresses in the piezoelectric matrix. d_{33} and d_{31} are the longitudinal and transverse piezoelectric constants of the matrix material, respectively.

There are usually two kinds of methods for measuring the ME voltage coefficient $\alpha_E \equiv \delta E/\delta H$ when an ac magnetic field $H_{ac}\sin(2\pi ft)$ superimposed on a dc magnetic field H_{dc} is applied on the sample, where f is the applied frequency. One is measuring the charge $Q = A\times\int_0^t J(t)dt$ generated from the sample under a short circuit condition where A is the sample area and $J(t)$ is the total current (density)

flowing through the circuit; the output voltage is obtained from the charge and the capacitance of the composite using $V = Q/C$, and α_E is given by the measured voltage divided by the thickness of the sample and magnitude of the a.c. magnetic field. The other method measures the open circuit voltage across the sample, and the output voltage divided by the thickness and the a.c. magnetic field gives the ME voltage coefficient of the sample. Under the short circuit condition, *E=0*, and in the open circuit condition, *J=0*. The longitudinal ME voltage coefficient is calculated by:

$$\alpha_{E33} = -\frac{\left\{(\varepsilon_i + 2\varepsilon_m)(1-\phi)\partial\langle P_m\rangle/\partial t + 3\phi(\varepsilon_m\sigma_i - \varepsilon_i\sigma_m)E_i\right\}_{\cos 2\pi ft}}{\varepsilon\left[(1-\phi)\varepsilon_i + (2+\phi)\varepsilon_m\right]2\pi fH_{ac}}, \tag{6.11a}$$

for short circuit and for open circuit

$$\alpha_{E33} = -\frac{\left\{(\varepsilon_i + 2\varepsilon_m)(1-\phi)\partial\langle P_m\rangle/\partial t + \left[(1+2\phi)\varepsilon_i + 2(1-\phi)\varepsilon_m\right]\sigma_m E + 3\phi(\varepsilon_m\sigma_i - \sigma_m\varepsilon_i)E_i\right\}_{\cos 2\pi ft}}{\varepsilon_m\left[(1+2\phi)\varepsilon_i + 2(1-\phi)\varepsilon_m\right]2\pi fH_{ac}} \tag{6.11b}$$

where $\{\ \}_{\cos 2\pi ft}$ is the $\cos(2\pi ft)-$Fourier component of the function within the bracket.

Herein, we briefly describe the procedures for numerically calculating α_{E33}. The relevant magnetostriction response functions $f(H)$'s of the inclusion material have to be determined. We use experimental longitudinal and transverse strains of the pure inclusion material under zero external stresses to determine the $f(H_i)'s$ by Eq. (6.6). The electric polarization $\langle P_m\rangle$ induced by stresses in the piezoelectric matrix can then be calculated from Eqs. (6.5)-(6.9). Finally, the longitudinal ME voltage coefficient α_{E33} is numerically solved from Eqs. (6.10)-(6.11) for a given composite system.

6.3 Results and discussion

To verify our model, we perform numerical calculations for the particulate NFO/PZT composites reported in [Zhai *et al.*, 2004] and compare with experimental data for $\phi = 0.07$, 0.2 and 0.32 therein. The following parameters are adopted [Zhai *et al.*, 2004; Bichurin *et al.*, 2003; Chew *et al.*, 2003; Chan *et al.*, 1995; Liu and Gao, 2005; Said, 1998]: $k_i = 197GPa$, $\mu_i = 56GPa$, $k_m = 62.3GPa$, $\mu_m = 27.1GPa$, $d_{33} = 375pC/N$, $d_{31} = -175pC/N$, $\varepsilon_i = 10\varepsilon_0$, $\varepsilon_m = 1560\varepsilon_0$, $\xi_i = 3\xi_0$, $H_{ac} = 2Oe$, f=1kHz, $\sigma_i = 6\times10^{-6}\Omega^{-1}m^{-1}$, $\sigma_m = 5\times10^{-12}\Omega^{-1}m^{-1}$. The magnetostriction response functions are found by using data on the longitudinal and transverse magnetostrictive strain responses of polycrystalline NFO taken from [Bozorth *et al.*, 1955] (Fig. 6.1).

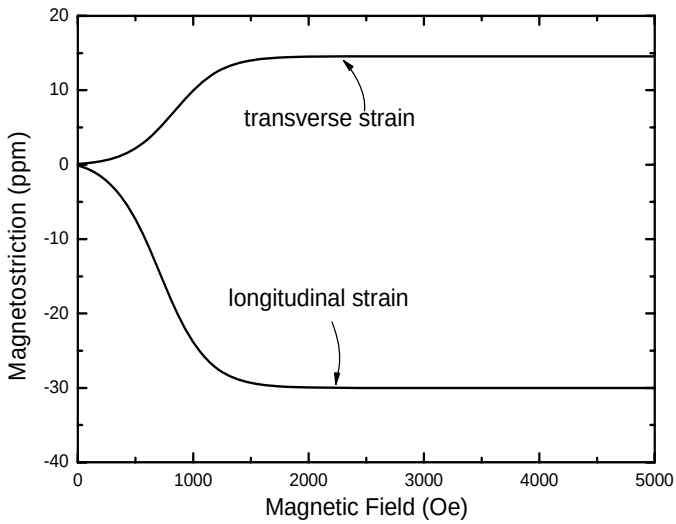

FIG. 6.1 The experimental longitudinal and transverse strains of NFO subjected to magnetic fields under zero external stresses.

Fig. 6.2 shows a comparison between the calculations by Eq. (6.11a) and reported experimental data [Zhai *et al.*, 2004] for the longitudinal magnetoelectric voltage coefficients of particulate NFO/PZT composites obtained by measuring the charge generated from the composites under short circuit condition. Good agreement up to

32% volume fraction of NFO with the experimental data is shown. Some key experimental features are reproduced by our calculation: α_{E33} increases with the volume fraction of NFO in the range $0\% < \phi < 32\%$, and the magnetic field values corresponding to maximum α_{E33} are about 1 kOe. It is noted that our calculation will give a much larger value, e.g. a peak value of 130 mV/cm Oe for the sample with 32% volume fraction of NFO, if no conductivity is considered. In addition, we have tried different conductivity values for the inclusion and matrix materials. It is also found that the theory will show a shift in the value of the magnetic field corresponding to maximum α_{E33} as the volume fraction increases, the same trend as observed in the experiments.

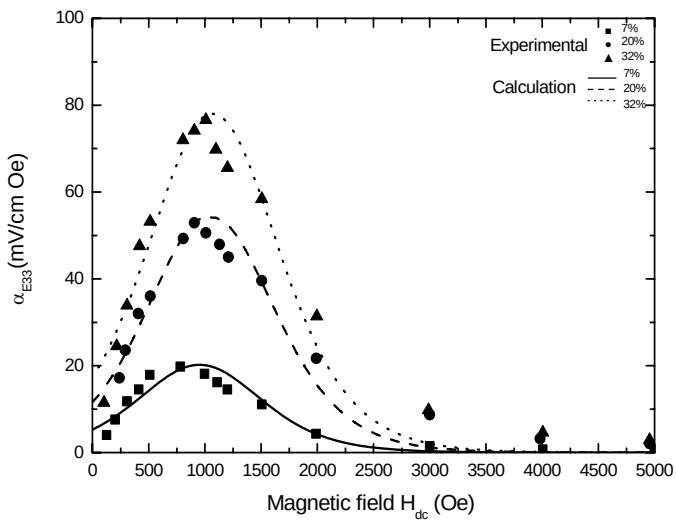

FIG. 6.2 Measured and calculated magnetic-field-dependent α_{E33} of NFO/PZT composites for $\phi = 0.07$, 0.2 and 0.32.

In recent experiments [Laletin and Srinivasan, 2002; Srinivasan, 2004], it is found that the measured ME voltage coefficients depended on the constituent's conductivity or, alternatively, the applied frequency, for bulk composites of NFO/PZT,

NZFO/PZT and NFO/BLZT by measuring the voltage induced under a small ac magnetic field. Fig. 6.3 elucidates the effects of electrical conductivity of the inclusion and matrix, respectively; the calculation is performed on the NFO/PZT system with $\phi = 10\%$. It is shown from the figure that the ME voltage coefficients decrease as the conductivity of the constituent materials increases. The resistivity of the composite will decrease with increasing conductivity of either inclusion or matrix, or both. Our calculation therefore demonstrates that larger resistance of the composite will enhance the ME effect and that the range over which notable ME effect is observed becomes smaller when decreasing the resistivity of the composites. These trends are observed in recent experiments with particulate composites of NZFO/PZT and NFO/BLZT [Laletin and Srinivasan, 2002; Srinivasan, 2004]. The solid line in Fig. 6.3 represents the calculated ME voltage coefficients by considering short circuit condition, which is about 1.5 times as large as the value under open circuit condition with the same electrical conductivities of constituents (the dashed line in Fig. 6.3). The absence of finite electrical conductivity in the materials should give the same values under the two different methods of calculation. Interesting to note, the calculated α_{E33} will gradually increase with increasing frequency *f*, a trend also experimentally observed in particulate composites [Zeng *et al.*, 2004]. From the above calculation results, we can see that the conductivity of either inclusion or matrix material is one of the possible key factors determining the magnetoelectric behavior of particulate composites.

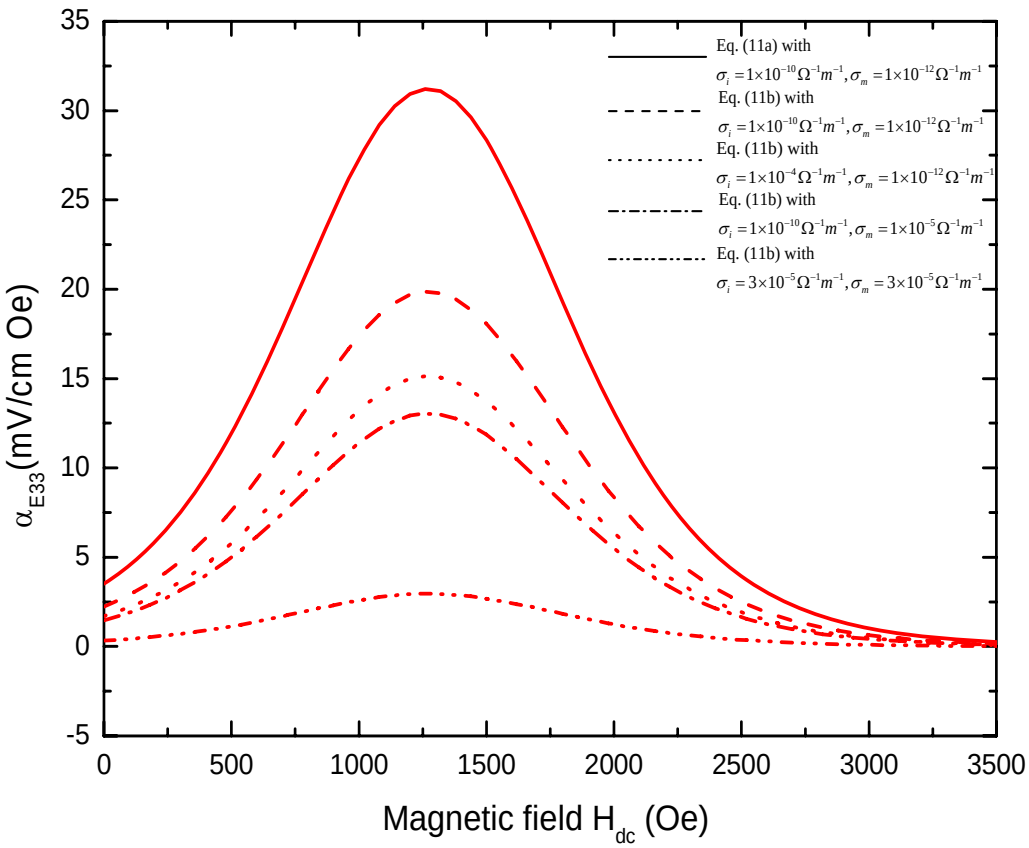

FIG. 6.3 The effects of inclusion and matrix conductivities on the calculated ME voltage coefficients.

Conclusions

We have been, in the first part of this project, focusing on the anomalous shift phenomena, namely vertical and horizontal shifts, widely observed in the hysteresis loop measurements of compositionally graded and other ferroelectric thin films. We have proposed a thermodynamic model to account for the possible origin of the polarization offsets observed in compositionally graded ferroelectric thin films and investigated the effects of polarization gradient, permittivity gradient, charge carrier mobility, film thickness on the vertical shift behavior of hysteresis loops of graded ferroelectrics by taking the TDSCL conduction into account. Our simulation results show that apart from polarization and permittivity gradients, the effects of charge carrier mobility and film thickness are also important factors determining the vertical offset behaviour. Although the cases discussed here are simplified and not exhaustive, they however represent reasonable first approximations to some possible variation in properties within realistic graded ferroelectric films (e.g. both P_r and ε are almost linearly varied with Zr concentration for the continuous compositionally graded $Pb(Zr_yTi_{1-y})O_3$ ferroelectric structures where y varies from 0.2 to 0.56). Our results indicate that the effect of vertical offset can be enhanced by the following conditions:

(1) The remanent polarization and permittivity gradients are in the same direction, and large enough within the graded ferroelectric;

(2) Either the positive or negative charge mobility is reasonably large, with a

nonzero difference between them;

(3) The film should be thin enough, e.g. $\leq 3\mu m$ for PZT.

Our simulation results are valid for films with continuous gradient, but should also be valid for films in which polarization increases or decreases in steps from one layer to the other. This study has provided direction for obtaining large vertical offsets in graded ferroelectric thin films for developing new applications. However, further efforts are required to understand the detailed charge dynamics of the shift mechanism.

On the other hand, the TDSCL conduction is also found likely to be one of the possible origins for the occurrence of imprint where large horizontal shifts of hysteresis loops are observed in experiments. A model has been introduced to explain the occurence of imprint phenomena widely reported in the literature. This model adopts the Landau-Khalatnikov equation to describe hysteresis behaviour and takes the TDSCL conductivity into account to investigate the effects of stress, domain pinning and degradation of ferroelectric properties at film/electrode surface. Our calculation produces the large horizontally shifted loops by considering the effects of stress and non-switching layers. The qualitative agreement between simulation and experiment supports the notion that imprint phenomena may originate from stress induced by lattice mismatch or clamping effect of the substrate, domain pinning induced by defect-dipole alignments, and/or the existence of graded surface layer. However, further efforts are needed to better understand the physics behind the imprint effect.

A detailed discussion of the remanent polarization and dielectric permittivity of two typical ferroelectric superlattice systems: $BaTiO_3/SrTiO_3$ superlattice and multilayered $Pb(Zr,Ti)O_3$ thin films are given. For BTO/STO superlattices, the remanent polarization is found to be sensitively dependent on the macroscopic geometrical dimension; the heterolayered PZT thin films made from alternating layers of PZT60 and PZT40 exhibit quite different ferroelectric and dielectric properties compared with their single-phase thin films. Both ferroelectric superlattices show much larger remanent polarization values than their single-phase thin films, which can not be satisfactorily explained by traditional theoretical models. In addition, a remarkable enhancement of dielectric constant of PZT multilayered films is also given by our calculation.

We have also investigated the electrostriction strain and the magnetostriction behavior of 0-3 composites. We elucidate a method to account for the electrostriction strain of a 0-3 composite comprising ferroelectric ceramic particles embedded in a polymer matrix. A model based on elasticity in association with the ferroelectricity of inclusion constituent is proposed to calculate the electrostrictive strain of the composite for various ceramic volume fractions. It successfully reveals all the essential features of the measured hysteretic electrostrictive strains of a composite system of ferroelectric PZT particles in nonferroelectric polyurethane matrix. These results encourage the extended application of the model to a system with ferroelectric matrix. On the other hand, we have also developed a conceptually simple and convenient approach to magnetostriction for particulate composites of

magnetostrictive inclusions in elastically isotropic, nonmagnetostrictive matrices. We have illustrated the model by calculating the effective elastic and magnetostrictive behaviors of Terfenol-D/glass and nickel/epoxy composites. Comparison with published experimental data indicates that good agreement up to very high volume fraction of inclusion particles has been achieved. Our magnetostriction model description appears to be useful in providing a general guide for the evaluation and technical improvement of magnetostrictive composites under development. The method can also be extended to model other inhomogeneous magnetostrictive materials to develop criteria for choosing the best combination of different constituent materials for magnetostrictive actuators and sensors.

This magnetostriction model is extendable to study the magnetoelectric (ME) effect of mildly conducting magnetostrictive/piezoelectric particulate composites by taking the constituents' Ohmic conductivity into account. We have proposed a relatively simple model to include the effect of electric conductivity in mildly conducting inclusion and matrix phases on the magnetoelectric effect of particulate composites comprising a dilute suspension of spherical magnetostrictive particles uniformly distributed in a piezoelectric matrix, for which our model has successfully reproduced some key characteristic experimental features. Our results may stimulate further interest in these kinds of materials for various applications. The study of particulate magnetoelectric composites with high inclusion volume fractions is very interesting because then the effective conductivity may increase rapidly with ϕ, implying the tendency of a decreasing α_E with higher ϕ.

In summary, we have included the effect of electrical conductivity to study some anomalous phenomena widely observed in the literature. It has been shown that electrical conductivity in ferroelectric thin films could be responsible for quite a few anomalous ferroelectric and dielectric behaviours. In addition, electrical conductivity in both inclusion and matrix materials have been demonstrated to play a significant role in the prediction of electrostriction strain and magnetoelectric effect of 0-3 composites.

On the other hand, the effects of electrical conductivity have been experimentally utilized to optimize the ferroelectric and dielectric properties in ferroelectric thin films and composites. It is often found that the presence of conductivity in ferroelectric polymers can be utilized to control the polarization buildup process, particularly under high fields. The conductivity induced by impurity doping has also been variously utilized to enhance the pyroelectric and piezoelectric properties of 0-3 composites. Under the circumstance of a general lack of theoretical investigations in this direction, we believe our work has clarified and furnished a deeper understanding of the effect of electrical conductivity in some ferroelectric structures, the results of which already suggest that it is necessary and beneficial to engage in a careful consideration of electrical conductivity in materials or device design and optimization.

List of Publications

1. Journal articles:

Yan Zhou, H. K. Chan, C. H. Lam and F. G. Shin. "Effects of polarization and permittivity gradients and other parameters on the anomalous vertical shift behaviour of graded ferroelectric thin films", *Journal of Applied Physics*, Vol. 98, pp. 034105/1-6 (August 2005).

Yan Zhou, H. K. Chan, C. H. Lam and F. G. Shin. "Mechanisms of Imprint Effect in Ferroelectric Thin Films", *Journal of Applied Physics*, Vol. 98, pp. 024111/1-9 (July 2005).

Yan Zhou, and F. G. Shin. "Modeling of Magnetostriction in Particulate Composite Materials", *IEEE Transactions on Magnetics*, Vol. 41, pp. 2071-2076 (June 2005).

K. S. Lam, Yan Zhou, Y. W. Wong and F. G. Shin. "Electrostriction of lead zirconate titanate/polyurethane composites", *Journal of Applied Physics*, Vol. 97, pp. 104112/1-6 (May 2005).

Yan Zhou, and F. G. Shin. "Magnetoelectric effect of mildly conducting magnetostrictive/piezoelectric particulate composite", *Applied Physics Letters*, 2005 (submitted).

Yan Zhou, and F. G. Shin. "Enhancement of dielectric and ferroelectric properties in interface-coupled ferroelectric superlattices", *Journal of Applied Physics*, 2005 (submitted).

2. Conference articles:

Yan Zhou, and F. G. Shin. “Modeling of Magnetostriction in Particulate Composite Materials”, poster, 21-25 March 2005, Annual March Meeting of the American Physical Society, Los Angeles, USA.

Yan Zhou, and F. G. Shin. “Investigation of the Anomalous Polarization Offsets Phenomenon in Ferroelectric Thin Films”, oral presentation, 3-8 July 2005, 3rd International Conference on Materials for Advanced Technologies (ICMAT 2005), Suntec Singapore International Convention Center, Singapore.

Yan Zhou, attendee, 8-10 August 2005, 2005 International Conference on NanoTechnology and Advanced Materials, Hong Kong Convention and Exhibition Center, Hong Kong.

References

Abe, K. and Komatsu, S. "Ferroelectric properties in epitaxially grown $BaxSr_{1-x}TiO_3$ thin films", *Journal of Applied Physics*, Vol. 77, 6461-6465 (1995)

Abe, K., Komatsu, S., Yanase, N., Sano, K. and Kawakubo, T. "Asymmetric ferroelectricity and anomalous current conduction in heteroepitaxial $BaTiO_3$ thin films" *Japanese Journal of Applied Physics*, Vol. 36, pp. 5846-5853 (1997)

Abe, K., Yanase, N., Yasumoto, T. and Kawakubo, T. "Nonswitching layer model for voltage shift phenomena in heteroepitaxial barium titanate thin films". *Japanese Journal of Applied Physics*, Vol. 41, pp. 6065-6071 (2002)

Al-Shareef, H.N., Dimos, D., Warren, W.L. and Tuttle, B.A. "A model for optical and electrical polarization fatigue in $SrBi_2Ta_2O_9$ and $Pb(Zr,Ti)O_3$". *Integrated Ferroelectrics*, Vol. 15, 53-67 (1997)

Alpay, S.P., Ban, Z.G. and Mantese, J.V. "Thermodynamic analysis of temperature-graded ferroelectrics". *Applied Physics Letters*, Vol. 82, pp. 1269-1271 (2003)

Armstrong, W.D. "The non-linear deformation of magnetically dilute magnetostrictive particulate composites". *Materials Science and Engineering*, pp. 13-17 (2000)

Armstrong, W.D. “A general magneto-elastic model of Terfenol-D particle actuated composite materials”. *Journal of Intelligent Material Systems and Structures*, Vol. 13, pp. 137-141 (2002)

Baerwald, H.G. and Berlincourt, D.A. “Electromechanical response and dielectric loss of prepolarized barium titanate”. *The Journal of the Acoustical Society of America*, Vol. 25, 703 (1953)

Ban, Z.G., Alpay, S.P. and Mantese, J.V. “Fundamentals of graded ferroic materials and devices”. *Physical Review B*, Vol. 67, pp. 184104/1-6 (2003)

Bao, D., Wakiya, N., Shinozaki, K., Mizutani, N. and Yao, X. “Abnormal ferroelectric properties of compositionally graded $Pb(Zr,Ti)O_3$ thin films with $LaNiO_3$ bottom electrodes” *Journal of Applied Physics*, Vol. 90, 506 (2001)

Baudry, L. “Theoretical investigation of the influence of space charges on ferroelectric properties of $PbZrTiO_3$ thin film capacitor”. *Journal of Applied Physics*, Vol. 90, pp. 1442-1454 (1999)

Baudry, L. and Tournier, J. “Lattice model for ferroelectric thin film materials including surface effects: Investigation on the "depolarizing" field properties”. *Journal of Applied Physics*, Vol. 86, pp. 1096-1105 (2001)

Bichurin, M.I., Petrov, V.M. and Srinivasan, G. "Theory of low-frequency magnetoelectric coupling in magnetostrictive-piezoelectric bilayers". *Physical Review B* Vol. 68, pp. 054402/1-5 (2003)

Bracke, L.P.M. and Vanvliet, R.G. "A broad-band magnetoelectric transducer using a composite material". *International Journal of Electronics*, Vol. 51, pp. 255-262 (1981)

Brazier, M., Mansour, S. and McElfresh, M. "Electrochemical potential gradients in Pb(Zr,Ti)O3 thin films". *Material Research Society Symposium Proceeding*, Vol. 541, pp. 507-510 (1999)

Bouregba, R. and Poullain, G. "Numerical extraction of the true ferroelectric polarization due to switching domains from hysteresis loops measured using a Sawyer-Tower circuit". *Ferroelectrics*, Vol. 274, pp. 165-181 (2002)

Bouregba, R. and Poullain, G. Vilquin, B. and Le Rhun, G. "Asymmetrical leakage currents as a possible origin of the polarization offsets observed in compositionally graded ferroelectric films". *Journal of Applied Physics*, Vol. 93, No. 9, pp. 5583-5591 (2003)

Bozorth, R.M., Tilden, E.F. and Williams, A.J. "Anisotropy and Magnetostriction of Some Ferrites", *Physical Review*, Vol. 99, pp. 1788–1798 (1955)

Brazier, M., McElfresh, M. and Mansour, S. "Unconventional hysteresis behavior in compositionally graded Pb(Zr,Ti)O_3 thin films". *Applied Physics Letters*, Vol. 72, pp. 1121-1123 (1998)

Brazier, M., McElfresh, M. and Mansour, S. "Origin of anomalous polarization offsets in compositionally graded Pb(Zr, Ti)O_3 thin films". *Applied Physics Letters*, Vol. 74, pp. 299-301 (1999)

Cao, H.X., Gao, Y.H., Jiang, Q. and Li, Z.X. "Thermodynamic properties of compositionally graded $Ba_{1-x}Sr_xTiO_3$ thin films". *Journal of Applied Physics*, Vol. 96, No. 3, pp. 1628-1634 (2004)

Chan, H.L.W., Chen, Y. and Choy, C.L. "A poling study of PZT/P(VDF-TRFE) copolymer 0-3 composites". *Integrated Ferroelectrics*, Vol. 9, pp. 207-214 (1995)

Chan, H.K., Lam, C.H. and Shin, F.G. "Time-dependent space-charge-limited conduction as a possible origin of the polarization offsets observed in compositionally graded ferroelectric films". *Journal of Applied Physics*, Vol. 95, No. 5, pp. 2665-2671 (2004)

Chen, Y., Snyder, J.E., Schwichtenberg, C.R., Dennis, K.W., Falzgraf, D.K., McCallum, R.W. and Jiles, D.C. "Effect of the elastic modulus of the matrix on magnetostrictive strain in composites". *Applied Physics Letters*, Vol. 74, No. 8, pp. 1159-1161 (1999a)

Chen, Z. Arita, K., Lim, M. and Paz De Araujo, C.A. "Graded PZT thin film capacitors with stoichimetric variation by MOD technique". *Integrated Ferroelectrics*, Vol. 24, pp. 181-188 (1999b)

Chew, K.H., Ishibashi, Y. and Shin, F.G. "Ferroelectric hysteresis loops as the manifestation of interface-aided polarization reversals in heterostructures". *Journal of Physical Society of Japan*, Vol. 74, pp. 2338-2346 (2005)

Chew, K.H, Shin, F.G., Ploss, B., Chan, H.L.W. and Choy, C.L. "Primary and secondary pyroelectric effects of ferroelectric 0-3 composites". *Journal of Applied Physics*, Vol. 94, pp. 1134-1145 (2003)

Christen, H.M., Specht, E.D., Siliman, S.S. and Harshavardhan, K.S. "Ferroelectric and antiferroelectric coupling in superlattices of paraelectric perovskites at room temperature". *Physical Review B*, Vol. 68, pp. 020101R (2003)

Christensen, R.M. Mechanics of Composite Materials, Krieger Publishing Company, Florida, pp. 41-44 (1979)

Coelho, R. *Physics of Dielectrics for the Engineer.* Elsevier Scientific, New York, pp. 123-125 (1979)

Das-Gupta, D.K. "Pyroelectricity in polymers". *Ferroelectrics*, Vol. 118, pp. 165-189, (1991)

Desu, S.B. "Influence of stresses on the properties of ferroelectric $BaTiO_3$ thin films". *Journal of The Electrochemical Society*, Vol. 140, pp. 2981-2987 (1993)

Dey, S.K., Lee, J.J. and Alluri, P. "Electrical-properties of paraelectric $(Pb_{0.72}La_{0.28})TiO_3$ thin-films with high linear dielectric permittivity-schottky and Ohmic contacts". *Japanese Journal of Applied Physics*, Vol. 34, pp. 3142-3152 (1995)

Erbil, A., Kim, Y. and Gerhardt, R.A. "Giant Permittivity in Epitaxial Ferroelectric Heterostructures". *Physical Review Letters*, Vol. 77, pp. 1628-1631 (1996)

Folen, V.J., Rado, G.T. and Stalder, E.W. "Anisotropy of the Magnetoelectric Effect in Cr_2O_3". *Physical Review Letters*, Vol. 6, pp. 607–608 (1961)

Fong, D.D., Stephenson, G.B., Streiffer, S.K., Eastman, J.A., Auciehho, O., Fuoss, P.H. and Thompson, C. "Ferroelectricity in ultrathin perovskite films". *Science*, Vol. 304, pp. 1650-1653 (2004)

Foster, C.M., Bai, G.R., Csencsits, R., Vetrone, J., Jammy, R., Wills, L.A., Carr, E. and Amano, J. "Single-crystal $Pb(Zr_xTi_{1-x})O_3$ thin films prepared by metal-organic

chemical vapor deposition: Systematic compositional variation of electronic and optical properties". *Journal of Applied Physics*, Vol. 81, pp. 2349-2357 (1997)

Furukawa, T., Fujino, K. and Fukada, E. "Electromechanical properties in composites of epoxy-resin and PZT ceramics". *Japanese Journal of Applied Physics*, Vol. 15, pp. 2119-2129 (1976)

Furuya, A. and Cuchiaro, J.D. "Compositional dependence of electrical characteristics of $SrBi_2(Ta_{1-x}Nb_x)_2O_9$ thin-film capacitors". *Journal of Applied Physics*, Vol. 84, pp. 6788-6794 (1998)

Goodier, J.N. "Concentration of stress around spherical and cylindrical inclusions and flaws". *Transactions of the ASME*, Vol. 55, pp. 39-44 (1933)

Grossmann, M., Lohse, O., Bolten, D., Boettger, U. and Waser, R. "The interface screening model as origin of imprint in $PbZr_xTi_{1-x}O_3$ thin films. II. Numerical simulation and verification". *Journal of Applied Physics*, Vol. 92, pp. 2688-2696 (2002)

Hase, T., Sakuma, T., Miyasaka, Y., Hirata, K. and Hosokawa, N. "Preparation of Ba $(Zr,Ti)O_3$ thin films by multitarget sputtering". *Japanese Journal of Applied Physics*, Vol. 32, pp. 4061-4064 (1993)

He, L.X. and Vanderbilt, D. "First-principles study of oxygen-vacancy pinning of domain walls in $PbTiO_3$". *Physical Review B*, Vol. 68, pp. 134103/1-7 (2003)

Hook, J.R. and Hall, H.E. *Solid State Physics*. John Wiley and Sons Ltd., Chichester, pp. 139-143 (1974)

Kumazawa, T., Kumagai, Y., Miura, H. and Kitano, M. "Effect of external stress on polarization in ferroelectric thin films". *Applied Physics Letters*, Vol. 72, 608-610 (1998)

Jin, F., Auner, G.W., Naik, R., Schubring, N.W., Mantese, J.V., Catalan, A.B. and Micheli, A.L. "Giant effective pyroelectric coefficients from graded ferroelectric devices". *Applied Physics Letters*, Vol. 73, pp. 2838-2840 (1998)

Hill, R. "A self-consistent mechanics of composite materials," *Journal of Mechanics and Phyical Solids*, vol. 13, pp. 213-222, (1965)

Hong, S., Colla, E.L., Kim, E., Taylor, D.V., Tagantsev, A.K., Muralt, P., No, K. and Setter, N. "High resolution study of domain nucleation and growth during polarization switching in $Pb(Zr,Ti)O_3$ ferroelectric thin film capacitors". *Journal of Applied Physics*, Vol. 86, pp. 607-613 (1999)

Laletin, V.M. and Srinivasan, G. "Magnetoelectric Effects in Composites of Nickel Ferrite and Barium Lead Zirconate Titanate". *Ferroelectrics*, Vol. 280, pp. 177-185

(2002)

Lam, K.S., Wong, Y.W., Tai, L.S., Poon, Y.M. and Shin, F.G. "Dielectric and pyroelectric properties of lead zirconate titanate/polyurethane composites". *Journal of Applied Physics*, Vol. 96, pp. 3896-3899 (2004)

Lam, K.S., Zhou, Y., Wong, Y.W. and Shin, F.G. "Electrostriction of lead zirconate titanate/polyurethane composites". *Journal of Applied Physics*, Vol. 97, pp. 104112/1-6 (2005)

Landau, L.D. and Lifshitz, E.M. Electrodynamics of Continuous Media, Pergamon Press, pp. 43-44 (1960)

Laletin, V.M. and Srinivasan, G. "Magnetoelectric effects in composites of nickel ferrite and barium lead zirconate titanate". *Ferroelectrics*, Vol. 280, pp. 343-351 (2002)

Lee, H.N., Christen, H.M., Chisholm, M.F., Rouleau, C.M. and Lowndes, D.H. "Strong polarization enhancement in asymmetric three-component ferroelectric superlattices". *Nature* Vol. 433, pp. 395-399 (2005)

Lee, K.W., Kim, Y.I. and Lee, W.J. "Physical modeling of the effect of the asymmetric electrode configuration on the hysteresis curves of ferroelectric film capacitors". Ferroelectrics Vol. 271, pp. 1769-1775 (2002)

Lee, J., Safari, A. and Pfeffer, R.L. "Growth of epitaxial $Pb(Zr,Ti)O_3$ films by pulsed laser deposition". *Applied Physics Letters*, Vol. 61, pp. 1643-1645 (1992)

Li, C.L., Chen, Z.H., Zhou, Y.L. and Cui, D.F. "Effect of oxygen content on the dielectric and ferroelectric properties of laser-deposited $BaTiO_3$ thin films". *Journal of Physics D-Condensed Matter*, Vol. 13, pp. 5261-5268 (2001)

Li, Y., Nagarajan, V., Aggarwal, S., Ramesh, R., Salamanca-Riba, L.G. and Martinez-Miranda, L.J. "Depth profile study of ferroelectric $PbZr_{0.2}Ti_{0.8}O_3$ films". *Journal of Applied Physics*, Vol. 92, pp. 6762-6767 (2002)

Liu, W., Ko, J. and Zhu, W. "Asymmetric switching behavior of $Ni/Pb_{1.1}(Zr_{0.3}Ti_{0.7})O_3/Pt$ thin films". *Materials Letter*, Vol. 49, pp. 122-126 (2001)

Liu, Y.Q. and Gao, L. "A study of the electrical properties of carbon nanotube-$NiFe_2O_4$ composites: Effect of the surface treatment of the carbon nanotubes". Carbon, Vol. 43, pp. 47-52 (2005)

Lo, V.C. "Simulation of thickness effect in thin ferroelectric films using

Landau–Khalatnikov theory". *Journal of Applied Physics*, Vol. 94, pp. 3353-3359 (2003)

Lo, V.C. and Chen, Z.J. "Simulation of the effects of space charge and Schottky barriers on ferroelectric thin film capacitor using Landau Khalatnikov theory". *IEEE transactions on ultrasonics ferroelectrics and frequency control*, Vol. 49, pp. 980-986 (2002)

Loloee, R. and Crimp, M.A. "Effect of growth temperature on the structure and magnetic properties of sputtered biepitaxial (111) permalloy films". *Journal of Applied Physics*, Vol. 92, pp. 4541-4544 (2002)

Lü, T. and Cao, W. "Generalized continuum theory for ferroelectric thin films". *Physical Review B*, Vol. 66, pp. 024102/1-5 (2002)

Lü, T. and Cao, W. "Influence of imperfect surface on properties of ferroelectric thin film". *Microelectronic Engineering*, Vol. 66, pp. 818-824 (2003)

Mantese, J.V., Schubring, N.W., Micheli, A.L., Catalan, A.B., Mohammed, M.S., Naik, R. and Auner, G.W. "Slater model applied to polarization graded ferroelectrics". *Applied Physics Letters*, Vol. 71, No. 14, pp. 2047-2049 (1997)

Mantese, J.V. and Schubring, N.W. "Polarization-graded ferroelectrics: The dielectric analogues of semiconductor junctions devices". *Integrated Ferroelectrics*,

Vol. 37, pp. 575-587 (2001)

Mantese, J.V., Schubring, N.W., Micheli, A.L., Thompson, M.P., Naik, R., Auner, G.W., Misirlioglu, I.B. and Alpay, S.P. "Stress-induced polarization-graded ferroelectrics". *Applied Physics Letters*, Vol. 81, pp. 1068-1070 (2002)

Mark, J.E. *Polymer Data Handbook*, Oxford, New York, pp. 874 (1999)

Ma, Y and Reneker D.H. "Electrostriction of rubber sheets". *Rubber Chemistry and Technology*, Vol. 69, pp. 674-685 (1996)

Miller, S.L., Nasby, R.D., Schwank, J.R., Rodgers, M.S. and Dressendorfer, P.V. "Device modeling of ferroelectric capacitors". *Journal of Applied Physics*, Vol. 68, pp. 6463-6471 (1990)

Mohammed, M.S. Naik, R., Mantese, J.V., Schubring, N.W., Micheli, A.L. and Catalan, A.B. "Microstructure and ferroelectric properties of fine-grained $Ba_xSr_{1-x}TiO_3$ thin films prepared by metalorganic decomposition". *Journal of Materials Research*, Vol. 11, pp. 2588-2593 (1996)

Müller , P. and Thomas, O. "Asymptotic behaviour of stress establishment in thin films". *Surface Science*, Vol. 465, pp. L764-L770, (2000)

Nagasawa, D. and Nozawa, H. "Imprint Model Based on Thermionic Electron Emission Under Local Fields in Ferroelectric Thin Films". *Japanese Journal of Applied Physics*, Vol. 38, pp. 5406-5410 (1999)

Nakamura, T., Nakao, Y., Kamisawa A. and Takasu, H. "Preparation of $Pb(Zr,Ti)O_3$ thin films on Ir and IrO_2 electrodes". *Japanese Journal of Applied Physics*, Vol. 33, pp. 5207-5210 (1994)

Nan, C.W. and Weng, G.J. "Theoretical approach to effective electrostriction in inhomogeneous materials". *Physical Review B*, Vol. 61, No. 1, pp. 258-265 (2000)

Nan, C.W., Li, M. and Huang, J.H. "Calculations of giant magnetoelectric effects in ferroic composites of rare-earth-iron alloys and ferroelectric polymers". *Physical Review B*, Vol. 63, pp. 144415/1-9 (2001)

Nan, C.W., Li, M., Feng, X.Q. and Yu. S.W. "Possible giant mangetoelectric effect of ferromagnetic rare-earth-iron-alloys-filled ferroelectric polymers". *Applied Physics Letters*, Vol. 78, No. 17, pp. 2527-2529 (2001)

Nersessian, N., Or, S.W., Carman, G.P., Chow, W.Y. and Radousky, H.B. "Hollow and solid spherical magnetostrictive particulate composites". *Journal of Applied Physics*, Vol. 96, No. 6, pp. 3362-3365 (2004)

Park, B.H., Noh, T.W., Lee, J., Kim, C.Y. and Jo, W. "Effects of interface charges

on imprint of epitaxial $Bi_4Ti_3O_{12}$ thin films". *Applied Physics Letters*, Vol. 70, pp. 1101-1103 (1997)

Park, B.H., Hyun, S.J., Moon, C.R., Choe, B.D., Lee, J., Kim, C.Y., Jo, W. and Noh, T.W. "Imprint failures and asymmetric electrical properties induced by thermal processes in epitaxial $Bi_4Ti_3O_{12}$ thin films". *Journal of Applied Physics*, Vol. 84, pp. 4428-4435 (1998)

Pike, G.E., Warren, W.L., Dimos, D., Tuttle, B.A., Ramesh, R., Lee, J., Keramidas, V.G. and Evans, J.T. "Voltage offsets in (Pb,La)(Zr,Ti)O_3 thin films". *Applied Physics Letters*, Vol. 66, pp. 484-486 (1995)

Pintilie, L., Boerasu, I. and Gomes, M.J.M. "Simple model of polarization offset of graded ferroelectric structures". *Journal of Applied Physics*, Vol. 93, No. 12, pp. 9961-9967 (2003)

Pontes, F.M., Longo, E., Leite, E.R. and Varela, J.A. "Improvement of the dielectric and ferroelectric properties in superlattice structure of Pb(Zr,Ti)O_3 thin films grown by a chemical solution route". *Applied Physics Letters*, Vol. 84, pp. 5470-5472 (2004)

Poullain, G., Bouregba, R., Vilquin, B., Rhun, G.L. and Murray, H. "Graded

ferroelectric thin films: Possible origin of the shift along the polarization axis". *Applied Physics Letters*, Vol. 81, pp. 5015-5017 (2002)

Poon, Y.M. and Shin, F.G. "A Simple Explicit Formula for the Effective Dielectric Constant of Binary 0-3 Composites". *Journal of Materials Sciences*, vol. 39, pp. 1277-1281, (2004)

Qu, B.D., Zhong, W.L. and Prince, R.H. "Interfacial coupling in ferroelectric superlattices". *Physical Review B*, Vol. 55, pp. 11218-11224 (1997)

Ricinschi, D., Harnagea, C., Papusoi, C., Mitoseriu, L., Tura, V. and Okuyama, M. "Analysis of ferroelectric switching in finite media as a Landau-type phase transition". *Journal of Physics D: Condensed Matter*, Vol. 10, pp. 477-492 (1998)

Robels, U., Calderwood, J.H. and Arlt, G. "Shift and deformation of the hysteresis curve of ferroelectrics by defects-electrostatic model". *Journal of Applied Physics*, Vol. 77, pp. 4002-4008 (1995)

Sadashivan, S., Aggarwal, S., Song, T.K., Ramesh, R., Evans, J.T., Tuttle, B.A., Warren, W.L. and Dimos, D. "Evaluation of imprint in fully integrated $(La,Sr)CoO_3/Pb(Nb,Zr,Ti)O_3/(La,Sr)CoO_3$ ferroelectric capacitors". *Journal of Applied Physics*, Vol. 83, pp. 2165-2171 (1998)

Sakamoto, W.K., Shibatta-Kagesawa, S.T., Melo, W.L.B. “Voltage responsivity of pyroelectric sensor”. *Sensors and Actuators*, Vol. 77, pp. 28-33 (1999)

Sakashita, Y., Segawa, H., Tominaga, K. and Okada, M. “Dependence of electrical properties on film thickness in $Pb(Zr_xTi_{1-x})O_3$ thin films produced by metalorganic chemical vapor deposition”. *Journal of Applied Physics*, Vol. 73, pp. 7857-7863 (1993)

Said, M.Z. “Effect of gadolinium substitutions on the structure and electrical conductivity of Ni-ferrite”. *Materials Letters*, Vol. 34, pp. 305-307 (1998)

Sawyer, C.B. and Tower, C.H. “Rochelle Salt as a Dielectric”, *Physical Review*, Vol. 35, pp. 269–273 (1930)

Saya, Y., Watanabe, S., Kawai, M., Yamada, H. and Matsushige, K. “Investigation of nonswitching regions in ferroelectric thin films using scanning force microscopy”. *Japanese Journal of Applied Physics*, Vol. 39, pp. 3799-3803 (2000)

Schubring, N.W., Mantese, J.V., Micheli, A.L., Catalan, A.B. and Lopez, R.J. “Charge pumping and pseudopyroelectric effect in active ferroelectric relaxor-type films”. *Physical Review Letters*, Vol. 68, pp. 1778-1781 (1992)

Sepliarsky, M., Phillpot, S.R., Stachiotti, M.G. and Migoni, R.L. “Ferroelectric phase transitions and dynamical behavior in $KNbO_3/KTaO_3$ superlattices by molecular-dynamics simulation”. *Journal of Applied Physics,* Vol. 91, pp. 3165-3171 (2002)

Shimuta, T., Nakagawara, O., Makino, T., Arai, S., Tabata, H. and Kawai, T. “Enhancement of remanent polarization in epitaxial $BaTiO_3/SrTiO_3$ superlattices with "asymmetric" structure”. *Journal of Applied Physics,* Vol. 91, pp. 2290-2294 (2002)

Shimizu, M., Okaniwa, M., Fujisawa, H. and Niu, H. “Crystalline and ferroelectric properties of $Pb(Zr, Ti)O_3$ thin films grown by low-temperature metalorganic chemical vapor deposition”. *Japanese Journal of Applied Physics,* Vol. 41, pp. 6686-6689 (2002)

Slater, J.C. “The Lorentz correction in barium titanate”. *Physical Review,* Vol. 78, pp. 748-761 (1950)

Song, T.K., Kim, J.S., Kim, M.H., Lim, W., Kim Y.S. and Lee, J. “Landau-Khalatnikov simulations for the effects of external stresses on the ferroelectric properties of $Pb(Zr,Ti)O_3$ thin films”. *Thin Solid Films,* Vol. 424, pp. 84-87 (2003)

Spierings, G.A.C.M., Dormans, G.J.M., Moors, W.G.J., Ulenaers, M.J.E. and Larsen, P.K. “Stresses in Pt/Pb(Zr,Ti)O_3/Pt thin-film stacks for integrated ferroelectric capacitors”. *Journal of Applied Physics*, Vol. 78, pp. 1926-1933 (1995)

Srinivasan, G., Devreugd, C.P., Flattery, C.S., Laletsin, V.M. and Paddubnaya, N. “Magnetoelectric interactions in hot-pressed nickel zinc ferrite and lead zirconante titanate composites”. *Applied Physics Letters*, Vol. 85, No. 13, pp. 2550-2552 (2004)

Stoilichnov, A. Tagantsev, E. Colla, S. Gentil, S. Hiboux, J. Baborowski, P. Muralt, and N. Setter, “Downscaling of Pb(Zr,Ti)O_3 film thickness for low-voltage ferroelectric capacitors: Effect of charge relaxation at the interfaces”. *Journal of Applied Physics*, Vol. 88, pp. 2154-2156 (2000)

Tai, L.S., *M. Phil. Thesis*, The Hong Kong Polytechnic University, (2001)

Tagantsev, A.K., Landivar, M., Colla, E. and Setter, N. “Identification of passive layer in ferroelectric thin films from their switching parameters”. *Journal of Applied Physics*, Vol. 78, pp. 2623-2630 (1995)

Tsang, C.H., Chew, K.H., Ishibashi, Y. and Shin, F.G. “Structure of interfaces in layered ferroelectrics of first and/or second order transition”. *Journal of Physical*

Society of Japan, Vol. 73, pp. 3158-3165 (2004).

Wang, C., Fang, Q.F., Zhu, Z.G., Jiang, A.Q., Wang, S.Y., Cheng, B.L. and Chen, Z.H. "Dielectric properties of $Pb(Zr_{20}Ti_{80})O_3/Pb(Zr_{80}Ti_{20})O_3$ multilayered thin films prepared by rf magnetron sputtering". *Applied Physics Letters*, Vol. 82, pp. 2880-2882 (2003)

Wang, C.L., Zhang, L., Peng, Y.P., Zhong, W.L., Zhang, P.L. and Wang, Y.X. "Landau theory of asymmetric ferroelectric films under external electric fields". Solid State Communications, Vol. 109, pp. 213-216 (1999)

Warren, W.L., Tuttle, B.A., Dimos, D., Pike, G.E., Al-Shareef, H.N., Ramesh R. and Evans, J.T. "Imprint in ferroelectric capacitors". *Japanese Journal of Applied Physics*, Vol. 35, pp. 1521-1524 (1996)

Wong, C.K. and Shin, F.G. "Role of interfacial charge in the piezoelectric properties of ferroelectric 0-3 composites". *Journal of Applied Physics*, Vol. 97, pp. 034111/1-9 (2005)

Wong, C.K., Wong, Y.W. and Shin, F.G. "Effect of interfacial charge on polarization switching of lead zirconate titanate particles in lead zirconate

titanate/polyurethane composites". *Journal of Applied Physics*, Vol. 92, No. 7, pp. 3974-3978 (2002)

Wong, C.K., Poon, Y.M. and Shin, F.G. "Explicit formulas for effective piezoelectric coefficients of ferroelectric 0-3 composites". *Journal of Applied Physics*, Vol. 90, pp. 4690-4700 (2001)

Wu, W.B., Wong, K.H. and Mak, C.L. "Effect of oxygen stoichiometry on the ferroelectric property of epitaxial all oxide $La_{0.7}S_{0.3}MnO_3Pb(Zr_{0.52}Ti_{0.48})O_3/La_{0.7}Sr_{0.3}$ thin film capacitors". *Journal of Vacuum of Science and Technology*, Vol. 18, pp. 2412-2416 (2000)

Xu, Y.H., Chen, C.J. and Xu, R. "The self-biased heterojunction effect of ferroelectric thin film on silicon substrate". *Journal of Applied Physics*, Vol. 67, pp. 2985-2991 (1990)

Yang, P. Carroll, D.L., Ballato, J. and Schwartz, R.W. "Electrical properties of $SrBi_2Ta_2O_9$ ferroelectric thin films at low temperature". *Applied Physics Letters*, Vol. 81, pp. 4583-4585 (2002)

Zeng, M., Wan, J.G., Wang, Y., Yu, H., Liu, J.M., Jiang, X.P. and Nan, C.W. "Resonance magnetoelectric effect in bulk composites of lead zirconate titanate and nickel ferrite". *Journal of Applied Physics*, Vol. 95, No. 12, pp. 8069-8073 (2004)

Zhai, J.Y., Cai, N., Shi, Z., Lin, Y.H. and Nan, C.W. "Magnetic-dielectric properties of $NiFe_2O_4$/PZT particulate composites". *Journal of Physics D: Applied Physics*. Vol. 37, pp. 823-827 (2004)

Zhang, Q.M., Bharti V. and Zhao X. "Giant electrostriction and relaxor ferroelectric behavior in electron-irradiated poly(vinylidene fluoride-trifluoroethylene) copolymer". *Science*, Vol. 280, pp. 2101-2104 (1998)

Zheng, L., Lin, C. and Ma, T.P. "Current-voltage characteristic of asymmetric ferroelectric capacitors". *Journal of Physics D: Applied Physics*, Vol. 29, pp. 457-461 (1996)

Zhengyl, M., Scheinbeim, J.I., Lee, J.W. and Newman, B.A. "High-field electrostrictive response of polymers". *Journal of Polymer Science*, Vol. 32, pp. 2721-2731 (1994)

Zhou, Y. and Shin, F.G. "Modeling of Magnetostriction in Particulate Composite Materials". *IEEE Transactions on Magnetics*, Vol. 41, pp. 2071-2076 (2005)

Zhou, Y., Chan, H.K., Lam, C.H. and Shin, F.G. "Effects of polarization and permittivity gradients and other parameters on the anomalous vertical shift behavior of graded ferroelectric thin films". *Journal of Applied Physics*, Vol. 98, pp. 034105/1-6 (2005)

Appendix A

First, consider the case when the composite is subjected to a hydrostatic compression. From [Chew *et al.*, 2003] we know the stress-strain relationship can be expressed as

$$\langle \sigma_m \rangle = \langle \sigma_i \rangle + \frac{4}{3}\mu_m(\langle e_i \rangle - \langle e_m \rangle) \ , \tag{A1}$$

where $\langle \sigma \rangle = \langle \sigma_x \rangle = \langle \sigma_y \rangle = \langle \sigma_z \rangle$ and $\langle e \rangle = \langle e_x \rangle + \langle e_y \rangle + \langle e_z \rangle$ are the volume-averaged hydrostatic stress and volume-averaged hydrostatic strain of the composite, respectively. Since in the hydrostatic case $\langle \sigma_x \rangle = \langle \sigma_y \rangle = \langle \sigma_z \rangle$ and $\langle e_x \rangle = \langle e_y \rangle = \langle e_z \rangle$, the constitutive equations are given by

$$\langle \sigma_{ix} \rangle = (k_i - \frac{2}{3}\mu_i)(3\langle e_{ix} \rangle) + 2\mu_i \langle e_{ix} \rangle \ , \tag{A2}$$

$$\langle \sigma_{mx} \rangle = (k_m - \frac{2}{3}\mu_m)(3\langle e_{mx} \rangle) + 2\mu_m \langle e_{mx} \rangle \ . \tag{A3}$$

The strain and stress of the composite in the *x*-direction are calculated by

$$\langle e_x \rangle = \phi \langle e_{ix} \rangle + (1-\phi)\langle e_{mx} \rangle \ , \tag{A4}$$

$$\langle \sigma_x \rangle = \phi \langle \sigma_{ix} \rangle + (1-\phi)\langle \sigma_{mx} \rangle \ . \tag{A5}$$

Eqs. (5.1), (5.2) and (5.3) give

$$\langle \sigma_{ix} \rangle - \langle \sigma_{mx} \rangle = (A+2B)(\langle e_{ix} \rangle - \langle e_{mx} \rangle) \ . \tag{A6}$$

Comparing (A1) and (A6) yields

$$A + 2B = -4\mu_m \ . \tag{A7}$$

For later use in Appendix C, we need an expression for the bulk modulus of the composite. This can be calculated by using (A2)-(A6) as

$$k = \frac{\langle \sigma_x \rangle}{3\langle e_x \rangle} = \frac{(A+2B)(1-\phi)k_m + k_i[(A+2B)\phi - 3k_m]}{A+2B-3(1-\phi)k_i - 3\phi k_m} \ . \tag{A8}$$

When the composite is subjected to the pure shear stresses, we refer e.g. to the Hashin [Hashin, 1962] shear modulus

$$\mu = \mu_m + \frac{15(1-\nu_m)(\mu_i/\mu_m - 1)\phi}{7-5\nu_m + 2(4-5\nu_m)[\mu_i/\mu_m - (\mu_i/\mu_m - 1)\phi]} \ , \tag{A9}$$

where $\nu_m = \dfrac{3k_m - 2\mu_m}{6k_m - 2\mu_m}$ is Poisson's ratio of the matrix material. Considering the shear deformation case $\langle\sigma_{ix}\rangle = -\langle\sigma_{iy}\rangle, \langle\sigma_{mx}\rangle = -\langle\sigma_{my}\rangle, \langle e_{ix}\rangle = -\langle e_{iy}\rangle, \langle e_{mx}\rangle = -\langle e_{my}\rangle$, Eqs. (5.1) and (5.2) become

$$\langle\sigma_{ix}\rangle - \langle\sigma_{mx}\rangle = A\times(\langle e_{ix}\rangle - \langle e_{mx}\rangle) + B\times(\langle e_{iy}\rangle - \langle e_{my}\rangle) \ , \tag{A10}$$

$$\langle\sigma_{iy}\rangle - \langle\sigma_{my}\rangle = B\times(\langle e_{ix}\rangle - \langle e_{mx}\rangle) + A\times(\langle e_{iy}\rangle - \langle e_{my}\rangle) \ . \tag{A11}$$

The constitutive equations are given by

$$\langle\sigma_{ix}\rangle = 2\mu_i\langle e_{ix}\rangle \ , \tag{A12}$$

$$\langle\sigma_{iy}\rangle = 2\mu_i\langle e_{iy}\rangle \ , \tag{A13}$$

$$\langle\sigma_{mx}\rangle = 2\mu_m\langle e_{mx}\rangle \ , \tag{A14}$$

$$\langle\sigma_{my}\rangle = 2\mu_m\langle e_{my}\rangle \ . \tag{A15}$$

The strain and stress of the composite in the *x*-direction are calculated by

$$\langle e_x\rangle = \phi\langle e_{ix}\rangle + (1-\phi)\langle e_{mx}\rangle \ , \tag{A16}$$

$$\langle\sigma_x\rangle = \phi\langle\sigma_{ix}\rangle + (1-\phi)\langle\sigma_{mx}\rangle \ . \tag{A17}$$

Using (A10) to (A17), the shear modulus of the composite μ can be expressed, after some manipulation, as

$$\mu = \frac{\langle\sigma_x\rangle}{2\langle e_x\rangle} = \frac{\mu_i[(A-B)\phi - 2\mu_m] + (A-B)(1-\phi)\mu_m}{A-B-2(1-\phi)\mu_i - 2\phi\mu_m} \ . \tag{A18}$$

Then, (A9) and (A18) yield

$$A - B = -\mu_m \frac{9k_m + 8\mu_m}{3(k_m + 2\mu_m)} \quad . \tag{A19}$$

Hence, A and B are solved from (A8) and (A19)

$$A = \frac{10}{9}\mu_m(-3 + \frac{2\mu_m}{k_m + 2\mu_m}) \ , \tag{A20}$$

$$B = \frac{1}{9}\mu_m(-3 - \frac{10\mu_m}{k_m + 2\mu_m}) \ . \tag{A21}$$

Appendix B

Consider a magnetostrictive sphere of radius a with magnetic permeability ξ_i situated at the origin and subjected to a uniform magnetic field $\langle B_m \rangle$ in the z direction sufficiently far away from the sphere. The sphere is surrounded by a medium with permeability ξ_m. The problem is to solve the Laplace's equation:

$$\nabla^2 \varphi_l(r,\theta) = 0, \qquad l = i, m \ , \tag{B1}$$

where $\varphi_i(r,\theta)$ is the magnetic potential for $r < R$ inside the spherical inclusion and $\varphi_m(r,\theta)$ is the potential for $r > R$ outside of the inclusion.

With the condition that potential must not have a singularity at the center of sphere (r=0), and the boundary condition at infinity:

$$(\varphi_m)_{r\to\infty} = -\langle H_m \rangle z = -\langle H_m \rangle r\cos\theta \ , \tag{B2}$$

the general solutions for the spherical inclusion and matrix are

$$\varphi_i = \sum_{l=0}^{\infty} A_l r^l P_l(\cos\theta) \ , \tag{B3}$$

$$\varphi_m = -\langle H_m \rangle r\cos\theta + \sum_{l=0}^{\infty} C_l r^{-(l+1)} P_l(\cos\theta) \ , \tag{B4}$$

where $P_l(\cos\theta)$ are the Legendre polynomials.

On the inclusion surface, the boundary condition of the tangential component of magnetic field is

$$-\frac{1}{r}\frac{\partial \varphi_i}{\partial \theta}\bigg|_{r=a} = -\frac{1}{r}\frac{\partial \varphi_m}{\partial \theta}\bigg|_{r=a} \tag{B5}$$

and the boundary condition of the normal component of magnetic induction is

$$[-\xi_i \frac{\partial \varphi_i}{\partial r} + \langle M_i \rangle \cos\theta]\big|_{r=a} = [-\xi_m \frac{\partial \varphi_m}{\partial r} + \langle M_m \rangle \cos\theta]\big|_{r=a} \ . \tag{B6}$$

Using (B3) and (B4) together with boundary conditions (B5) and (B6), we obtain

$$A_1 = -(\frac{3\xi_m}{\xi_i + 2\xi_m})\langle H_m \rangle + \frac{\langle M_i \rangle - \langle M_m \rangle}{\xi_i + 2\xi_m} \ , \tag{B7}$$

$$C_1 = a^3 \left[(\frac{\xi_i - \xi_m}{\xi_i + 2\xi_m})\langle H_m \rangle + \frac{\langle M_i \rangle - \langle M_m \rangle}{\xi_i + 2\xi_m} \right] , \tag{B8}$$

and

$$A_n = C_n = 0 \quad for \quad n \neq 1 \ . \tag{B9}$$

The expression for the field in the inclusion is thus

$$\langle H_i \rangle = \frac{(\xi_m \langle H_m \rangle + \langle M_m \rangle) - (\xi_i \langle H_i \rangle + \langle M_i \rangle)}{\xi_i + 2\xi_m} \ , \tag{B10}$$

which can be rewritten in terms of the average magnetic induction and magnetic field as

$$\langle B_i \rangle - \langle B_m \rangle = -2\xi_m (\langle H_i \rangle - \langle H_m \rangle) \ . \tag{B11}$$

Appendix C

We assume that the inclusion particles are surrounded by a “matrix” material which has the same effective elastic properties as the whole composite material. Thus the effective bulk and shear modulus are likewise obtained from (A8) and (A18) by replacing k_m and μ_m by k and μ, respectively:

$$k = \frac{(A+2B)(1-\phi)k + k_i[(A+2B)\phi - 3k]}{A+2B-3(1-\phi)k_i - 3\phi k} \ , \tag{C1}$$

$$\mu = \frac{\mu_i[(A-B)\phi - 2\mu] + (A-B)(1-\phi)\mu}{A-B-2(1-\phi)\mu_i - 2\phi\mu} \ , \tag{C2}$$

where also A and B are replaced by

$$A = \frac{10}{9}\mu(-3 + \frac{2\mu}{k+2\mu}) \ , \tag{C3}$$

$$B = \frac{1}{9}\mu(-3 - \frac{10\mu}{k+2\mu}) \ . \tag{C4}$$

Thus (C1) and (C2) can be rewritten as

$$\frac{3}{3k+4\mu} = \frac{3\phi}{3k_i+4\mu} + \frac{3(1-\phi)}{3k_m+4\mu} \ , \tag{C5}$$

$$\frac{3\phi k_i}{3k_i+4\mu} + \frac{3(1-\phi)k_m}{3k_m+4\mu} + 5[\frac{\phi\mu_m}{\mu-\mu_m} + \frac{(1-\phi)\mu_i}{\mu-\mu_i}] + 2 = 0 \ , \tag{C6}$$

which are the same with Hill’s equations [Hill, 1965].